

# **Carbohydrate Polymer Based Nanocomposite Hydrogel Membrane for Enhanced Antimicrobial Activity**



**By  
Fatima Amir**

**School of Chemical and Materials Engineering  
National University of Sciences and Technology  
2023**

# **Carbohydrate Polymer Based Nanocomposite Hydrogel Membrane for Enhanced Antimicrobial Activity**



Name: Fatima Amir

Reg No.: 00000329147

**This thesis is submitted as partial fulfilment of the requirements for  
the degree of**

**MS in Chemical Engineering**

**Supervisor: Dr. Muhammad Bilal Khan Niazi**

**School of Chemical and Materials Engineering (SCME)**

**National University of Sciences and Technology (NUST)**

**H-12 Islamabad, Pakistan**

**July, 2023**



### THESIS ACCEPTANCE CERTIFICATE

Certified that final copy of MS thesis written by Fatima Amir (Registration No 00000329147), of School of Chemical & Materials Engineering (SCME) has been vetted by undersigned, found complete in all respects as per NUST Statues/Regulations, is free of plagiarism, errors, and mistakes and is accepted as partial fulfillment for award of MS degree. It is further certified that necessary amendments as pointed out by GEC members of the scholar have also been incorporated in the said thesis.

Signature: \_\_\_\_\_

*N. M. Bilal Khan Niazi*

Name of Supervisor: Dr.M. Bilal Khan Niazi

Date: 30<sup>th</sup> October 2023

Signature (HOD): \_\_\_\_\_

*SB*

Date: \_\_\_\_\_

31/10/23

Signature (Dean/Principal): \_\_\_\_\_

*AA*

Date: \_\_\_\_\_

31.10.2023



Form TH-1  
(Must be typewritten)

National University of Sciences & Technology (NUST)

MASTER'S THESIS WORK

Formulation of Guidance and Examination Committee (GEC)

Name: Fatima Amir

NUST Regn No: 00000320147

Department: SCME

Specialization: Chemical Engineering

Credit Hour Completed: (18) 24

CGPA: (3.45) 3.50

Course Work Completed

S/No	Code	Title	Core/Elective	CH	Grade
1	CHE-843	Separation Processes in Chemical Engineering	Core	3.0	B+
2	EME-921	Momentum, Heat & Mass Transfer	Core	3.0	B+
3	CHE-847	Chemical Kinetics and Reactor Design	Core	3.0	C+
4	ENE-809	Wastewater Treatment and Design	Elective	3.0	B+
5	CHE-814	Product Technology	Elective	3.0	A
6	CHE-823	Advanced Analytical Techniques	Elective	3.0	B+
7	RM-898	Research Methodology	Additional	2.0	Q
8	CHE-848	Consolidation Processes	Elective	3.0	A
9	ESE-911	Carbon capture & Utilization	Elective	3.0	B+

Date 06-10-2021

Student's Signature Fatima Amir

Thesis Committee

- Name: Dr Muhammad Bilal Khan Niazi (Supervisor)  
Department: Chemical Engineering, SCME, NUST
- Name: Dr Usman Liaqat (Co-Supervisor)  
Department: Material Engineering, SCME, NUST
- Name: Dr. Salik Javed Kakar  
Department: Healthcare Biotechnology, ASAB, NUST
- Name: Dr. Zakir Hussain  
Department: Material Engineering, SCME, NUST

Signature: [Signature]

Signature: [Signature]

Signature: [Signature]

Signature: [Signature]

DR. SALIK J. KAKAR  
Assistant Professor  
Applied Biosciences School of  
Applied Biosciences (ASAB)  
NUST-Islamabad

Date: 22/10/21

Signature of Head of Department: [Signature]

APPROVAL

Date: 25-10-2021

Dean/Principal [Signature]

Distribution

- 1x copy to Exam Branch, Main Office NUST
- 1x copy to PGPDte, Main Office NUST
- 1x copy to Exam branch, respective Institute

School of Chemical and Materials Engineering (SCME) Sector H-12, Islamabad



National University of Sciences & Technology (NUST)

FORM TH-4

MASTER'S THESIS WORK

We hereby recommend that the dissertation prepared under our supervision by

Regn No & Name: 00000329147 Fatima Amir

Title: Carbohydrate polymer-based nanocomposite hydrogel membrane for enhanced antimicrobial activity.


Presented on: 26 Oct 2023 at: 1430 hrs in SCME Seminar Hall

Be accepted in partial fulfillment of the requirements for the award of Master of Science degree in Chemical Engineering.


Members

Guidance & Examination Committee Members

Name: Dr Salik Javed Kakar

Signature: 

Name: Dr Zakir Hussain

Signature: 


Name: Dr Usman Liaqat (Co-Supervisor)

Signature: 

Supervisor's Name: Dr M. Bilal Khan Niazi

Signature: 

Dated: 31/10/2023

  
Head of Department

Date 1/11/23

  
Dean/Principal

Date 1.11.2023

School of Chemical & Materials Engineering (SCME)

# **Dedication**

This thesis is dedicated to my parents who had faith in me and prayed for me in my every decision. And to my brother my supporting pillar who always supported me and helped me continuously throughout my journey.

# Declaration

I, *Fatima Amir* declare that this thesis titled “Carbohydrate polymer-based nanocomposite hydrogel membrane for enhanced antimicrobial activity” and the work presented in it are my own and has been generated by me because of my own original research.

I confirm that:

1. This work was done wholly or mainly while in candidature for a Master of Science degree at NUST.
2. Where any part of this thesis has previously been submitted for a degree or any other qualification at NUST or any other institution, this has been clearly stated.
3. Where I have consulted the published work of others, this is always clearly attributed.
4. Where I have quoted from the work of others, the source is always given. With the exception of such quotations, this thesis is entirely my own work.
5. I have acknowledged all main sources of help.
6. Where the thesis is based on work done by myself jointly with others, I have made clear exactly what was done by others and what I have contributed myself.

Fatima Amir,  
Reg no: 329147

## Acknowledgement

I would like to express my gratitude and indebtedness to Almighty ALLAH for showering His blessing on me. This work would not be possible without His permission and help. All praise to Him.

I owe a deep debt of gratitude to my respected supervisor, **Dr. Muhammad Bilal Khan Niazi**, for choosing me as his student and believing in my abilities. His incessant direction, encouragement and support was the driving force behind the success of this project. Not only did Dr. Bilal Niazi, introduce me to this fascinating research field but also provide me with priceless advice and guidance during the research phase. It was an honor working under his esteemed supervision.

Furthermore, I would like to thank my co-supervisor **Dr. Usman Liaquat** for his vast knowledge and guidance that helped me lay base of this project without which I would have not been able to form a direction in my work.

I would also like to extend my deepest thankfulness to my GEC members, **Dr. Salik Javed Kakar** and **Dr. Zakir Hussain**.

Moreover, I would like to extend my gratitude to Dr. Sarah Farrukh and Dr. Tahir Baig for all the help and support in completing my work. I would also like to extend my gratitude to all my friends especially Ayesha Sultan for always providing me with emotional and spiritual support and encouraging me through difficult times. Moreover, I would also like to heartily thank Aqsa, Rabia, Hizbullah, Inamullah, Mashal, Zoraiz, Mahad and Arslan Maqbool for always being there to support and help me.

Lastly, I would like to thank my father, M. Amir; my mother, Fozia and my brothers Adrish and Husham Amir who stood by me throughout this journey and always supported me in my every decision. Their love and compassion have helped me to overcome many obstacles. Without their moral support, this thesis would have been much difficult. My heartiest thanks to everyone for this incredible experience.

**Fatima Amir**



## Abstract

Wound healing is an intricate and ever-evolving phenomenon that involves a series of biological processes and multiple stages. Despite the growing utilization of nanoparticles to enhance wound healing through antibacterial activity and cell proliferation, these approaches often overlook important properties such as mechanical stability, degradability, toxicity, and efficacy. Therefore, there is a need for a multifunctional dressing material that can promote optimum wound healing and possess multiple properties. In this study, a Chitosan-PVA membrane crosslinked with vanillin and reinforced with nano-cellulose and CuO-Ag nanoparticles was used for wound healing. Various characterization techniques, including FTIR, SEM, XRD, TGA, mechanical testing, surface roughness and contact angle measurement, were employed to study the morphology and structural properties of the membrane. In addition, biomedical tests such as moisture retention ability, water vapour transmission rate, gel fraction, porosity, swelling behaviour, biodegradability, antimicrobial study, cytotoxicity, and animal models were conducted to evaluate the membrane's performance as a wound healing material. The membrane displayed impressive mechanical strength, measuring as high as  $49.985 \pm 2.31$  MPa, and had a hydrophilic nature, with moisture retention values up to 98.84% and swelling percentages as high as 191.67%. It also demonstrated biodegradable properties and high cell viability of up to 94.63%. Additionally, the fabricated membranes exhibited excellent antimicrobial activity against both gram-positive and gram-negative bacteria, with maximum zone of inhibition measuring  $17 \pm 0.5$ mm and  $8 \pm 0.1$ mm, respectively. Moreover, the membranes were tested in an animal model and demonstrated superior wound healing properties with wound healing efficiency upto 70%. These results suggest that the fabricated membranes hold potential as an effective wound dressing material.

**Keywords:** Hydrogel Membrane, Polyvinyl Alcohol, Chitosan, Vanillin, Nanocellulose, Copper Oxide, Silver Nanoparticles, Wound Healing, Antibacterial Activity

# Table of Contents

<b>1 Introduction</b> .....	<b>1</b>
<b>2 Literature Review</b> .....	<b>5</b>
2.1 Skin .....	5
2.2 Wound and its classification .....	6
2.2.1 Wound Healing .....	7
2.2.2 Wound Dressing .....	9
2.2.3 Characteristic of Ideal Wound Dressing .....	10
2.3 Hydrogel Wound Dressing .....	11
2.3.1 Classification of Hydrogel .....	12
2.3.2 Hydrophilicity in Hydrogels .....	13
2.3.3 Synthesis Mechanism .....	14
2.3.4 Properties of Hydrogels .....	15
2.3.5 Applications of Hydrogel .....	17
2.4 Polymers for Hydrogels .....	18
2.4.1 Polyvinyl Alcohol (PVA) .....	18
2.4.2 PVA Blends .....	19
2.4.3 Chitosan .....	22
2.5 Nanocellulose .....	24
2.5.1 Nanocellulose Structure .....	24
2.5.2 Classification of Nanocellulose .....	25
2.5.3 Properties of Nanocellulose .....	26
2.6 Nanoparticle .....	26
2.6.1 Metallic Nanoparticle .....	27
2.6.2 Synthesis of NP .....	27
2.6.3 Nanoparticles as Antibacterial Agents .....	29
<b>3 Materials and Methods</b> .....	<b>31</b>
3.1 Materials .....	31
3.2 Synthesis of Nanocellulose .....	32
3.3 Fabrication of Membrane (PVA/Chitosan/ Vanillin/ NC) .....	32
3.4 Synthesis of CuO/Ag nanoparticles using wet chemical precipitation .....	33
3.5 Fabrication of Membrane (PVA/Chitosan/Vanillin/NC/CuO-Ag NPs) .....	34
3.6 Characterization Techniques .....	36
3.6.1 X-ray Diffraction Analysis (XRD) .....	37
3.6.2 Scanning Electron Microscopy (SEM) .....	38
3.6.3 Fourier Transform Infra-Red Spectroscopy (FTIR) .....	41
3.6.4 Mechanical Testing .....	42
3.6.5 Thermogravimetric Analysis (TGA) .....	44
3.6.6 Drop Shape Analyzer .....	45
3.6.7 Surface Roughness Measurement .....	46

3.6.8	Moisture Retention Capability (MRC) .....	47
3.6.9	Water Vapour Transmission Rate (WVTR).....	47
3.6.10	Gel Fraction.....	47
3.6.11	Porosity .....	48
3.6.12	Swelling Behaviour .....	48
3.6.13	Biodegradability .....	49
3.6.14	Cytotoxicity Assay .....	49
3.6.15	Antibacterial Activity.....	49
3.7	In-Vivo Wound Healing Experiment .....	50
3.7.1	Experimental Protocol.....	50
3.7.2	Full Thickness Wound Excision .....	50
3.7.3	Pro-Healing Parameters .....	50
<b>4</b>	<b>Results and Discussions .....</b>	<b>51</b>
4.1	X-Ray Diffraction Analysis (XRD).....	51
4.1.1	Nanocellulose and NC incorporated membranes.....	51
4.1.2	CuO-Ag NPs and NPs incorporated membranes .....	52
4.2	Fourier Transform Infrared Spectroscopy (FTIR).....	53
4.2.1	Nanocellulose and their incorporated membranes .....	53
4.2.2	CuO-Ag NPs and their incorporated membranes .....	54
4.3	Scanning Electron Microscopy (SEM).....	55
4.3.1	Nanocellulose incorporated membranes .....	55
4.3.2	CuO-Ag NPs and their incorporated membranes .....	57
4.4	Mechanical Properties .....	59
4.4.1	Nanocellulose incorporated membranes .....	59
4.4.2	CuO-Ag incorporated membranes .....	60
4.5	Thermogravimetric Analysis (TGA) .....	61
4.5.1	Nanocellulose incorporated membranes .....	61
4.5.2	CuO-Ag incorporated membranes .....	63
4.6	Surface Roughness .....	65
4.6.1	Nanocellulose incorporated membranes .....	65
4.6.2	CuO-Ag incorporated membranes .....	66
4.7	Contact Angle Measurement .....	67
4.7.1	Nanocellulose incorporated membranes .....	67
4.7.2	CuO-Ag incorporated membranes .....	68
4.8	Moisture Retention Capability.....	70
4.8.1	Nanocellulose incorporated membranes .....	70
4.8.2	CuO-Ag incorporated membranes .....	71
4.9	Water Vapor Transmission Rate (WVTR) .....	72
4.9.1	Nanocellulose incorporated membranes .....	72
4.9.2	CuO-Ag incorporated membranes .....	73
4.10	Gel Fraction .....	74

4.10.1 Nanocellulose incorporated membranes .....	74
4.10.2 CuO-Ag incorporated membranes .....	74
4.11 Porosity .....	75
4.11.1 Nanocellulose incorporated membranes .....	75
4.11.2 CuO-Ag incorporated membranes .....	76
4.12 Swelling Ability .....	77
4.12.1 Nanocellulose incorporated membranes .....	77
4.12.2 CuO-Ag incorporated membranes .....	78
4.13 Biodegradability .....	79
4.13.1 Nanocellulose incorporated membranes .....	79
4.13.2 CuO-Ag incorporated membranes .....	80
4.14 Cell-based Cytotoxicity Assay .....	81
4.15 Antibacterial Activity Measurement .....	82
4.16 In-vivo Wound Healing Experiment .....	83
<b>Conclusion.....</b>	<b>86</b>
<b>Future Recommendations.....</b>	<b>88</b>
<b>Reference.....</b>	<b>89</b>

# List of Figures

Figure 1: Schematic Illustration of Skin.....	5
Figure 2: Classification of Wound.....	6
Figure 3: Stages of Wound Healing for Skin.....	7
Figure 4: Different types of Wound Dressing.....	9
Figure 5: Types of Hydrogels.....	13
Figure 6: Synthesis of Hydrogel through Polymerization of monomer.....	14
Figure 7: Synthesis of Hydrogel through Cross-linking of water-soluble polymer.....	14
Figure 8: Applications of Hydrogel Membranes.....	17
Figure 9: Classification of Hydrogel based on the nature of polymer.....	18
Figure 10: Chemical structure of PVA.....	19
Figure 11: Chemical Structure of Chitosan.....	22
Figure 12-1: Single Cellulose Chain Repeat Unit.....	25
Figure 12-2: Cellulose microfibril having structure of the crystalline and amorphous region.....	25
Figure 13: Different methods for nanoparticle synthesis.....	29
Figure 14: Synthesis of nanocellulose from microcrystalline cellulose through ultrasonication probe.....	32
Figure 15: Fabrication of PVA/Chitosan/Vanillin/NC membranes.....	33
Figure 16: Synthesis of CuO/Ag nanoparticles using wet chemical precipitation method.....	34
Figure 17: Fabrication of PVA/Chitosan/Vanillin/NC/CuO-Ag NP membranes.....	34
Figure 18: XRD Analyzer by STOE-Germany.....	37
Figure 19: Scanning Electron Microscope (JSM-64900) combined with an EDX spectrometer.....	39
Figure 20: The working mechanism and components of SEM.....	40
Figure 21: ATR-FTIR Analyzer by BRUKER.....	41
Figure 22: The components and working mechanism of FTIR.....	42
Figure 23: Universal Testing Machine (AG-20RRKNXD Plus) by Shimadzu Corporation.....	43
Figure 24: SDT 650-TA analyzer for thermogravimetric analysis.....	44
Figure 25: The components and working mechanism of TGA.....	45

Figure 26: DSA25 KRUSS Drop Shape Analyzer.....	46
Figure 27: Compact Optical Profilometer (NANOVEA PS50).....	46
Figure 28: XRD Analysis of (a)Nanocellulose and (b)hydrogel membranes with varying NC compositions.....	52
Figure 29: FTIR Spectrum of a) NC and b) hydrogel membranes with varying NC compositions.....	54
Figure 30: FTIR spectra of (a) CuO-Ag nanoparticles and (b) composite membranes, as well as XRD patterns of (c) CuO-Ag nanoparticles and (d) composite membranes.....	55
Figure 31: SEM images of surface and cross section of a) CVN0, b) CVN12, c) CVN16.....	56
Figure 32: Copper oxide and silver nanoparticle blend a) SEM image b) EDX.....	57
Figure 33: SEM images and EDX analysis of CVN12, CNP0.5, CNP1, CNP1.5, and CNP2 membranes. (a-e) SEM images showcasing the surface morphologies and nanoparticle distributions of the membranes respectively. (f-j) EDX analysis displaying the elemental composition and distribution across the membrane surface respectively.....	58
Figure 34: Mechanical properties of hydrogel membranes with varying NC compositions ..	60
Figure 35: Mechanical properties of hydrogel membranes with varying CuO-Ag NP composition.....	61
Figure 36: Thermal degradation (TGA) study of hydrogel membranes with varying NC composition.....	63
Figure 37: Thermal degradation (TGA) study of hydrogel membranes with varying CuO-Ag NPs concentration.....	65
Figure 38: Surface roughness of hydrogel membranes with varying NC compositions	66
Figure 39: Surface roughness of hydrogel membranes with varying CuO-Ag NP concentration.....	67
Figure 40: Contact angle measurement of hydrogel membranes with varying NC compositions.....	68
Figure 41: Contact angle measurement of hydrogel membranes with varying CuO-Ag NP concentration.....	69
Figure 42: Moisture retention capability of hydrogel membranes with varying NC compositions.....	70

Figure 43: Moisture retention capability of hydrogel membranes with varying CuO-Ag NP concentration.....	71
Figure44: a) Positive and negative controls b) WVTR of hydrogel membranes with varying NC composition.....	72
Figure 45: a) Positive and negative controls b) WVTR of hydrogel membranes with varying CuO-Ag NP concentration.....	73
Figure 46: Gel Fraction of hydrogel membranes with varying NC concentration.....	74
Figure 47: Gel Fraction of hydrogel membranes with varying CuO-Ag concentration.....	75
Figure 48: Porosity of hydrogel membranes with varying NC concentration.....	76
Figure 49: Porosity of hydrogel membranes with varying CuO-Ag concentration.....	77
Figure 50: Swelling behaviour of hydrogel membranes with varying NC concentration a) with deionized water b) phosphate buffer solution.....	78
Figure 51: Swelling behaviour of hydrogel membranes with varying CuO-Ag NP concentration a) with deionized water b) phosphate buffer solution.....	79
Figure 52: Biodegradability of hydrogel membranes with varying NC concentration.....	80
Figure 53: Biodegradability of hydrogel membranes with varying CuO-Ag concentration.....	81
Figure 54: Depiction of cytotoxicity evaluation of fabricated membranes through cell viability assay.....	82
Figure 55: Photograph showing the zone of inhibition formed around PVA-Chitosan hydrogel membranes against E. coli.and S. aureus (a,b,c,d) and e) graphical representation of antibacterial activity.....	83

Figure 56: Photographic representation of burn wounds induced in the animal model a)  
Photographic results b) Graphical representation of wound healing  
efficiency.....85



## **List of Tables**

Table 1: Characteristics of Ideal Wound Dressing .....	10
Table 2: The detailed description for fabrication of PVA/Chitosan/Vanillin/Nanocellulose and CuO-Ag nanocomposite membrane .....	35
Table 3: Characterization Techniques carried out for the nanocomposite membranes .....	36

## List of Abbreviations

Ag	Silver
CaCl <sub>2</sub>	Calcium Chloride
Ch	Chitosan
CuO	Copper Oxide
DNA	Deoxyribonucleic acid
ECM	Extracellular Matrix
FTIR	Fourier Transform Infrared Spectroscopy
LPS	Lipopolysaccharides
NaOH	Sodium Hydroxide
NaBH <sub>4</sub>	Sodium Borohydride
NP	Nanoparticles
NC	Nanocellulose
PVA	Polyvinyl Alcohol
TGA	Thermogravimetric Analysis
SEM	Scanning Electron Microscope
V	Vanillin
WVTR	Water Vapour Transmission Rate
XRD	X-ray Diffraction

# Chapter 1:

## Introduction

Chronic wounds arising from bacterial infection have emerged as a prominent medical predicament [1], as bacteria possess the ability to impede the immune system and subsequently infiltrate viable tissue [2]. This phenomenon is particularly noteworthy in cases of *Staphylococcus aureus*-related skin wound infections, which typically result in severe tissue impairment[3]. Conversely, while irritation assumes an essential part in the injury healing process, delayed irritation can incite tissue crumbling and thwart the convenient progression of wound healing. Therefore, there is an urgent need for wound dressings that possess antibacterial and anti-inflammatory properties.

With its pivotal functions in diverse physiological mechanisms, the skin serves as a vital organ system and acts as the principal barrier against harmful microorganisms and external stressors. The skin, being the most external and vulnerable organ, is prone to various forms of disturbances, such as ulceration, trauma, injuries, burns, and inflammation, which are commonly known as cutaneous wounds[4]. Hemostasis, inflammation, proliferation, and remodeling are the main phases involved in the healing of the skin. These stages are regulated by a multitude of cellular and molecular mechanisms, including growth factors, extracellular matrix constituents, and immune cells. As individuals undergo the natural process of aging, the presence of underlying medical conditions, as well as the utilization of unsuitable treatment modalities, have the potential to interfere with this intricate process. Consequently, such disruptions can result in compromised wound healing and heightened vulnerability to infections[5]. Bacterial infiltration into wounds presents a notable concern within the medical field due to its potential to intensify inflammation, impair wound healing processes, and heighten the likelihood of systemic infection, ultimately resulting in substantial morbidity and mortality. Hence, imperativeness of developing efficient wound dressings that can attenuate colonization of bacteria and facilitate healing of injuries holds utmost significance in achieving ideal patient outcomes.

The procedure of healing and management has posed a recurring challenge within the global healthcare system, especially in instances where wounds become infected by pathogens,

thereby leading to prolonged and persistent chronic conditions. The presence of bacteria at the site of a wound has the potential to undergo rapid proliferation, colonization, and subsequently inflict harm upon the integrity of the skin, resulting in the onset of pronounced systemic symptoms[6].

In medical science, many dressings have been used to obstruct the multiplication of microscopic organisms and improve the course of wound healing. However, it has been observed that conventional dressings which utilize inorganic antibacterial agents can potentially induce toxic effects while also contributing to the development of microbial drug resistance[7]. Furthermore, it should be noted that most of monetarily accessible dressings are explicitly intended for a particular reason, rendering them vulnerable to complications originating from the microenvironment present at the site of the wound. As a result, it is imperative to create and execute innovative dressing materials that can efficiently address wounds, eradicate microbial infections, reinstate the necessary growth factors in the surrounding environment, and accelerate the healing process in instances of bacterial infection.

The long-term management and treatment of chronic wounds, particularly those afflicted with bacterial pathogens, have remained a consistently challenging concern within the broader framework of the global healthcare system[8]. Traditional wound dressings, such as foams, sponges, and gauze, have been designed with the intention of facilitating wound healing. Nevertheless, these conventional materials frequently fall short in terms of delivering an ideal fit and sufficient protection, consequently resulting in an environment that lacks freedom from bacteria[9]. Therefore, it is imperative to prioritize the advancement of wound dressings capable of complete conformity to the wound site and endurance of mechanical stress, while simultaneously acting against microbial infections and promoting an optimal environment for the healing process.

Hydrogels definitely stand out in the course of wound healing research, owing to their notable ability to effectively absorb tissue exudates while facilitating oxygen permeability. These materials have characteristic feature to create a favorable moist environment that facilitates the growth and division of cells, as well as chemically adhering to the skin surface and promoting the process of blood clotting by interrupting the actions of naturally occurring tissue proteins[10]. Hydrogels possess the capacity to decrease skin temperature and restrict blood vessel dilation, consequently mitigating pain levels. In addition, hydrogels have

demonstrated significant potential as effective vehicles for drug delivery and growth factor transport, including nanoparticles, for the purpose of addressing infections and facilitating wound healing[11].

Various biocompatible polymers, such as sodium alginate, hyaluronic acid, gelatin, and chitosan, have been employed to create hydrogels for applications in healing of wound [12]. Considerable research has been done to explore the utilization of chitosan as a remarkably suitable polymer for the synthesis of hydrogels and for promoting wound healing owing to its hemostatic, mucoadhesive, and antibacterial characteristics. Chitosan demonstrates structural attributes that bear resemblance to glycosaminoglycans (GAGs), constituents of the extracellular matrix[13]. The inherent characteristics of chitosan render it an appropriate substance for employment in tissue engineering endeavors. Polyvinyl alcohol (PVA), derived through the hydrolysis of vinyl acetate, is recognized as a biocompatible, biodegradable, and non-toxic polymer, making it highly valued in various medical contexts owing to its room temperature chemical stability and remarkable elasticity[14]. The hybrid nanofibrous hydrogels, composed of a blend of natural and manufactured polymers, show a synergistic impact by integrating the profitable properties of both biopolymers. These biomaterials, specifically chitosan and PVA, exhibit bioactivity and biocompatibility akin to natural compounds, while also possessing the strength and durability characteristic of synthetic biopolymers[15]. To expand the injury recuperating properties of chitosan and work with the crosslinking among chitosan and PVA, the utilization of vanillin, a compound derived from vanilla beans, as an active cross-linker has been employed due to its possession of aldehyde and hydroxyl functional groups[16].

The mechanical fragility of traditional hydrogels, specifically those derived from biological sources, remains a recurring concern despite their extensive use in dressing applications. In order to tackle this issue, scholars are integrating synthetic and natural polymers, including nanocellulose - an inherently sourced organic filler possessing advantageous features such as low density, biodegradability, biocompatibility, and renewability. Through this combination, the objective is to amplify the strength of bio-based hydrogels[17]. Moreover, the incorporation of nanomaterials, such as silver nanoparticles, into hydrogels has been investigated in order to augment their antibacterial efficacy and improve their physical and chemical attributes. Combining silver nanoparticles with inorganic antibacterial materials has been proposed as a means to enhance their antibacterial efficacy in a cost-effective manner,

given the high cost of silver nanoparticles[18]. Recently, CuO-Ag nanoparticles have been utilized in light of their stability with mammalian cells, heightened environmental friendliness, and reduced toxicity[19].

In summary, the process of wound healing is intricate, encompassing numerous factors, and necessitates a multifaceted approach. The objective of this research endeavor was to confront the aforementioned dilemma through the creation of an innovative chitosan-PVA hydrogel fortified with nanocellulose and CuO-Ag nanoparticles. Through the application of these constituents, a multifaceted hydrogel compound was generated, possessing the capacity to proficiently regulate the discharge of enclosed nanoparticles, furnish a propitious microenvironment for the process of wound healing, and bestow mechanical fortitude onto the injured area. Furthermore, the hydrogel exhibited potent antimicrobial properties against pathogenic microorganisms frequently associated with wound infections. This study elucidates the considerable prospects of employing sophisticated materials in the progression of wound dressings capable of expediting the healing procedure.

## Chapter 2:

### Literature Review

#### 2.1. Skin

The skin, which constitutes the biggest organ within the human body, encompasses an area of approximately 1.856 square meters[20]. The skin serves a dual function by not solely providing protection against microbial invasion, but also playing part in the regulation of our body's temperature[21]. The skin possesses incredible strength and flexibility due to its layered structure. The skin of human beings possesses incredible regenerative abilities that function as a strong shield, controlling the entry of pollutants from the environment and inhibiting excessive moisture loss. Furthermore, it plays a vital function in sustaining the body's temperature and protecting against harmful microorganisms. The mentioned entity serves as a protection against physical forces, alterations in the surroundings, and microscopic organisms. Additionally, it maintains influence over different bodily functions such as temperature regulation, changes in blood flow to the extremities, and the balance of fluids by means of sweating. The entity stated before functions as a depot for generating Vitamin D. Nevertheless, each time a wound appears, the disruption of the barricade's purpose leads to an elevated risk of infection.

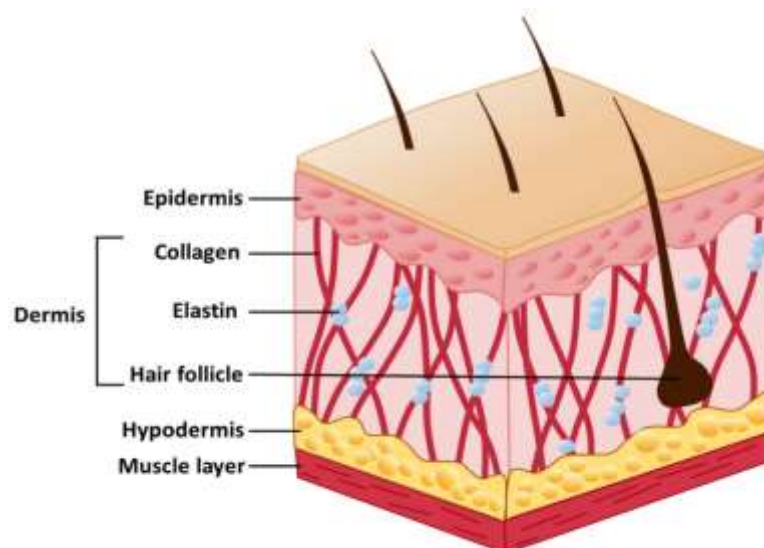


*Figure 1: Schematic Illustration of Skin*

The skin's functionality and anatomical structure result in distinct attributes for each layer. The integumentary system comprises three discrete layers, specifically the hypodermis, epidermis, and dermis. The epidermis, outermost layer of the skin, exhibits a robust and resilient characteristic, primarily fulfilling the crucial function of providing protection for the underlying structures. The cellular architecture of this organism confers a remarkably efficient defense mechanism against microbial invasion. The epidermis possesses a unique characteristic that distinguishes it from other bodily cells, namely its capacity for self-reproduction. In the event of bodily injury, the afflicted cells undergo a process of healing and subsequently give way to the replenishment of new cells. The underlying layer of tissue adjacent to the epidermis is known as the dermis. Consisting of hair follicles, lymphatic vessels, and sweat glands, dermis plays a crucial role in regulating body temperature and producing sebum to help preserve skin moisture. The substance imparts both tensile strength and resilience to the integumentary system. The underlying stratum below the dermis is referred to as the hypodermis, which serves the purpose of connecting the skin to the surrounding tissues of bones and muscles[22]. The demarcation point between the dermis and hypodermis remains indiscernible.

## 2.2. Wound and its Classification

A wound can be described as an imperfection or rupture in the outer covering of the body, known as the skin, resulting from either traumatic incidents or systemic impairments. Wound classification involves differentiating wounds according to the extent of injury suffered by the skin layers and the specific area of the dermis affected. The classifications mentioned cover superficial wounds that only affect the outermost layer of skin, partial thickness wounds that extend beyond the epidermis, and full thickness wounds that damage the underlying tissues and subcutaneous layers. Wounds are further categorized into subgroups;

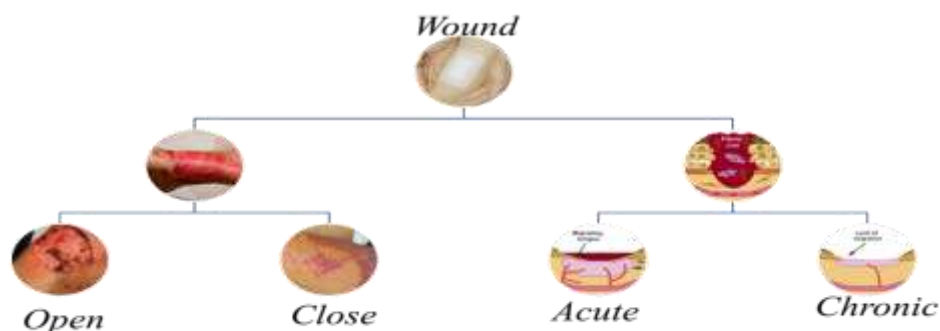


Figure 2: Classification of Wound



Acute wounds possess a characteristic healing trajectory that adheres to the conventional wound healing process, culminating in resolution typically occurring within a span of approximately 4-12 weeks. These injuries can stem from various mechanisms, including abrasion, incision, cuts caused by sharp objects, or the tearing of tissues as a result of powerful impacts. Chronic wounds originate from acute wounds but transition into a state of chronicity due to failure in adhering to the normal healing process, consequently leading to an extended recuperation phase lasting anywhere from months to years[23]. These manifestations, which arise from thermal burns, chronic ulcers, or incised wounds, among other causative factors, emerge as a consequence. Chronic wounds often result in enduring dermal markings and may necessitate an extended healing duration, spanning several months or even years. This protracted healing process necessitates the frequent substitution of dressings, thereby imparting a financial burden on patients and extending their hospitalization periods.

### 2.2.1. Wound Healing

The incredible regenerative capabilities of the human skin play a vital role in safeguarding against external substances and maintaining the proper transpiration of the epidermis. The intricate phenomenon within the human body that warrants particular attention is the process of wound repairing[24]. The wound healing process comprises a succession of concurrent stages including hemostasis, inflammation, tissue proliferation, and tissue remodeling.

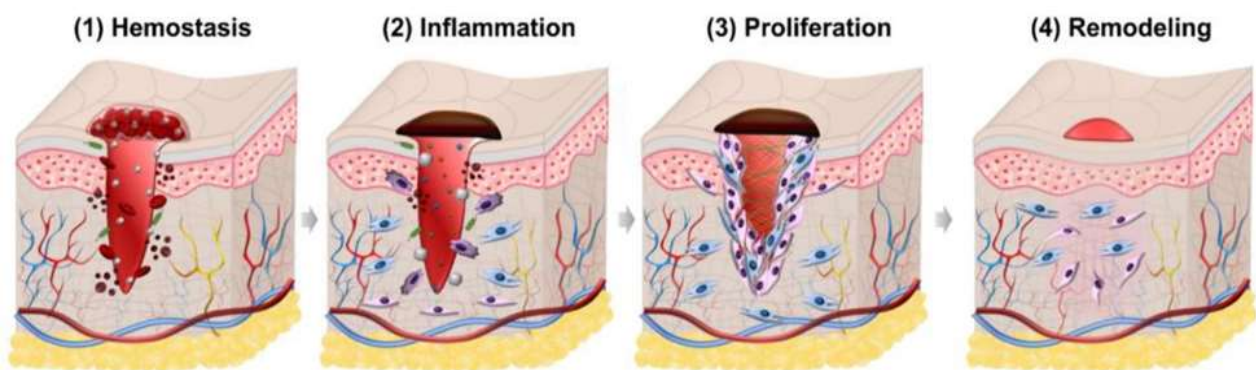


*Figure 3: Stages of Wound Healing for Skin*

Tissue restructuring following injury is a dynamic process characterized by intricate cell and extracellular matrix (ECM) interactions, along with the influence of growth factors[24]. The essential mechanisms for achieving complete wound healing and epithelialization involve the multiplication of fibroblasts and the movement of keratinocytes [25]. Following a cutaneous

injury, the activation of tissue factors and collagen initiates platelet aggregation, subsequently leading to the release of chemokine and growth factors which serve to orchestrate clot formation. The initial phase, denominated as hemostasis, represents the onset of the process under examination. The aforementioned phenomenon denotes the innate and principal reaction exhibited by the human body in response to an inflicted injury or trauma. The blood flow is decelerated, instigating the commencement of clot formation in order to avert hemorrhaging. At the subsequent phase, blood transitions from a liquid state to a gelatinous fluid. Neutrophils serve as vital contributors in establishing a favorable milieu for wound healing, being the initial cells to actively respond at the wound site. One of their primary functions is the removal of bacterial pathogens and extraneous cellular material from wound sites. In the subsequent phase, macrophages accumulate and facilitate the process of phagocytosis of damaged tissues. The successful completion of the inflammatory phase is achieved using this approach. Both of these stages require a time span of 72 hours to reach completion. The blood vessels undergo dilation, thereby facilitating the transportation of essential nutrients, antibodies, and leukocytes to the site of injury. This aids in mitigating the risk of infection. In this stage, patients encounter physiological manifestations such as edema, erythema, or nociception. The subsequent stage, known as proliferation, is distinguished by the accumulation of a substantial quantity of cells and connective tissues. The commencement of granulation tissue formation can be observed. These recently developed tissues comprise a composite blend of collagen and extracellular matrix (ECM), resulting in the formation of an intricate vascular network, thereby serving as a substitute for damaged blood vessels. Several strains of cytokines, growth factors, and the extracellular matrix are involved in this phase. The duration of this phase extends over a time span of several days to possibly weeks. The final stage of the process involves remodeling, which requires a meticulous equilibrium between pre-existing and newly generated cells. During this phase, the recently developed tissues undergo maturation. Skin tissues undergo a process of refurbishment in order to enhance their tensile strength. Ultimately, the non-functional fibroblasts are replaced by their functional counterparts.

### 2.2.2. Wound Dressing

Wound dressings are employed for the purpose of managing wounds. Wound dressings can be categorized based on their level of wettability as:

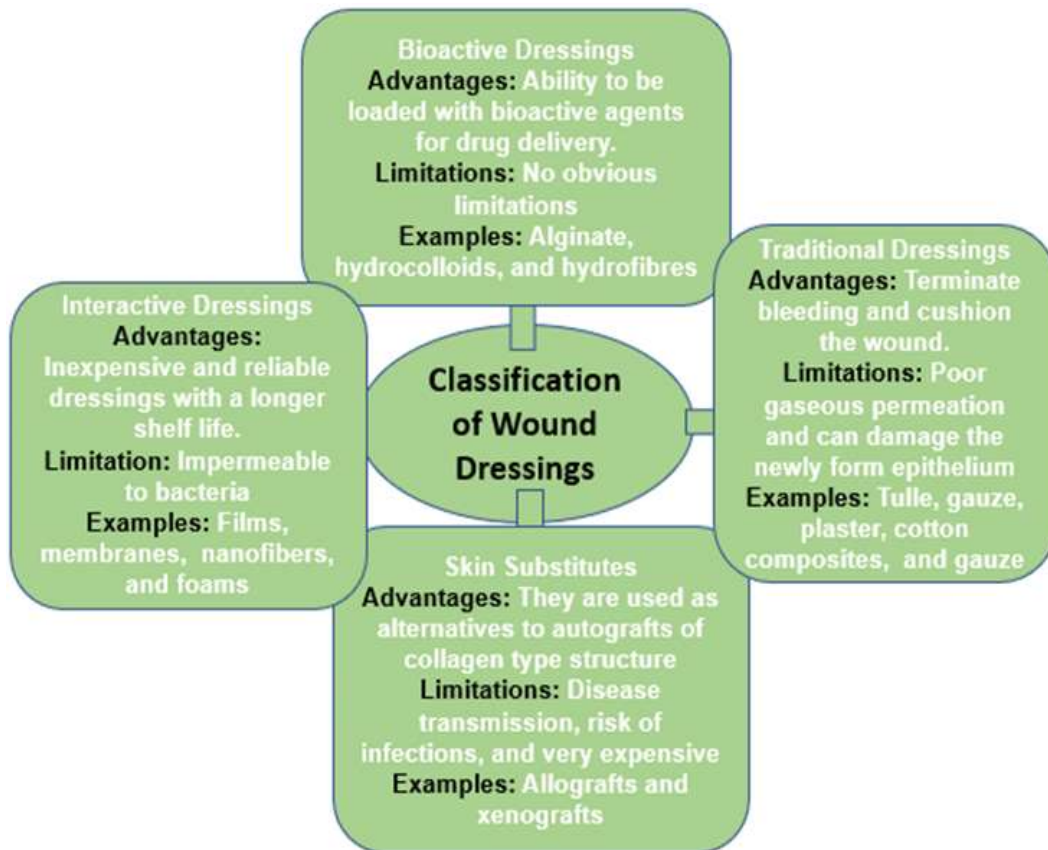


Figure 4: Different Types of Wound Dressings[26]

Up until the 1970s, cotton gauze or rayon blend dressings were widely considered to be dry dressings and were commonly utilized in the facilitation of wound healing[27]. In earlier perceptions, the phenomenon of wound healing was believed to be expedient and methodical when left uncovered and desiccated. Subsequent to the research conducted by Winter[24], it became evident that desiccated dressings are insufficient in creating the crucial environment required for the management of chronic wound conditions.

### 2.2.3. Characteristics of Ideal Wound Dressing

*Table 1: Characteristics of Ideal Wound Dressing*

<b>Feature</b>	<b>Description</b>
<b>Non-toxicity</b>	Exposure to toxic substances, regardless of the quantity, can result in adverse outcomes.
<b>Bacterial infection prevention</b>	Bacterial infections not only extend the time of the healing process, but also impede the occurrence of healing. Therefore, it is imperative to inhibit the occurrence of bacterial infection.
<b>Adhesiveness</b>	An excess of adhesive may result in sustained injury, it is imperative to provide an optimal level of adhesion healing process.
<b>Moisture</b>	Cell proliferation is enhanced in environments characterized by moisture, thereby establishing the necessity of moist wounds for the process of wound healing.
<b>Thermal insulation</b>	Thermal insulation offers an optimal temperature to the wounded surface, thereby promoting expedited recovery and mitigating pain sensation.
<b>Exudate adsorption</b>	In order to effectively control the exudate volume within a wound, it is imperative that dressing materials possess superior adsorption capabilities.
<b>Oxygen permeation</b>	The activity of cells is augmented by the presence of oxygen, necessitating use of wound dressings that allow for breathability. This allows for the diffusion of oxygen, thereby contributing to the healing process.
<b>Cost effective</b>	Cost plays a significant role among various attributes. In the context of medical care, wound dressings that are reasonably priced tend to be prioritized over those that are expensive.
<b>Easy availability</b>	Ensuring widespread availability of wound dressings across healthcare facilities and to patients constitutes a crucial element.
<b>Physical and Mechanical properties</b>	Mechanically wound dressings are required to exhibit a sufficient level of strength that closely approximates the structural integrity of the natural skin.

Chitosan has been extensively utilized for wound dressing purposes owing to its favorable characteristics that are well-suited for wound dressings, such as biocompatibility, immunostimulatory effects, and comparatively low toxicity.

Considering the aforementioned attributes, chitosan is deemed highly compatible with the task of wound healing, effectively exerting affirmative impacts on wounded regions. Several research studies have demonstrated the cytocompatibility of chitosan, yet its natural origin renders it susceptible to the presence of organic and inorganic contaminants and impurities.

### **2.3. Hydrogel Wound Dressing**

The initial creation of a synthetic hydrogel was undertaken by Wichterle and Lim in 1960[28]. A hydrogel refers to a tridimensional lattice composed of hydrophilic polymers that undergo cross-linking, either chemically or physically, resulting in the formation of a resilient framework. These substances exhibit hydrophilic properties and possess the capacity to undergo swelling or deswelling in response to changes in physical or chemical circumstances.

The capacity of these substances to increase in volume is significantly greater than their weight; however, they exhibit resistance to being dissolved in water, saline solutions, and various biological fluids, which is contingent upon the extent of crosslinking. Some possible approaches to cross-link water-soluble polymers involve the utilization of either natural or synthetic polymers by:[29]

1. Linking of polymer chains by chemical reaction
2. Ionic radiations
3. Physical interactions (electrostatics, entanglements, crystallite formation)

Hydrogels are a pragmatic, biocompatible and enduring platform for facilitating drug delivery, encompassing a diverse array of small molecules like non-steroidal anti-inflammatory drugs, in addition to larger entities like peptides, including proteins. The aforementioned attributes, namely surface functionality, biodegradability, bio recognition, and environmental friendliness, have rendered them of significant significance. The physical conditions encompass a range of factors, including temperature, pressure, electric or magnetic fields, light, sound, and pressure. On the other hand, the chemical conditions encompass various parameters such as the nature of the solvent, pH level, ionic strength, and the

molecular species involved[30]. These hydrogels exhibit environmental sensitivity and exhibit a stimulus-dependent release of therapeutic substances. These factors are of notable importance due to the fact that the internal environment within the human body is characterized by high temperatures and low pH levels[31]. All of these properties can be leveraged to optimize the drug release rate. Polymers exhibiting pH responsiveness often incorporate ionizable groups that possess the ability to either accept or donate protons in response to variations in the surrounding external conditions. Commonly observed polymers in scientific research include poly(acrylamide), poly (methacrylic acid), and poly (acrylic acid)[32].

### **2.3.1. Classification of Hydrogels**

There is currently no standardized methodology for the classification of hydrogels. However, hydrogels can be categorized based on variations in certain properties as:

#### **On the basis of degradation**

Hydrogels can be classified as:

1. Physical or reversible gels
2. Chemical or permanent gels

##### *2.3.1.1. Physical gels:*

In these types of hydrogels, the network is formed by secondary forces like ionic or hydrogen bonding. They are often reversible and can dissolve when change in environmental conditions like pH, ionic strength or temperature is experienced.

##### *2.3.1.2. Chemical gels:*

Here the molecular chains are joined together by covalent bonding through cross linking of polymer chains either in dry state or in the form of solution. Depending on the nature of functional groups they may be charged or uncharged.

They are prepared by:

- a) Three-dimensional polymerization
- b) Direct cross linking of water-soluble polymers

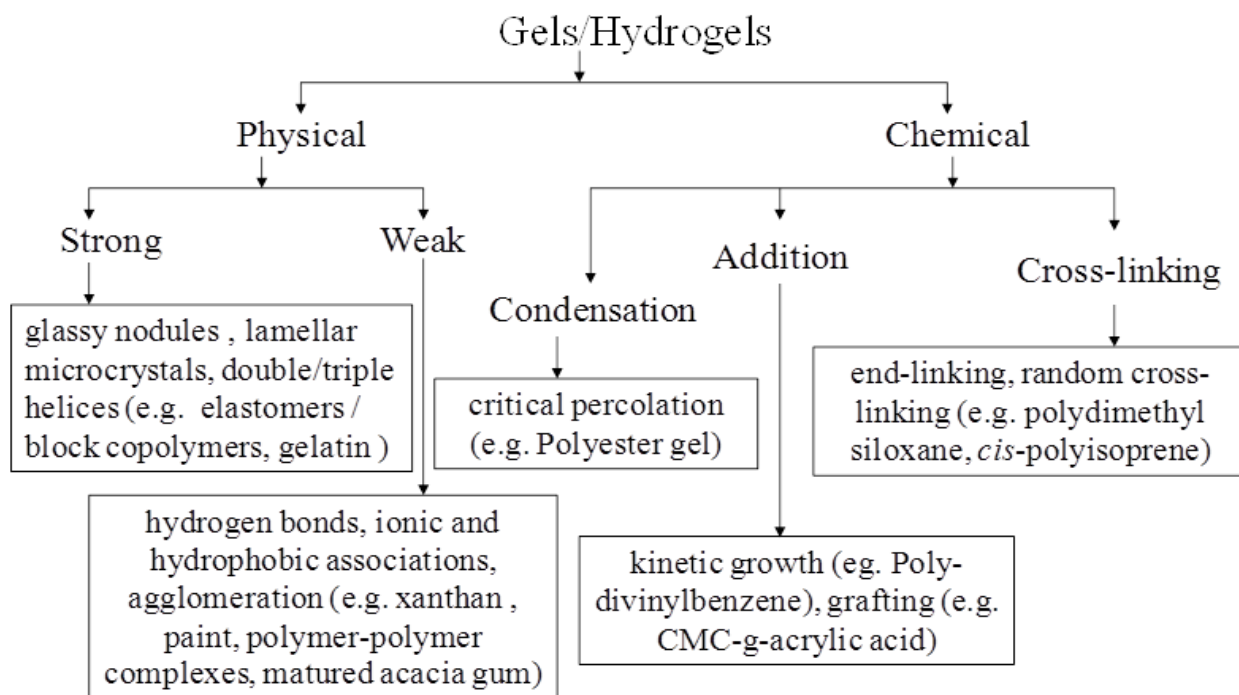


Figure 5: Types of Hydrogels

### 2.3.2. Hydrophilicity in Hydrogels

The inclusion of water within hydrogel structures assumes a pivotal function in the facilitation of nutrient and cellular product transportation. The onset of the absorption process prompts the initial interaction of incoming molecules with groups exhibiting the highest levels of hydrophilicity and polarity. The aforementioned process is commonly referred to as "primary attached water" in academic discourse. Upon completion of the hydration process within polar networks, the hydrogels exhibit an initial stage of swelling. The formation of hydrophobic bonds occurs after an increase in volume, resulting from the exposure of hydrophobic networks, and is commonly referred to as "secondary attached water". The total bond water is comprised of both primary and secondary attached water forms. The hydrogel exhibits the ability to uptake excess water, a phenomenon attributed to osmotic pressure, following the full hydration of its polar and non-polar constituents[33]. The phenomenon of revocation force that counteracts the occurrence of further swelling induces an inherent elasticity within the network. The hydrogel attains the maximum swelling point using this approach. When the polar, non-polar, and ionic groups within the network become fully saturated, the remaining voids are then occupied by unbound water molecules. The dissolution and dissociation of the polymer occur as water is absorbed, with the extent of this

process primarily contingent upon the characteristics and makeup of the polymers under consideration.

### 2.3.3. Synthesis Mechanism

The synthesis of polymeric hydrogels can be achieved through one of two established methods, namely the polymerization of hydrophilic monomers or the modification through cross-linkage of existing polymers. Figure 6 depicts the process of monomer polymerization and the subsequent synthesis of the hydrogel. The formation of hydrogel through the interlinking of water-soluble polymers is illustrated in Figure 7. In both instances, covalent bonding assumes a crucial function in facilitating the interconnection of molecular chains via cross-linking of polymer chains. The achievement of polymer transformation can be approached through the utilization of either a solution or dry state method, the choice of which depends on the inherent characteristics of the polymer[29, 34].

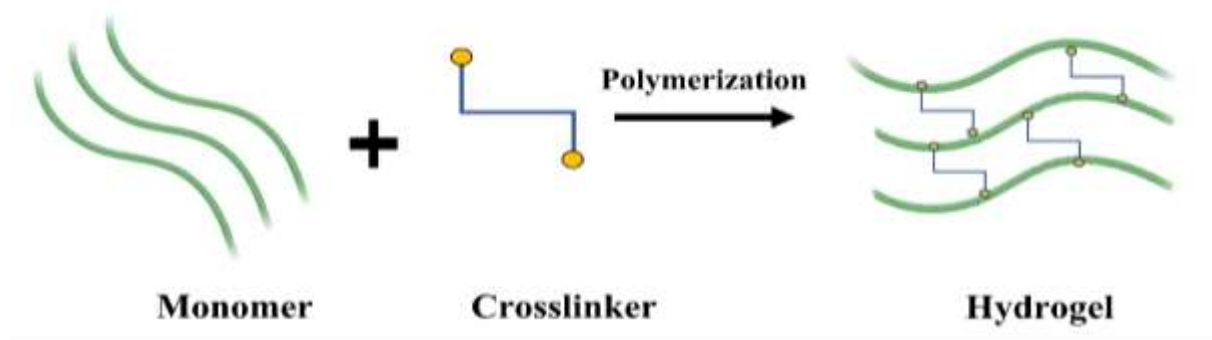


Figure 6: Synthesis of Hydrogel through Polymerization of monomer

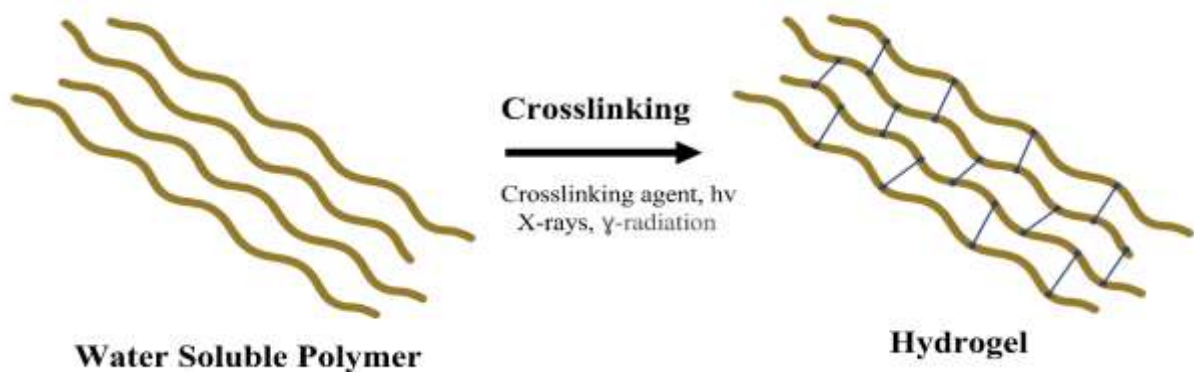


Figure 7: Synthesis of Hydrogel through Cross-linking of water-soluble polymer



### **2.3.4. Properties of Hydrogel**

When developing hydrogels for medical applications, the inclusion of hydrophilic pendant groups within natural or synthetic polymers presents several benefits. These groups can enhance the water absorption capacity of the hydrogels, facilitating improved interactions with epithelial tissues and mucous membranes. In their fully hydrated state, hydrogels commonly display qualities associated with viscoelastic behavior, softness, lubricity, and reduced interfacial angle when in contact with biological fluids. These properties are pivotal in minimizing the probability of an unfavorable immune reaction. The aggregate presence of these factors serves to collectively contribute to the biocompatibility of hydrogels. The degree of degradation in hydrogels is typically variable and dependent on the specific crosslinker used[35].

#### *2.3.4.1. Swelling Behavior*

Hydrogels possess a pronounced swelling characteristic that holds considerable importance in their overall existence. The phenomenon of hydrogel swelling occurs through a sequential process consisting of three distinct stages. First, the ingress of water into the hydrogel matrix ensues, which is referred to as primary bound water and involves water molecules diffusing into the network. Subsequently, the relaxation of the polymer chains takes place, resulting in further water uptake known as secondary bound water. Ultimately, the hydrogel framework exhibits expansion when it undergoes infiltration of supplementary water, denoted as free water. The Flory-Reihner theory postulates a profound association between the swelling phenomenon and the elastic characteristics of polymer chains, specifically in relation to their capability to interact harmoniously with water molecules[36].

#### *2.3.4.2. Response to External Stimuli*

Hydrogels demonstrate a wide range of reactions to changes in their surroundings, which can primarily be categorized as both physical stimuli. There are three types of stimuli that can affect living organisms: physical stimuli (including heat, light, and pressure), chemical stimuli (such as changes in pH and salt concentration), and biological stimuli (involving enzymes). Chemical and biological stimuli are naturally occurring phenomena, while physical stimuli usually occur in the external surroundings, except for temperature, which can come from either external sources or from within an organism[37].

#### *2.3.4.3. Mechanical Properties*

Hydrogels have acquired significant attention in the pharmaceutical and biomedical domains due to their considerable mechanical resilience. The evaluation of the mechanical robustness of hydrogels holds great importance in guaranteeing their effective performance in diverse physiological settings. These areas encompass various aspects such as biomedical technology, tendon and ligament repair, cartilage replacement, tissue engineering, wound dressing, and drug delivery systems. The preservation of the physical integrity of the hydrogel is of utmost significance when considering its gradual release of therapeutic substances over a specified duration[35].

#### *2.3.4.4. Degree of Crosslinking*

The optimization of mechanical properties in hydrogels entails the inclusion of distinct polymers, co-monomers, and crosslinkers, as well as meticulous regulation of crosslinking intensity. Despite the multi-faceted interconnections, an overabundance of such connections can result in a diminishing capacity for elasticity and adaptability, concurrently leading to an increased propensity for fragility. The characteristic of elasticity holds utmost significance in conferring heightened adaptability to the interconnected system and facilitating the seamless mobility of synergistic therapeutic constituents. Hence, attaining the utmost level of crosslinking in hydrogels holds significant importance in preserving a delicate balance between structural integrity and flexibility[38].

#### *2.3.4.5. Biocompatibility*

It is imperative that hydrogels exhibit biocompatibility and non-toxicity. Biocompatibility is essentially defined as the inherent capability of a material to effectively interact with host tissues and accurately respond to a specific environmental context. Biological safety and biological functionality are integral components of biocompatibility. If the hydrogels fail to meet these specified criteria, they may subsequently become fouled. The utilization of toxic chemicals in the formulation process of hydrogels frequently presents difficulties in achieving *in vivo* biocompatibility. Polysaccharides are commonly acknowledged to be biologically compatible and non-toxic polymers thus they have received approval for utilization in dietary contexts. In a study conducted by Tokura et al. *In vivo* cytotoxicity studies were conducted on various biodegradable polysaccharides, as detailed in the reported literature. No signs of immediate harm were observed in the blood systems of rats[39]. In the present research, Chan et al. conducted an investigation into the potential detrimental effects

of chitosan, chitosan-PEG, and folic acid-conjugated chitosan-PEG/DNA complexes. The findings exhibited a mean cellular viability of 90% [40]. A specialized investigation was conducted to assess the impact of chitosan, O-carboxymethyl chitosan, and N, O-carboxymethyl chitosan on the proliferation of MCF-7 breast cancer cells within a controlled laboratory environment. The conducted investigation revealed that the examined substances exhibited significantly reduced levels of toxicity, consequently leading to a cell viability rate of 98% [41].

#### 2.3.4.6. Biodegradability

The utilization of biodegradable hydrogels serves as a pivotal undertaking within the domain of biomedical research. The term "biodegradability" refers to the enzymatic decomposition of hydrogels into non-toxic byproducts by an organism. The biodegradability of hydrogels is contingent upon the constituents within the systems and the methodology employed during their preparation. The mechanisms of deterioration encompass hydrolysis and solubilization of biological components within hydrogels, resulting in the formation of final substances or end products. The potential degradation and elimination of hydrogels from the human body can occur via mechanisms known as bio-absorption and bio-erosion [35].

#### 2.3.5. Applications of Hydrogel

Hydrogels have witnessed increasing employment across various disciplines in recent years, owing to their multifaceted characteristics [42]. Properties such as a gentle texture, exceptional swelling characteristics, and the ability to mimic natural tissue attributes. The application of hydrogel technology has proven its efficacy across a wide range of scientific disciplines.



Figure 8: Applications of Hydrogel Membranes [43]

## 2.4. Polymers for Hydrogels

Recently, natural polymers have garnered significant interest due to their biocompatibility, biodegradability, cost-effectiveness, and abundance[44]. However, a persistent issue inherent in natural polymers is their susceptibility to mechanical weakness. Polyvinyl alcohol (PVA) possesses limited hydrophilicity and elasticity[45], thereby hindering its ability to independently form a durable hydrogel. Consequently, a solution has been sought in blending PVA with natural and synthetic polymers to address these issues. PVA hybrid hydrogels have gained significant popularity as polymeric membranes for the management of wounds in the field of healthcare. The hydrogels comprising of PVA/Dextran[46], PVA/Sodium Alginate[47], PVA/Chitosan[48], PVA/Glucan[49], PVA/Gelatin[50], PVA/Hyaluronic Acid[51], and PVA/Keratin[52], have been effectively synthesized.

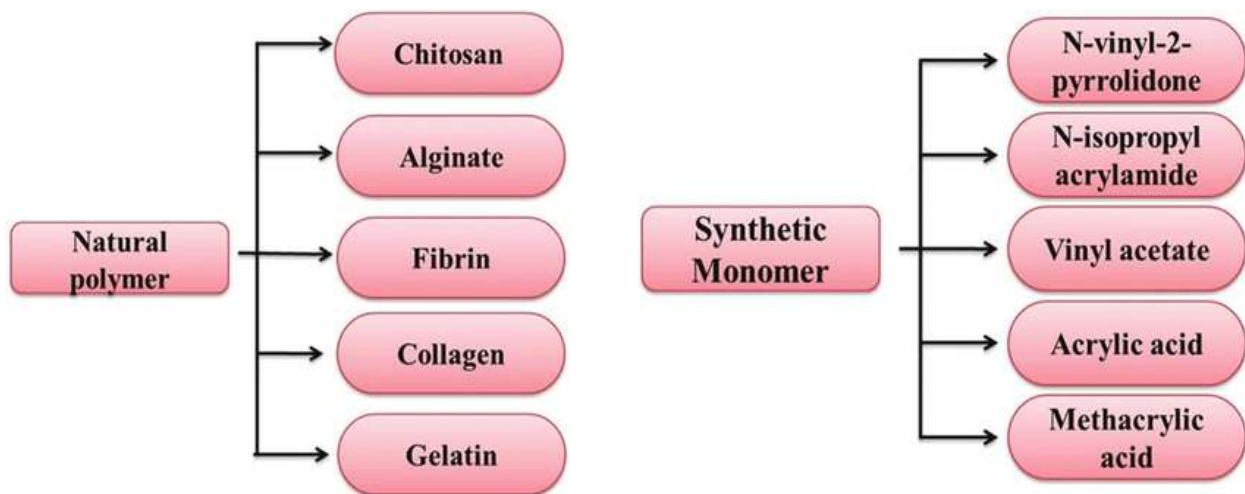
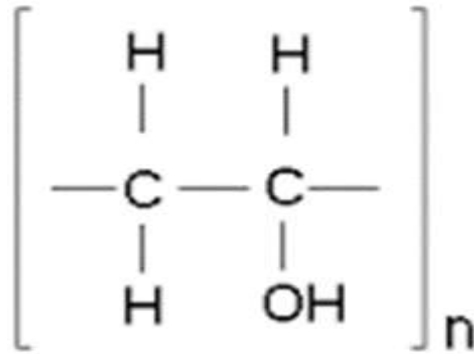


Figure 9: Classification of Hydrogel based on the nature of polymer[53]

### 2.4.1. Polyvinyl alcohol (PVA)

Polyvinyl alcohol (PVA) was discovered by F. Klatte in 1915. The process of stoichiometrically saponifying a polyvinyl acetic acid derivative with sodium hydroxide to produce polyvinyl alcohol (PVA) was first established in 1924 by W.O Hermann and W. Haehnel. According to the literature, the polyvinyl alcohol (PVA) demonstrates the presence of a recurring fundamental unit, which notably does not rely on a monomeric structure[54]. This phenomenon occurs due to the principle of free radical polymerization of vinyl acetate, followed by the incorporation of alcoholic functional groups within the acetate moieties[55].

The sub-atomic composition of PVA is visually depicted in Figure 10.



*Figure 10: Chemical structure of PVA*

Polyvinyl alcohol (PVA) is an artificial biopolymer. The substance exhibits exceptional qualities such as aqueous solubility, oxygen and oil retention capabilities, and noteworthy optical properties. Additionally, PVA exhibits an array of advantageous characteristics in an academic context. These include notable tensile properties, commendable thermal properties, resilience against organic solvents and oils, as well as the absence of toxicity as confirmed in reference[55]. The polyvinyl acetate (PVA) demonstrates a notable attribute of inhibiting the infiltration of solvents, oils, and greases. Upon dissolution in water, this substance yields a visibly clear and thick solution. The PVA films exhibited a remarkable degree of cleanliness and possessed a notably diminished propensity towards water absorption. The observed objects exhibit a lack of flexibility and resilience. In order to mitigate these challenges, the combination of polyvinyl alcohol (PVA) with various natural polymers such as chitosan, cellulose, starch, PLA, and gelatin is typically employed in the fabrication of hydrogels[56, 57].

#### **2.4.2. PVA Blends**

Blending techniques present a favorable prospect for accelerating the enhancement of material properties and achieving cost effectiveness in specific domains of medical sciences and packaging materials. Polymers exhibit solubility parameters which promote improved compatibility due to the presence of robust hydrogen bonding as opposed to weak van der Waals forces[58]. As a consequence, the resultant polymer blends can exhibit distinctive characteristics that deviate from those of the constituent polymers. The material cost of PVA is relatively high, and its biodegradability rate is low. Therefore, in order to enhance its properties for packaging applications, it is often necessary to incorporate other polymers, such as starch, chitosan, cellulose, and lignocellulose, through blending[59].

#### *2.4.2.1.PVA/Starch Blend*

Starch is classified as a member of the polysaccharide family, a ubiquitous entity in the natural world. This substance exhibits solubility in water, lack of taste and color, non-toxicity, biodegradability, and economic viability. Starch granules exhibit a size range varying from 0.5 to 175  $\mu\text{m}$ , contingent upon their origin as derived from sources such as potatoes, corn, wheat, rice, lentils, and peas [59]. The compound glutaraldehyde was employed as the chemical cross-linking agent, while glycerol served as the plasticizer in order to enhance the flexibility of the films. The hydrogel membranes were fabricated by incorporating a polyvinyl alcohol (PVA) solution with a starch solution. The hydrogel membranes synthesized via the application of heat treatment on starch exhibited transparency, in contrast to the white coloration observed for the hydrogel membranes derived from non-heated starch. The present study aimed to assess the phenomena of swelling behavior, mechanical strength, and diffusion coefficient pertinent to drug delivery applications. The aforementioned materials possessed promising capabilities as both wound dressings and for use in packaging applications[60].

#### *2.4.2.2.PVA/Chitosan Blend*

Chitosan represents a naturally derived biopolymer that exhibits notable antimicrobial properties, along with reduced oxygen permeability, exceptional film-forming characteristics, non-toxic nature, cost-efficiency, and widespread accessibility. The aforementioned intriguing attributes arise due to the formation of robust hydrogen bonds among molecular chains, coupled with the presence of hydroxyl and amine groups. Chitosan, a hydrophilic polymer, presents insolubility in water but can be easily dissolved in various acidic solvents and plasticizers. One of the most abundant biopolymers following cellulose is demonstrated by its plentiful presence[61]. The synergistic utilization of the favorable mechanical properties and hydrophilicity of PVA, in conjunction with the biologically active nature of chitosan, presents a promising opportunity for the development of blended films with advantageous attributes such as enhanced antibacterial efficacy, improved formability, superior mechanical integrity, and heightened barrier characteristics. Multiple studies have substantiated the influence of nanofillers on enhancing the mechanical properties of PVA/Chitosan blends[62].

#### *2.4.2.3.PVA/Gelatin Blend*

Gelatin is an inherently present protein that is obtained through the denaturation process of collagen. Collagen can be acquired through the process of simmering bones, skin, organs, and other such biological materials. Gelatin is commonly regarded as an insipid dietary substance. When in a dried state, it exhibits transparency and fragility. In a manner akin to polyvinyl alcohol (PVA), gelatin is also capable of producing high-quality films. The synthesis of hydrogel membranes was conducted through the incorporation of gelatin into the PVA solution. A minimal quantity of concentrated hydrochloric acid (HCl) was introduced as a cross-linking agent. Hydrogel membranes exhibit distinctive potential in the realm of wound dressing. Their versatile applications encompass drug delivery, artificial dermis development, the promotion of moist environment for wound healing, as well as utilization in packaging materials[63].

#### *2.4.2.4.PVA/PLA Blend*

Polylactic acid (PLA) is a naturally occurring polymer with the ability to degrade and interact harmoniously with living organisms. It is derived from agricultural sources such as potato, corn, and sugar beet. PLA exhibits linear polymerization, making it an attractive choice for various applications. PLA exhibits a significant hydrophobic character that contributes to its low rates of hydrolytic degradation. The material exhibits a limited water retention capacity, and the absorption of water plays a pivotal role in the process of degradation. As a means of facilitating its biodegradability, PVA is frequently conjoined with biopolymers[64]. The empirical findings further establish that the magnitude of tensile strength is notably amplified by augmenting the PVA concentration within the blend. This phenomenon can be attributed to the augmentation of hydrogen retention and chemical interplay among the polymers[65].

#### *2.4.4.5.PVA/Cellulose Nanocomposite Blend*

Nanofillers such as cellulose nanocrystals (CNCs) and cellulose nanofibers (CNFs) possess traits like biodegradability, biocompatibility, large surface area, high aspect ratio, high elastic modulus, low density, and cost-effectiveness. Environmentally-friendly fillers, including a variety of polymers like PVA and starch, have been utilized[66]. The hydrophilic nature of these substances lends them to a greater affinity with hydrophilic polymers such as PVA. Polymer matrices are prone to the formation of a three-dimensional structure. The hydroxyl (OH) groups in nanocomposite films significantly enhance their properties due to the occurrence of strong hydrogen bonding. Properties such as (mention specific properties)

exhibit an initial increase up until a certain threshold, beyond which there is a subsequent decrease due to the aggregation of nanocellulose in the PVA blend. Frone et al. also attained comparable findings. The presence of a considerable amount of 5% non-crystallizable component (NC) led to the conglomeration of particles within the PVA/Starch reinforced films. The composite blend exhibited positive dispersion with the inclusion of 1% NC[67]. The enhanced compatibility and intensive intermolecular interactions observed between polyvinyl alcohol (PVA) and nanocrystalline cellulose (NC) led to a notable rise in the glass transition temperature (T<sub>g</sub>) of the composite films. This effect can be attributed to the improved immobilization of the polymeric chains facilitated by the agglomeration of the nanofillers[68].

### 2.4.3. Chitosan

Chitosan has been proven to have both biocompatible and biodegradable characteristics, as supported by multiple studies[69, 70]. Furthermore, its degradation byproducts have been confirmed to be non-toxic and non-immunogenic, adding to its overall advantageous characteristics. Chitosan exhibits bio-adhesive and bacteriostatic properties[71].

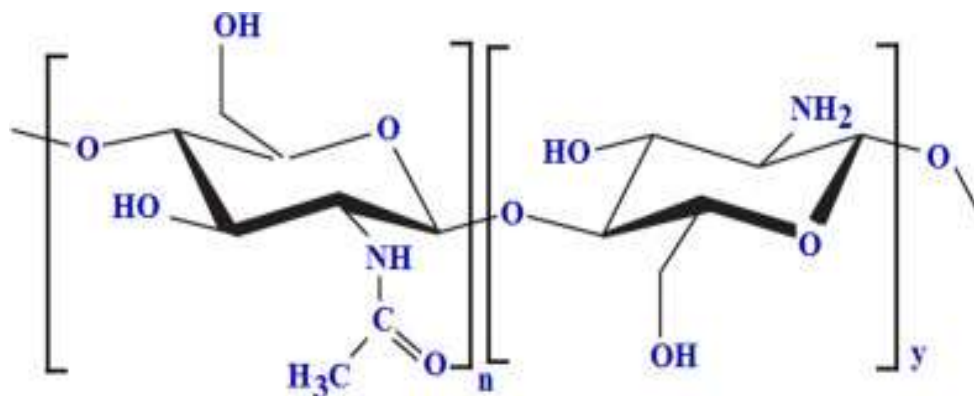


Figure 11: Chemical Structure of Chitosan

Moreover, it functions as a chelating agent[72] and possesses hemostatic properties alongside antioxidant activity[73]. This particular polymer possesses the ability to regulate hemorrhaging by means of incorporating a procoagulant agent that aids in expediting the clotting process[74]. Chitosan has garnered significant interest across various domains, namely pharmaceutical, medical, cosmetics, agricultural, and food industries[75]. Chitosan demonstrates great potential in various pharmaceutical contexts, encompassing drug and gene delivery, wound dressing, tissue repair, and tissue engineering[76-78].



#### *2.4.3.1. Drug Delivery*

The utilization of chitosan-based hydrogels and their chemically modified derivatives has been extensively explored in various drug delivery applications[79]. One characteristic of chitosan is its cationic nature, which arises from the inclusion of an amine group. Conversely, mucosal glycoproteins possess a negative charge, as indicated by previous studies[80, 81]. Hence, it exhibits the ability to attach itself to biologically charged surfaces, functioning aptly as a bioadhesive substance. The application of bioadhesive polymers, such as chitosan, serves to extend the duration of drug retention in a drug-loaded system and facilitate targeted drug distribution within specific regions[82]. Chitosan has been observed to play a critical role in facilitating the paracellular transport of drugs, thereby exerting a significant influence on the effectiveness of drug delivery systems[83]. Chitosan, due to its biocompatible and biodegradable nature, along with its easily modifiable structure, has been employed as a drug carrier for various routes of administration. The subsequent sections explicate several noteworthy avenues in chitosan-based drug delivery.

#### *2.4.3.2. Wound Healing*

Chitosan, when administered topically, is utilized for the purpose of enhancing wound healing. The potential mechanism underlying the process of healing involves the infiltration of inflammatory cells, specifically polymorphonuclear leukocytes, as well as the secretion of inflammatory mediators, including tumor necrosis factor- $\alpha$ . Additionally, it entails the migration of macrophages and an increase in collagen proliferation. The interaction between GlcNac (N-acetyl-D-glucosamine), an integral component of chitosan, and specific receptors within the human body promotes enhanced stimulation of macrophage activity, leading to subsequent cascades of events including the discharge of various biological mediators[84]. Moreover, chitosan elicits the activation of the complement system[85] and induces the release of interleukin-8 (IL-8) and various other cytokines by fibroblasts[86].

#### *2.4.3.3. Tissue Engineering*

Over the course of the previous two decades, chitosan hydrogels have been employed as scaffolds within the realm of tissue engineering. The fundamental basis of these systems is predicated upon two core constituents, namely cells and polymeric chains encompassing hydrogel material. The biodegradability of chitosan as a scaffold is considered one of its advantageous qualities. Chitosan, a polysaccharide, has the capacity to undergo degradation via human enzymes such as lysozyme[87]. Furthermore, it is possible to enhance the

biodegradability and biocompatibility attributes required in the domain of tissue engineering applications by undertaking N-acetylation modifications on chitosan. According to previous studies[88], chitosan with a deacetylation degree in close proximity to 100 is purported to exhibit a greater degradation rate, enhanced cell biocompatibility, and increased potential for cell adhesion. The rate at which a scaffold biodegrades should align with the temporal requirements for malfunctioning tissue to undergo repair.

## **2.5. Nanocellulose**

Cellulose represents the most abundant and environmentally sustainable biopolymer found in the biosphere. The annual production of this substance exceeds 75 billion tons[89]. Given the substantial volumetric presence of cellulose, it can be effectively utilized.

The utilization of cellulose can be categorized into the initial generation, wherein advantages were derived from a hierarchical structure design. Natural materials exhibit a remarkable array of properties such as exceptional functionality, flexibility, and mechanical strength. These intrinsic characteristics are achieved through the deliberate harnessing of hierarchical structural arrangements spanning from the nanoscale to macroscopic dimensions. Nevertheless, the initial iteration of cellulose material fails to meet the societal requirements for efficiency. Consequently, scientists and researchers are compelled to delve deeper into the examination of the reinforcement unit, nanocellulose, as exemplified in this study[90].

### **2.5.1. Nanocellulose Structure**

Cellulose is composed of a linear chain of glucose atoms arranged in a repeated ring structure, displaying a structural conformity akin to that of a latticed lace. The rehashing unit consists of two anhydroglucose rings ( $(C_6H_{10}O_5)_n$ ), where  $n$  ranges from 10000 to 15000, and is determined by the source material. These rings are connected through an oxygen covalently bonded to C1 of one glucose ring and C4 of the adjacent ring, forming a 1-4 glucosidic bond[90]. The intermolecular and intramolecular hydrogen bonding interactions occur between hydroxyl groups and adjacent oxygen atoms, providing stability to the linkage. Cellulose's linear configuration imparts structural stability to its polymer and imparts high rigidity to cell fibrils. These fibrils serve as the primary structural elements for trees, plants, algae, and microorganisms. The cellulose fibrils consist of a crystalline region (ordered) and an amorphous region (disordered), although the distribution of these regions has yet to be

properly addressed[91]. The presence of a crystalline region within cellulose microfibrils yields the extraction of cellulose nanocrystals, thereby initiating their formation.

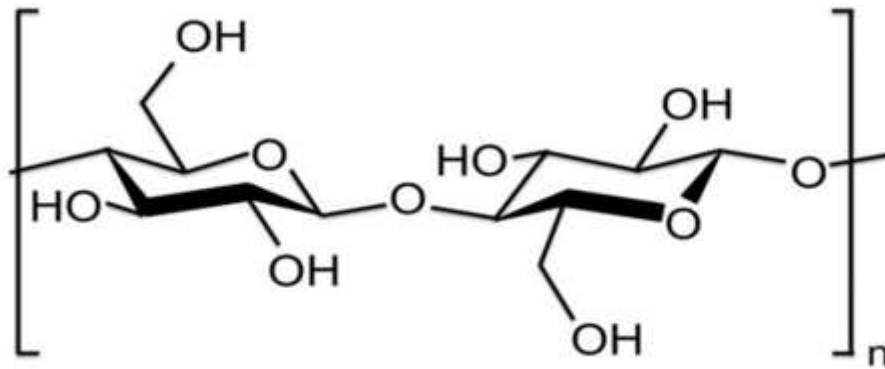


Figure 12-1: Single Cellulose Chain Repeat Unit

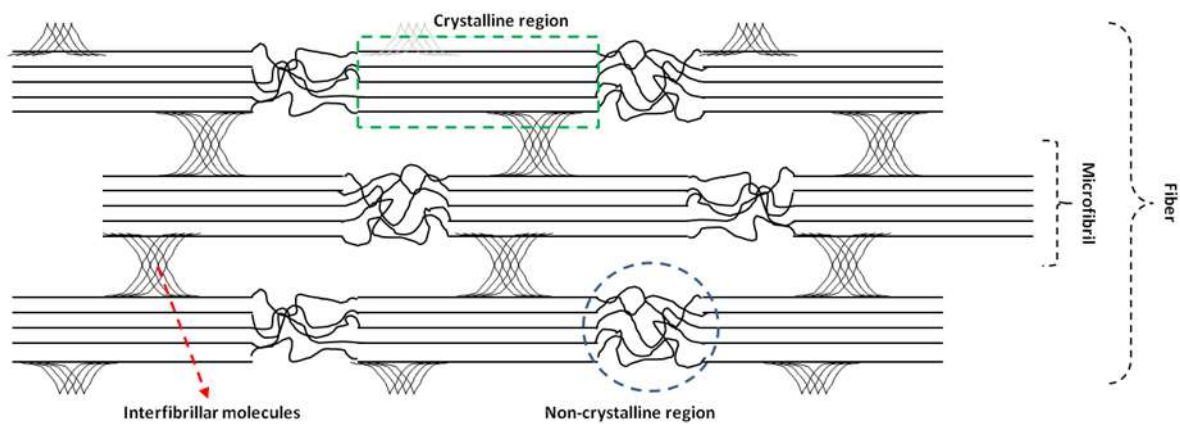


Figure 12-2: Cellulose microfibril having structure of the crystalline and amorphous regions

### 2.5.2. Classification of Nanocellulose

Nanocellulose is typically comprised of nanocellulose crystals, micro or nano-fibrillated cellulose (MFC or NFC), cellulose nanofibers oxidized with TEMPO (TOCN), and bacterial cellulose (BC). The latter products are typically synthesized through a process of mild hydrolysis, involving either acidic or enzymatic conditions, coupled with mechanical defibrillation treatments such as the use of ultra-blenders, grinders, and homogenizers[92].

### **2.5.3. Properties of Nanocellulose**

The properties of nanocellulose are listed below:

- Lightweight materials are characterized by their low density, typically below 5000 kg/m<sup>3</sup>, offering a high strength-to-weight ratio.
- They are widely utilized in various industries due to their favorable properties such as flexibility, thermal insulation, and corrosion resistance. Their reduced weight allows for improved energy efficiency, reduced environmental impact, and increased overall performance.
- The utilization of electrical conductivity is a pertinent aspect within the realm of scientific and technological advancements.
- The investigated substance is characterized by its non-toxic nature.
- The crystalline structure exhibits transparency and impermeability to gases.
- The substance can be efficiently manufactured in considerable quantities at a reasonable cost.
- The material possesses a significantly elevated tensile strength, measuring eightfold higher when compared to steel.
- The substance in question exhibits exceptional absorbency properties when employed as a foundational element in the synthesis of aerogels or foams.
- Cellulose, as a raw material, constitutes the most abundant polymer within the Earth's biosphere.

### **2.6. Nanoparticle**

Nanoparticles (NPs) enjoy a favorable standing for their cutting-edge technology, rendering them suitable for deployment in sophisticated applications and products. NPs are deemed as a viable solution to resolve outstanding challenges and offer the capacity to accomplish tasks that would otherwise pose significant difficulty. For instance, NP applications span a wide range, such as cancer treatment, water purification, solar energy harnessing, energy storage, and facilitation of industrial reactions. Laurent Richard P. Feynman, a renowned recipient of

the prestigious Nobel Prize, is a prominent figure in his field. Nanotechnology was initially introduced by Feynman, thereby establishing him as a pioneering figure in this field.

NPs have been present since antiquity, with naturally occurring instances encompassing carbon-based substances derived from volcanic activities and combustion[93]. Furthermore, these particular microorganisms have been observed to actively generate such compounds[94]. NPs consist of matter that includes metal, metal oxide, or carbon-based materials and typically exhibit a size distribution within the range of approximately 100nm. NPs particularly metallic nanoparticles, play a significant role in biomedical applications owing to their properties that vary with size[95]. The intrinsic characteristics of NP are contingent upon variables such as shape, size, composition, and crystallinity. The aforementioned factors are contingent upon the methodology and circumstances employed in the synthesis process[96]. The classification of NP can be delineated into four distinct categories, which are determined by their chemical properties, size, and morphology. The aforementioned categories encompass Polymeric Nanoparticles, Ceramic Nanoparticles, Carbon-Based Nanoparticles, and Metallic Nanoparticles.

### **2.6.1. Metallic Nanoparticle**

Metallic nanoparticles such as ZnO, CuO, FeO, Au, and Ag, among others, are of interest in academic studies. NPs have found usage across the industry in various applications, however, their emergence in the biomedical field stands out as one of the most prevalent and significant. The significance within the realm of biomedical application stems from the antimicrobial properties exhibited by these nanoparticles against both Gram-positive and Gram-negative bacteria. Metallic nanoparticles have found numerous applications in various fields including agriculture, information technology, optics, catalysis, and energy, among others[97]. The magnetic and chemical characteristics of NPs are contingent upon a distinct size parameter of NPs[98].

### **2.6.2. Synthesis of NP**

The utilization of the top-down and bottom-up approaches is prevalent in the synthesis of nanoparticles. In the top-down approach, bulk materials undergo a progressive reduction process, resulting in increasingly smaller dimensions. Conversely, the bottom-up approach involves the consolidation of atoms, molecules, or clusters to form larger structures.

**Chemical precipitation** constitutes a viable approach for the synthesis of NPs, involving three primary stages: chemical reaction, nucleation, and crystal growth. It is recognized in the chemical precipitation method that achieving complete control over reaction kinetics and solid phase nucleation and growth is not entirely certain[99].

The **sol-gel process** has been extensively recorded in scientific literature as an effective technique for producing colloidal powders or films. The sol-gel method has been noted as a feasible approach to create metallic sulfides. The sol-gel method has a significant advantage in its capacity to control the microstructure of the produced item[100].

The method of **microwave synthesis** has been employed for creating nanoparticles. This technique utilizes the interaction between microwaves and either liquids or solids, which leads to a phenomenon called dielectric heating[101]. Dielectric heating provides a faster and uniform environment for producing nanoparticles, as opposed to the conventional heating method. This phenomenon is associated with the use of microwave radiation, which allows for quick and uniform heating[102].

The **vapor-phase synthesis** of nanoparticles involves the consideration of the thermodynamically unstable state of the vapor mixture in contrast to the solid-state synthesis of nanoparticles. In the context of vapor-phase synthesis, the vapor undergoes supersaturation, facilitating chemical reactions among the vapor-phase molecules and subsequently resulting in the formation of a condensed phase. The formation of particles is contingent upon the level of supersaturation and the condensation kinetic parameter. If both conditions are present, nucleation will occur in a homogeneous manner. Particle growth is the subsequent stage following nucleation when the oversaturated vapors are engaged with the resultant particles[103].

The **hydrothermal/solvothermal method** employed in the synthesis of nanoparticles constitutes a crystallization process encompassing two distinct phases. The initial phase entails the nucleation of crystals, followed by the subsequent growth phase. The manipulation of process variables, such as additives, temperature, reactant concentration, and pH, enables the fabrication of particles with the desired size and morphology[104].

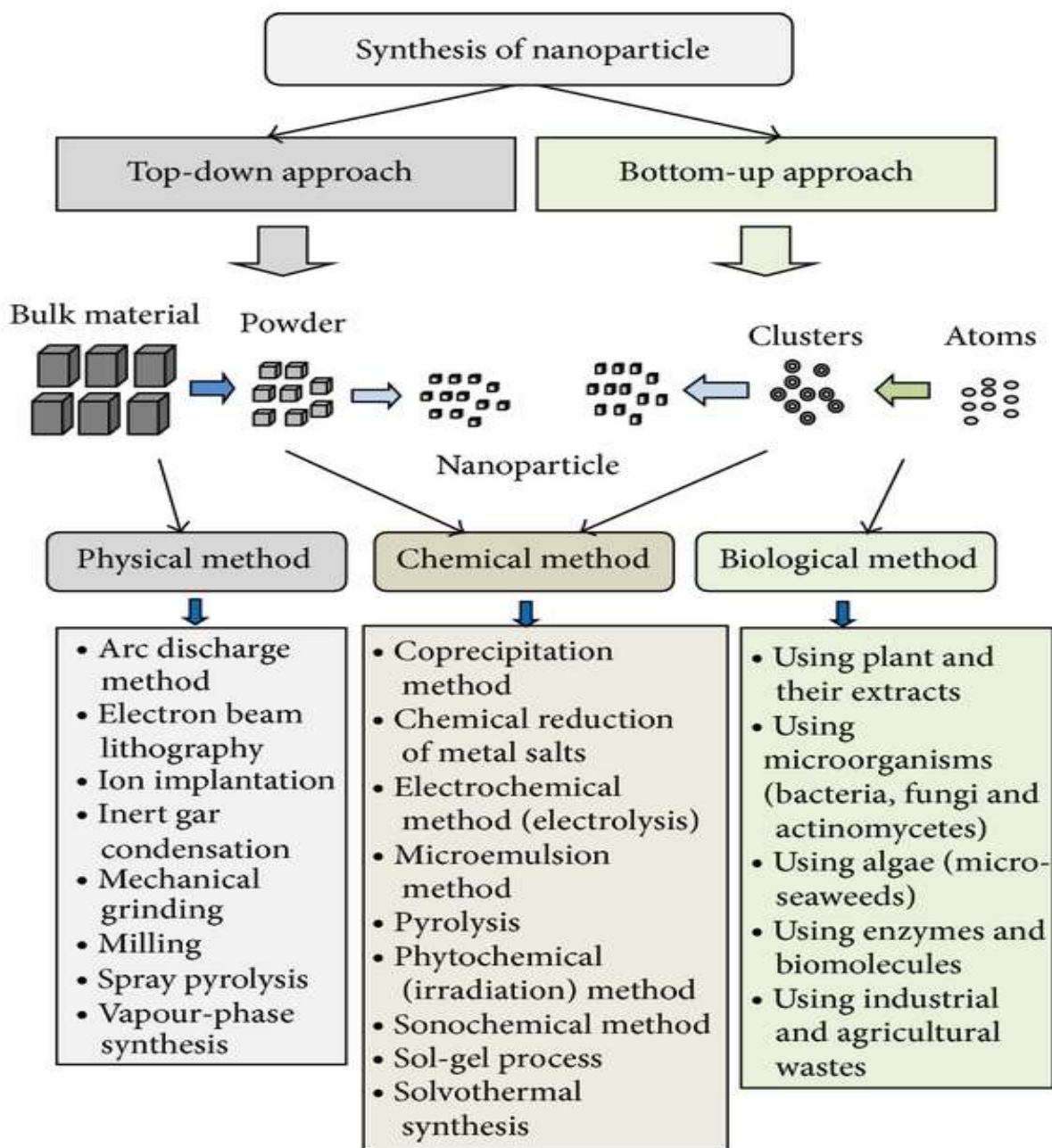


Figure 13: Different methods for nanoparticle synthesis[105]

### 2.6.3. Nanoparticles as Antibacterial Agents

Antibacterial nanoparticles (NPs) are minuscule particles, typically less than 100nm in size, that can be fabricated using an assortment of materials including metals, metal oxides, and polymers. Silver nanoparticles (AgNP) are commonly recognized as a highly prevalent type of antibacterial nanoparticles[106-108]. For many years, people have acknowledged the antimicrobial properties of silver, particularly silver nanoparticles, which have proven to be effective against a wide range of bacteria, including those that are resistant to antibiotics.

Other types of nanoparticles, specifically copper, gold, and zinc oxide nanoparticles, have been investigated and analyzed for their effectiveness in killing bacteria[109, 110].

Antimicrobial nanoparticles offer a wide range of applications in different areas, such as medicine[111], water purification[112], and packaging of food products[113]. Bioactive substances have been used in medicine to cover medical devices and prevent bacterial infections. They are also used in wound dressings to promote healing and prevent bacterial infections. In the realm of water treatment, these agents have been utilized with the purpose of water purification, achieving the eradication of bacteria and other microorganisms. In the realm of food packaging, nanoparticles have been employed to effectively enhance the longevity of food products through the inhibition of bacterial proliferation.



# Chapter 3:

## Materials and Methods

### 3.1. Materials

Following are the materials that were used for the preparation of hydrogel films:

- Polyvinyl Alcohol 1500 (density: 1.091 kg/m<sup>3</sup>, melting point: 44-48 °C) was purchased from Daejung Chemicals Korea
- Chitosan (density > 0.6 g/ml) was obtained from Macklin Chemicals China.
- Microcrystalline Cellulose (particle size: 51 µm, density: 0.6 g/ml) was obtained from Macklin Chemicals China.
- Vanillin (molecular weight: 152.15 g/mol, vapor pressure: >0.01 mmHg)
- Acetic acid (1% w/w) was purchased from Sigma Aldrich Germany.
- Copper Acetate and silver nitrate (AgNO<sub>3</sub>) were purchased from Sigma Aldrich Germany.
- De-ionized water was used throughout the experiment

### 3.2. Synthesis of Nanocellulose

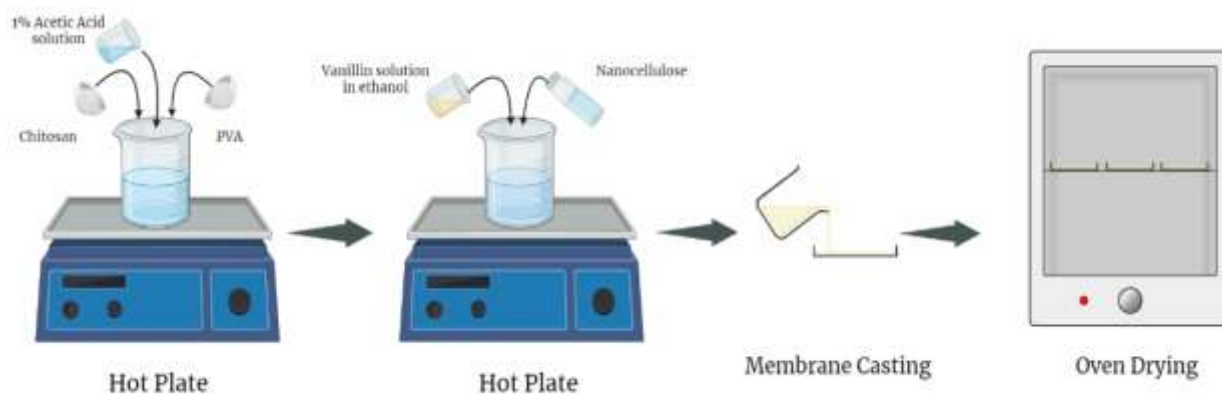
In 500 ml of deionized water, 5g of microcrystalline cellulose (MCC) was dissolved over the course of 24 hours with steady stirring. The mixture was then homogenized for 60 minutes using an ultrasonic homogenizer fitted with a sonication probe. After a two-hour ultrasonication procedure, nanocellulose was removed from the water suspension by transferring the supernatant into a new container.[114].



Figure 14: Synthesis of nanocellulose from microcrystalline cellulose through ultrasonication probe

### 3.3. Fabrication of Membrane (PVA/Chitosan/ Vanillin/ NC)

Membranes made of nanocomposite hydrogel were created utilizing the solution casting technique. PVA 10% weight/volume solution was made in preparation for the hydrogel membrane casting process. In a 1% volume/volume solution of acetic acid, chitosan was dissolved. Vanillin 0.3 gm was dissolved in ethanol. Vanillin and chitosan were combined to create a solution. After adding nanocellulose, the chitosan/vanillin solution was agitated for two hours. The resulting mixture was combined with PVA, which was then agitated for three hours at a temperature of 60 °C and 250 rpm. Place the solution in a Teflon petri dish and let it dry for 10 hours at 40 °C in a drying oven. The hydrogel membranes were taken out of the petri plates after drying and put in pouches that were later sealed to be used in further study.[115].



*Figure 15: Fabrication of PVA/Chitosan/Vanillin/NC membranes*

### **3.4. Synthesis of CuO/Ag nanoparticles using wet chemical precipitation method**

Wet chemical precipitation was used to create the CuO/Ag nanoparticles, albeit with a few alterations from earlier research. [116]. First, 100 ml of deionized water was used to dissolve 1 M copper acetate, and a magnetic stirrer hotplate was used to stir the mixture. Once pH 11 was reached, 2M NaOH was added dropwise, and a dark suspension appeared, indicating the presence of copper oxide. CuO/Ag nanoparticles were created by mixing 100 ml of CuO aqueous precipitate with 0.5 M silver nitrate. To reduce the silver ions in the reaction solution, 5 ml of 2 M sodium borohydride was next added dropwise. The resultant nanocomposites were then centrifuged to separate them, cleaned with distilled water to remove extra ions, and baked at 80°C to dry them.

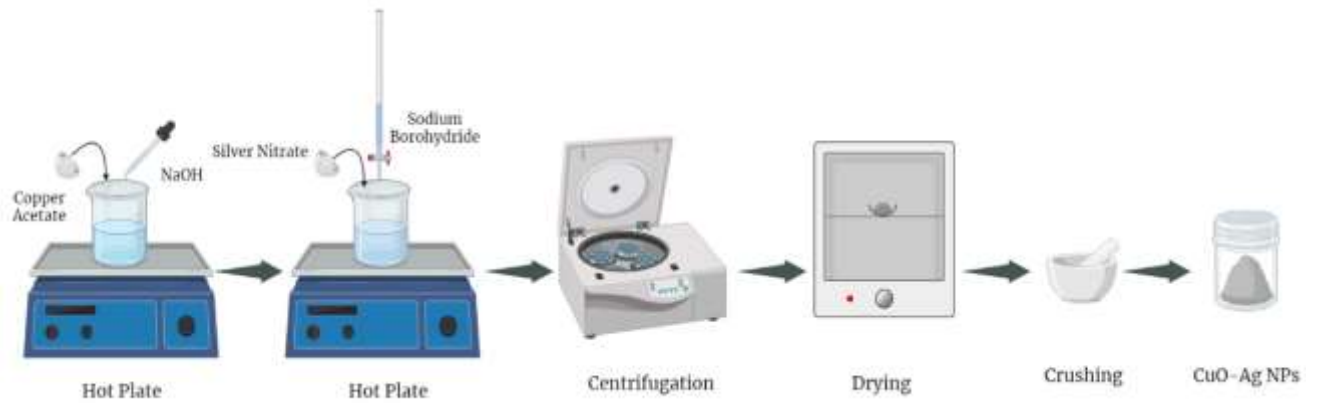


Figure 16: Synthesis of CuO/Ag nanoparticles using wet chemical precipitation method

### 3.5. Fabrication of Membrane (PVA/Chitosan/Vanillin/NC/CuO-Ag NPs)

Solution casting was employed in the creation of the hydrogels. Initially, 10 ml of acetic acid and 0.5g of chitosan were well stirred for 20 minutes to dissolve the chitosan. In order to create a cross-linker solution, 0.3g of vanillin was dissolved in 2 ml of ethanol. The cross-linker solution was then added after the CuO-Ag nanoparticles and nanocellulose were mixed with the chitosan solution in various ratios. Before being poured onto petri dishes, the resultant mixture was agitated at room temperature for 30 minutes. The resulting membranes were peeled off and stored in airtight containers after being dried at 30° C for a whole night.

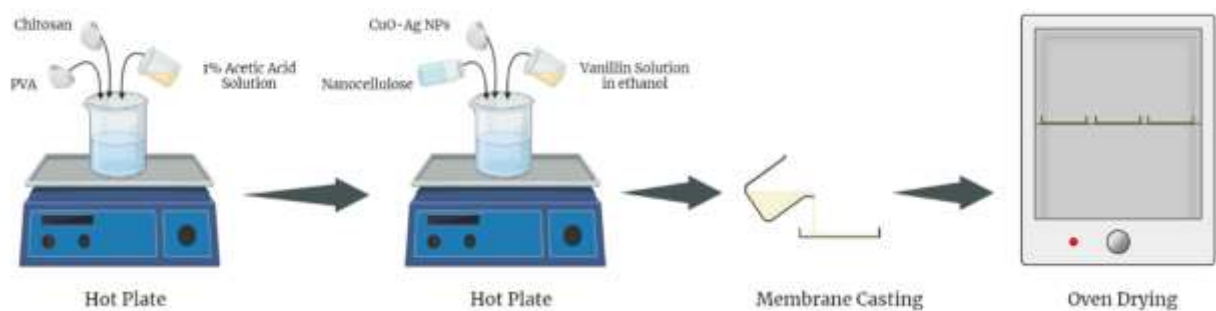


Figure 17: Fabrication of PVA/Chitosan/Vanillin/NC/CuO-Ag NP membrane

Table 2: The detailed description for fabrication of PVA/Chitosan/Vanillin/Nanocellulose and CuO-Ag nanocomposite membrane

<b>Membrane</b>	<b>Abb.</b>	<b>PVA (g)</b>	<b>Chitosan (g)</b>	<b>Vanillin (g)</b>	<b>Nanocellulose (%)</b>	<b>CuO/Ag NPs (mg)</b>
PVA/ Chitosan/ Vanillin	CVN0	1	0.15	0.3	0	0
PVA/ Chitosan/ Vanillin/ NC	CVN4	1	0.15	0.3	4	0
PVA/ Chitosan/ Vanillin/ NC	CVN8	1	0.15	0.3	8	0
PVA/ Chitosan/ Vanillin/ NC	CVN12	1	0.15	0.3	12*	0
PVA/ Chitosan/ Vanillin/ NC	CVN16	1	0.15	0.3	16	0
PVA/ Chitosan/ Vanillin/ NC/ CuO-Ag	CNP0.5	1	0.15	0.3	12	0.5
PVA/ Chitosan/ Vanillin/ NC/ CuO-Ag	CNP1	1	0.15	0.3	12	1
PVA/ Chitosan/ Vanillin/ NC/ CuO-Ag	CNP1.5	1	0.15	0.3	12	1.5
PVA/ Chitosan/ Vanillin/ NC/ CuO-Ag	CNP2	1	0.15	0.3	12	2

\* Subjected to best acceptable tensile strength

### 3.6. Characterization Techniques

Following characterizations of the nanocomposite membranes were performed to analyze the effect of filler and antibacterial agent.

*Table 3: Characterization Techniques carried out for the nanocomposite membranes*

<b>Characterization Techniques</b>	<b>PVA/Ch/V/NC</b>	<b>PVA/Ch/V/NC/CuO-Ag NPs</b>
XRD	✓	✓
FTIR	✓	✓
SEM	✓	✓
Mechanical Strength	✓	✓
Contact Angle	✓	✓
Surface Roughness	✓	✓
Moisture Retention Capability	✓	✓
WVTR	✓	✓
Gel Fraction	✓	✓
Porosity	✓	✓
Swelling Behaviour	✓	✓
Biodegradability	✓	✓
TGA	✓	✓
Cytotoxicity Assay	✗	✓
Antibacterial Activity Measurement	✗	✓
Animal Study (Rat Model)	✗	✓

### 3.6.1. X-ray Diffraction Analysis (XRD)

The STOE-Germany instrument was used to conduct an XRD examination to examine the crystalline nature of the nanocomposite membranes. An acceleration voltage of 40 kV and a current of 40 mA were used to obtain the X-ray diffraction (XRD) patterns. Step size was set to 0.04 s and the scan speed to 0.5 s. During the measurement, Cu-K radiation with a wavelength of 1.54060 was employed. The crystal structure and lattice properties of the materials could be identified thanks to the XRD investigation.



*Figure 18: XRD Analyzer by STOE-Germany*

XRD is employed as a technique within the realm of materials science for elucidating the crystallographic architecture of a given material. XRD operates through the exposure of a substance to incident X-rays, followed by the quantification of the intensity and scattering angles of the X-rays as they dissipate from the substance.

One of the primary applications of XRD analysis lies in the conclusive determination of materials by analyzing their distinct diffraction patterns. In addition to its application in phase identification, XRD analysis also provides useful information into the differences between the real structure and the predicted structure as well as the ideal structure, which can be caused by internal stressors and imperfections.

### **Objectives of XRD:**

The objectives of XRD are:

- I. Identification of crystallinity of material
- II. Identification of fingerprints of different polymeric forms
- III. Differentiation between crystalline and amorphous forms
- IV. Calculation of the percent crystallinity of the specimen

### **Working Principle:**

The underlying basis for X-ray diffraction (XRD) investigation is the phenomenon of constructive interference caused by the interaction of monochromatic X-rays with a crystalline material.[117]. The Cathode Ray Tube is capable of generating X-rays, which are subsequently subjected to filtration processes to yield monochromatic radiations. The rays undergo collimation to concentrate and subsequently direct their orientation towards the specimen. Due to the interaction between the aforementioned rays and the specimen, constructive interference occurred, provided that the conditions align with Bragg's Law. Bragg's Law describes the link between the wavelength of electromagnetic radiation, the lattice spacing, and the diffraction angle of the specimen. The given mathematical value is expressed symbolically as[118]:

$$n\lambda=2d \sin \theta \text{ _____ (1)}$$

In this equation, n stands for the order of reflection,  $\lambda$  for the X-ray wavelength, d for the typical distance between crystal planes inside a particular specimen, and  $\theta$  for the angle produced between the incident beam and the normal to the lattice plane.

### **3.6.2. Scanning Electron Microscopy (SEM)**

Utilizing an energy-dispersive X-ray (EDX) spectrometer and a scanning electron microscope (JSM-64900), the surface morphology of the hydrogel films was examined. Earlier to investigation, a thin palladium/platinum layer was set to test sample to extend conductivity.



An auxiliary electron locator was utilized to observe the surface structure, and an speeding up voltage of 20 kV was utilized all through the examination.



*Figure 19: Scanning Electron Microscope (JSM-64900) combined with an EDX spectrometer*

### **Objective of SEM:**

The Scanning Electron Microscope (SEM) is an exemplary method employed for the examination of material surfaces, yielding highly detailed information pertaining to surface topography[119]. It provides information about:

- I. Texture (External Morphology)
- II. Chemical composition
- III. Orientation
- IV. Crystalline Structure

### **Working Principle:**

The utilization of an electron beam is employed in order to generate a visual representation of a substance, while the amplification is achieved through the utilization of electromagnetic fields.

At the apex of the column, the electrons are produced through the utilization of an electron source. Electrons are generated and directed as a beam. When the thermal energy of the electrons surpasses the minimum energy threshold, known as the work function, required for emission, the electrons are released. The electrons subsequently undergo acceleration and are subsequently drawn towards the anode, which possesses a positive charge. The diameter of the electron beam can be controlled through the utilization of a lens. The production of a broader beam occurs when it is weakened, and conversely, a narrower beam is generated when it is strengthened. The trajectory of electrons is additionally regulated by the lens. An electromagnetic lens is employed due to the absence of electron permeability in glass material. Initially, the electrons encounter the condenser lens in the conducted experiment. After being focused by the condenser lens, the electrons undergo further condensation through the objective lens.

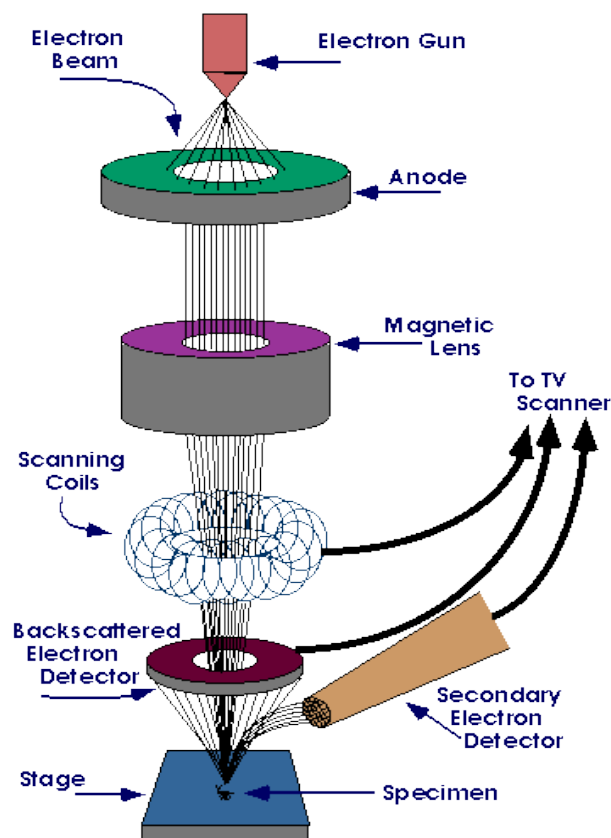


Figure 20: The working mechanism and components of SEM

### 3.6.3. Fourier Transform Infra-Red Spectroscopy (FTIR)

To investigate the functional groups identified in the nanocomposite membranes, fourier transform infrared spectroscopy (FTIR) was performed using the attenuated total reflectance (ATR) technique (ATR-FTIR, BRUKER). The FTIR spectra were obtained in the 500 to 4000  $\text{cm}^{-1}$  region with a scanning frequency of 32 and a resolution of 4  $\text{cm}^{-1}$ . The molecular compositions and architectures of nanoparticles and nanocellulose in the samples were also examined using this technique.



*Figure 21: ATR-FTIR Analyzer by BRUKER*

#### **Objectives of FTIR:**

The objective of FITR is to:

- I. Recognize organic, polymeric or sometimes inorganic compounds
- II. Characterize unknown materials
- III. Identify contaminations (in or on the materials)
- IV. In failure analysis, identify decomposition, oxidation or uncured substances

### Working Principle:

The underlying principle governing the functioning of Fourier Transform Infrared Spectroscopy is predicated on the phenomenon of molecular absorption of light within the infrared region of the electromagnetic spectrum. The absorption spectra are distinctly associated with the molecular bonds in the molecules. In customary practice, the frequencies are assessed within the spectrum of 4000 to 500  $\text{cm}^{-1}$ .

The emissions are produced by the source. The interferometer is traversed by the radiations mentioned above before they reach the specimen, where they are detected afterwards. The signals undergo amplification through the utilization of an amplifier, subsequently being transformed into digital signals via the implementation of an analog-to-digital converter. In conclusion, the transmission of the signal culminates in its transfer to a computational device, where it undergoes the significant process of Fourier Transformation.

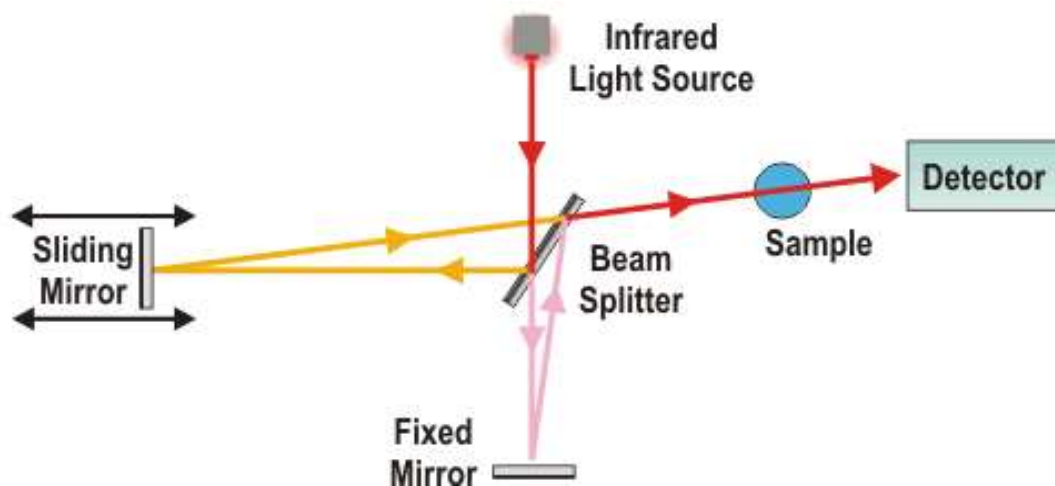


Figure 22: The components and working mechanism of FTIR

### 3.6.4. Mechanical Testing

With the help of Shimadzu Corporation's Trapezium-X Universal Testing Machine (AG-20RRKNXD Plus), the mechanical characteristics of the hydrogel membranes were evaluated. For testing, rectangular specimens with 20 mm length and 20 mm width were made from the membranes. Following the advice of earlier investigations, the experiments were carried out at a crosshead speed of 10 mm/min and a gauge length of 40 mm.[114]. To

ensure the accuracy and reliability of the results, each membrane was tested thrice, and the average value was recorded.



*Figure 23: Universal Testing Machine (AG-20RRKNXD Plus) by Shimadzu Corporation*

In order to execute the analysis, a rectangular membrane specimen was affixed with clamps at both ends and subjected to tension until its ultimate failure occurred. This conveys an understanding regarding the structural integrity of material, referred to as tensile strength, and its capacity to undergo elongation.

The measurement of tensile strength involves evaluating the force exerted on a given material in relation to the area it encompasses, alternatively referred to as stress. The Ultimate Tensile Strength (UTS) represents an intrinsic characteristic that manifests as the highest point observable on the stress-strain curve.

### **Objective of UTM:**

The objective of UTM is to test:

- I. Tensile Strength
- II. Compressive Strength

### 3.6.5. Thermogravimetric Analysis (TGA)

The thermogravimetric tests were carried out with the help of an SDT 650-TA analyzer (TGA). The membranes were heated in a nitrogen environment at a rate of 10 °C/min from 20 °C to 550 °C. [115].



*Figure 24: SDT 650-TA analyzer for thermogravimetric analysis*

#### **Objective of TGA:**

TGA is a method of thermal analysis, that is used to

- examine the mass change or weight loss of the specimen with respect to change in temperature or time in a controlled environment.
- provides information about the thermal stability of a material.
- organic and inorganic content can be predicted.

#### **Working Principle:**

The analysis entails a gradual elevation of the temperature of the specimen within the furnace. The weight is quantified utilizing an analytical balance situated externally to the furnace. The phenomenon of mass decrease is observed concurrent with the volatilization process.

The necessity of balance in experimental protocols lies in its ability to uphold reproducibility, accuracy, and sensitivity. The furnace delivers linear temperature increase across a broad range, facilitating efficient heating. In accordance with general standards, the temperature range typically spans from -150°C to 2000 °C. The process of temperature measurement and regulation is conducted through the utilization of thermocouples. There exist two commonly utilized thermocouples. One instrument is utilized for the quantification of temperature fluctuations, while the other is responsible for initiating the control mechanism. The recording unit is responsible for the function of acquiring digital data and capturing measurements.

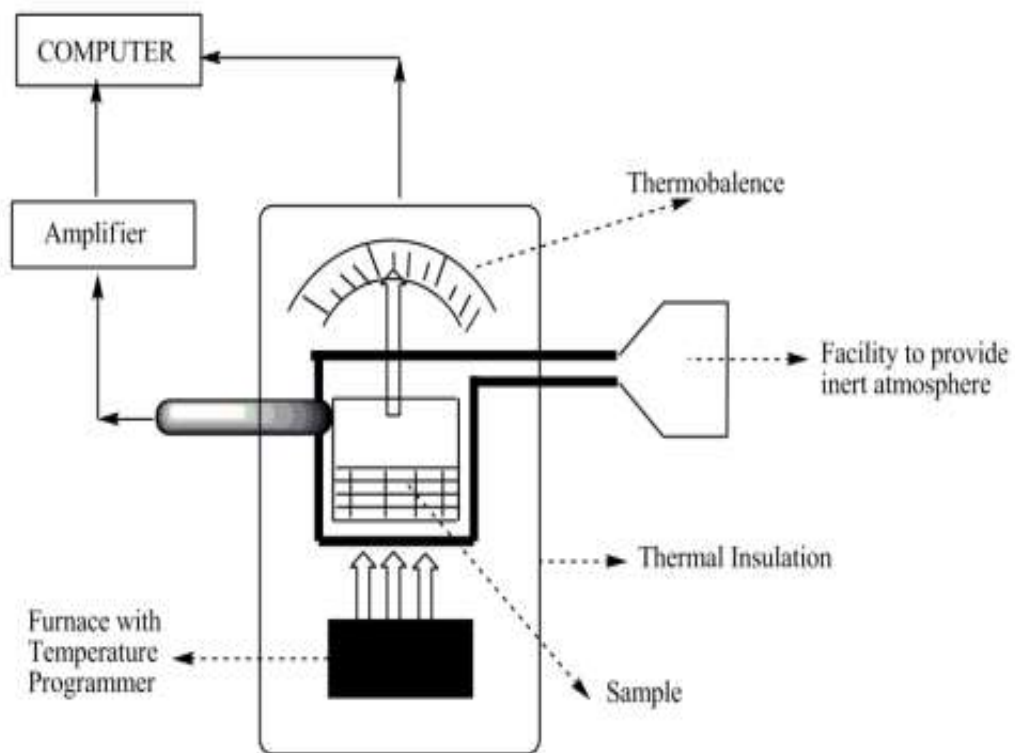


Figure 25: The components and working mechanism of TGA

### 3.6.6. Drop Shape Analyzer

Interaction between water and polymeric membrane was evaluated using the Drop Shape Analyzer. Using this technique, the contact angle between the water and the hydrogel was measured. The contact angle was determined based on the form of the water droplet at the point of contact with the hydrogel membrane after a small water drop was deposited on the

surface of the hydrogel. The DSA was equipped with a camera that continuously captured the image, and the software processed the data and measured the contact angle.

By measuring the contact angle, the nature of the membrane could be determined as hydrophobic or hydrophilic. The continuous contact angle measurement provided valuable insights into the behavior of the hydrogel membranes in contact with water. The DSA25 KRUSS was an effective tool for studying the surface properties of hydrogels and understanding the interaction between hydrogels and water.



*Figure 26: DSA25 KRUSS Drop Shape Analyzer*

### **3.6.7. Surface Roughness Measurement**

Hydrogel membranes used for wound dressing require careful consideration of the substrate surface roughness during the design process. The roughness of the hydrogel membranes' outer surfaces was measured using a compact optical profilometer (NANOVEA PS50). A glass slide with two sides was used to display the samples. All samples had to be at least 10mm x 10mm in size. All tests were conducted five times.



*Figure 27: Compact Optical Profilometer (NANOVEA PS50)*



### 3.6.8. Moisture Retention Capability (MRC)

To measure moisture retention capabilities, identically thick hydrogel films were sliced into pieces and weighed. These films were heated at 40 °C for 6 hours. The following formulas were used to calculate MRC:

$$\text{MRC (\%)} = \frac{w_t}{w_i} \times 100 \quad (2)$$

Where  $w_i$  is the initial weight of the film before it was placed in the oven and  $w_t$  is the final weight of the film after it was removed from the oven[115].

### 3.6.9. Water Vapour Transmission Rate (WVTR)

The European Polymer (EP) guidelines were used to determine the WVTR[120]. Round bottles were filled with 10ml of purified water. The samples were sealed inside the bottles. The bottles' mouths were taped shut. The assembly was then heated at 40 °C for 24 hours after weighing it ( $w_1$ ). Afterwards, the bottles were taken out of the oven and measured ( $w_2$ ). An uncorked bottle served as a negative control, while a sealed bottle served as a positive one. The results were analyzed using the formula:

$$\text{WVTR (g/m.h)} = \frac{(w_1 - w_2)}{A \times T} \quad (3)$$

where  $A$  represents the hydrogel membranes' permeation area( $m^2$ )[17].

### 3.6.10. Gel Fraction

For gel fraction analysis, samples were cut into  $1 \times 1 \text{ cm}^2$  pieces. The sample's initial weight was recorded. The sample was then placed in an oven until it attained a constant weight ( $w_1$ ). The hydrogels were immersed in distilled water for four days each. The samples were then removed from the water and dried in an oven at a constant temperature of 30°C until a constant weight ( $w_2$ ) was reached. The percentage of gel fraction (GF) was calculated using the following equation [121]:

$$\text{GF (\%)} = \frac{w_2}{w_1} \times 100 \quad (4)$$

### 3.6.11. Porosity

The prepared membrane porosity and density were estimated using Archimedes' rule [122]. Ethanol was used as a displacement fluid. Measuring the weight of a beaker containing a specific volume of displacement fluid ( $w_1$ ). The sample weight ( $w_s$ ) was noted, and the sample was immersed in ethanol. The weight of the beaker was measured again ( $w_2$ ) after complete saturation. Afterward, the hydrogels were taken out of the beaker, and their mass was determined ( $w_3$ ). Following are the equations that were utilized to carry out the calculations:

$$V_s = \frac{W_2 - W_3 - W_s}{\rho_h} \quad (5)$$

$$V_p = \frac{W_1 - W_2 - W_s}{\rho_h} \quad (6)$$

$$\rho_s = \frac{W_s \rho_h}{W_1 - W_2 + W_s} = \frac{W_s}{V_s} \quad (7)$$

$$C = \frac{W_2 - W_3 - W_s}{W_1 - W_3} = \frac{V_s}{V_p + V_s} \quad (8)$$

where  $v_s$  is the specimen volume (ml),  $v_p$  is the pores volume(ml),  $\rho_s$  is the specimen density (g/ml),  $\rho_h$  is the fluid density being displaced (g/ml), and  $C$  is the specimen porosity

### 3.6.12. Swelling Behaviour

Hydrogel membrane's swelling behavior was also calculated. Samples were cut into 1cm x 1cm size. The sample's initial dry weights were recorded ( $w_d$ ). Phosphate buffer saline and distilled water were then used to submerge the specimens. The acidity or basicity of each solution was measured. The samples were collected and weighed daily for five days ( $w_s$ ). The swelling ratio (SR) was obtained using the equation as follow[123]:

$$SR (\%) = \frac{W_s - W_d}{W_d} \times 100 \quad (9)$$

### **3.6.13. Biodegradability**

To evaluate the extent of degradation, a biodegradability test was performed. Thus, 1cm x 1cm size of pre-weighed samples were buried in soil. pH of the soil is 8.02 and its texture is slit loam. The weight loss of each membrane was measured every week for continuous seven weeks[47].

### **3.6.14. Cytotoxicity Assay**

To evaluate the cytotoxicity of the membranes synthesized with copper oxide and silver nanoparticles at various concentrations, HEK-293 cells were used. The cells were obtained from ATCC (Manassas, VA) and cultured in DMEM medium supplemented with 10% FBS and 0.5% Penstrep (10,000 U/mL Penicillin, 10 µg/mL Streptomycin) to avoid bacterial contamination. The cell culture was conducted under controlled conditions of 37°C, 5% CO<sub>2</sub>, and 95% air until the cells reached the logarithmic growth phase. Triplicate samples were prepared for each concentration. After 24 hours of incubation, the culture medium was removed, and 100 µL of medium containing MTT dye (final concentration: 250 µg/mL) was added to each well. Following a 3-hour incubation period, formazan particles were formed. These particles were dissolved in 70 µL of DMSO, and the absorbance was measured at 580 nm.

### **3.6.15. Antibacterial Activity**

The agar disc diffusion method was utilized to test the antibacterial activity of the hydrogel membranes against Gram-positive *Staphylococcus aureus* and Gram-negative *Escherichia coli*. The bacterial strains were grown in broth and kept at a temperature of 37 °C. Agar and distilled water were combined to create agar media, which was then placed into petri dishes and allowed to set. After spreading the bacterial strains over the agar surface, 6mm hydrogel membrane discs were added on top. The petri dishes were kept at 37°C for 24 hours of incubation. With CVN12 membrane serving as the negative control and gentamicin serving as the positive control, the diameter of the zone of inhibition was assessed.

## 3.7. In-Vivo Wound Healing Experiment

### 3.7.1. Experimental Protocol

Male Wister rats were utilized as the animal model to investigate the efficacy of the synthesized hydrogel membrane in promoting wound healing. The rats were divided into four groups: (i) untreated, (ii) control group treated with gauze immersed in saline solution, (iii) CVN12 group treated with PVA/chitosan/vanillin/NC 12% hydrogel membrane, and (iv) CNP2 group treated with PVA/chitosan/vanillin/NC 12%/NPs 2mg hydrogel membrane. Each group consisted of three rats. The rats were housed in metabolic cages with a hygienic environment and provided with a balanced diet and water.

### 3.7.2. Full Thickness Wound Excision

For the wound creation, a Full Thickness Excision Wound Model was employed. Prior to the incision, the dorsal side of the rats was shaved using a hair clipper to remove the hairs. Rats were mildly sedated with anesthesia, and a secondary burn and wound of approximately  $1 \pm 0.2$  cm in diameter were created using a modified method based on previous study[121]. An aluminium rod was heated and applied to the shaved area for 10 seconds. Once the wound was created, dressings were applied, and hydrogel membranes were fixed in place using adhesive tape.

### 3.7.3. Pro-Healing Parameters

The healing progress was measured periodically on days 1, 3, 6, 9 and 11 until complete healing occurred. A transparent sheet was used to trace the wound, and wound healing efficiency was calculated using the formula mentioned in the following equation:

$$\text{Wound Healing Efficiency (\%)} = \frac{W_i - W_f}{W_i} \times 100 \quad (10)$$

where,  $W_i$  = diameter of wound at the time of incision (cm)

$W_f$  = diameter of wound at the respective day (cm)

The wound healing process was evaluated in terms of pro-healing parameters and monitored at regular intervals.

## Chapter 4:

### Results and Discussions

This chapter discusses the results of various experiments conducted in this project. The results are subjected to the objectives of the project and the objectives are

- a) To synthesize nanocellulose and analyze the effect of different concentrations in polymeric hydrogel in terms of thermal and mechanical stability.
- b) To synthesize copper oxide and silver nanoparticles.
- c) To synthesize a polymeric hydrogel incorporating nanocellulose and CuO-Ag nanoparticles
- d) To analyze the effect of nanocellulose and CuO-Ag NPs incorporated in hydrogel for wound dressing application.

#### 4.1. X-Ray Diffraction Analysis (XRD)

##### 4.1.1. Nanocellulose and NC incorporated membranes

X-ray diffractograms of pure NC and CVN with various concentrations of NC were used to assess the crystallinity of the formed membranes. Fig. 28 depicts the XRD patterns of all formulated membranes. Two peaks were found in Fig. 28(a), one at  $2\theta = 20.1^\circ$  corresponding to the (101) crystal plane of cellulose I, a common cellulose allomorph. The peak at  $2\theta = 43.5^\circ$  corresponds to the cellulose I (102) crystal plane. This peak is frequently utilized to evaluate the crystal orientation of the hydrogel membrane's cellulose fibrils.[120]. In Fig. 28(b), the XRD pattern of hydrogel membrane was shown, diffraction peak at  $2\theta = 19.6^\circ$  indicates presence of pure PVA which depicts hydrogen bonding that occurs between the hydroxyl groups of the PVA chains. It refers to the crystallographic plane. The peak at  $2\theta = 43.3^\circ$  refers to the presence of chitosan/vanillin blend. The peak at around  $2\theta = 20^\circ$  indicates presence of nanocellulose[124]. The peak appeared at  $2\theta = 44^\circ$  is due to increase in concentration of NC.

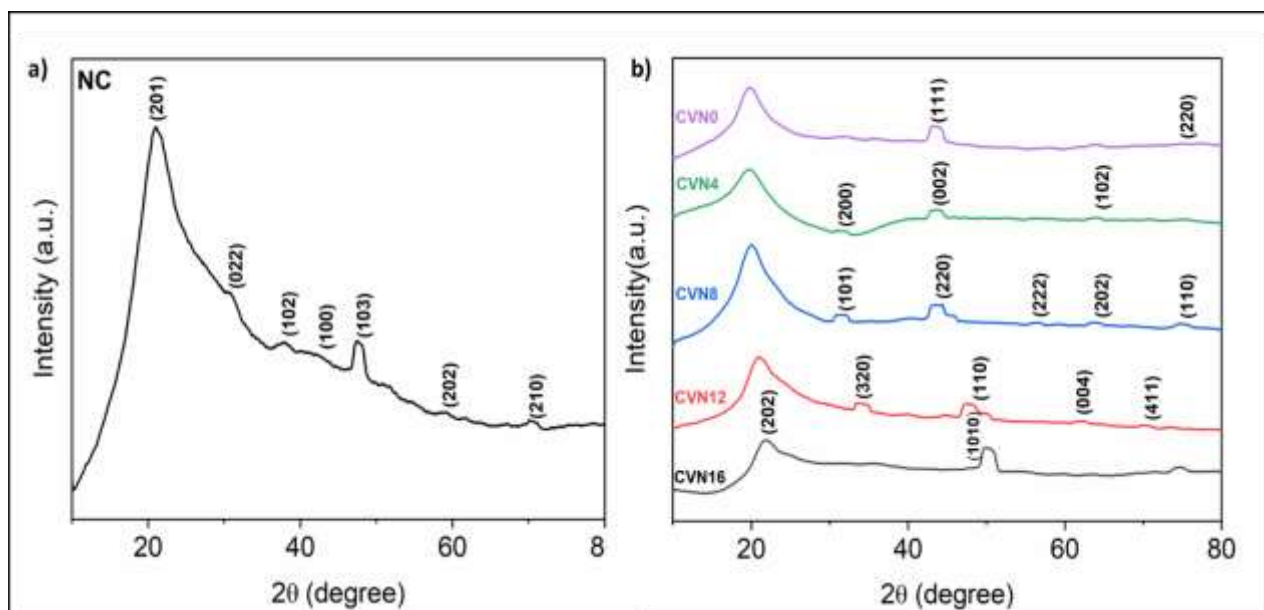


Figure 28: XRD Analysis of (a) Nanocellulose and (b) hydrogel membranes with varying NC compositions

#### 4.1.2. CuO-Ag NPs and NPs incorporated membranes

The structural study of synthesized CuO-Ag NPs was performed using X-ray diffraction analysis, as shown in Fig. 30(c). The diffraction peaks were observed at  $2\theta = 38.73^\circ$ ,  $44.49^\circ$ ,  $48.60^\circ$ ,  $57.47^\circ$ ,  $64.21^\circ$ , and  $76.43^\circ$ , corresponding to the diffraction planes (1 1 1) of Ag and CuO, (200) of Ag and CuO, and (220) of Ag and CuO respectively, which were in agreement Baker, Olga[125] and confirms the successful fabrication of CuO-Ag NPs. The X-ray diffraction patterns of the composite membranes with varying concentrations of CuO-Ag nanoparticles are shown in Fig. 30. The XRD patterns for all the membranes are presented in Fig.30 (d) show the presence of broad peaks centered around  $2\theta = 20\text{-}30^\circ$ , which indicate the amorphous nature of the composite membranes.

However, a few characteristic peaks can be observed for each membrane, which can be attributed to the crystalline nature of some of the components. For example, the peak observed at  $19.8^\circ$  for the CVN12 membrane can be assigned to the (110) plane of chitosan. Similarly, the peak observed at  $17.2^\circ$  for the CNP0.5 membrane can be assigned to the (101) plane of CuO.

Interestingly, a shift in the peak positions can be observed with increasing concentrations of CuO-Ag nanoparticles. For example, the peak observed at  $18.45^\circ$  for the CNP1 membrane

shifts to  $13.6^\circ$  for the CNP1.5 membrane and further to  $13^\circ$  for the CNP2 membrane. This peak shift can be attributed to the changes in the crystal structure of the composite membranes with increasing concentrations of CuO-Ag nanoparticles. Furthermore, the peak intensities also show a gradual increase with increasing concentrations of CuO-Ag nanoparticles. This increase in peak intensities can be attributed to the increased crystallinity of the composite membranes with increasing concentrations of CuO-Ag nanoparticles. Similar results were obtained by Gobi and Babu[126] in their study as well, where increasing contents of NPs in Chitosan/PVA membrane shown increase in peak intensities.

## **4.2. Fourier Transform Infrared Spectroscopy (FTIR)**

### **4.2.1. Nanocellulose and their incorporated membranes**

The FTIR spectra of NC and CVN with varying NC compositions was shown in Fig. 29. The peak at  $3434\text{ cm}^{-1}$  in Fig. 29(a) corresponds to the O-H stretching vibration of cellulose and absorbed water. The C=C stretching vibration of the aromatic ring in cellulose corresponds to the peak at  $1634\text{ cm}^{-1}$ . In the FTIR spectra of CVN0, the O-H stretching peak at  $3440\text{ cm}^{-1}$  and the  $sp^3$  hybridized aromatic C-H stretching peak at  $2925\text{ cm}^{-1}$  can be detected in Fig. 29(b).[17]. The  $1614\text{ cm}^{-1}$  peak in the FTIR spectrum of CVN4 is due to C=O stretching[115]. The peak at  $1412\text{ cm}^{-1}$  showed the bending vibrations of C-H and CH<sub>2</sub> bonds[127]. The peaks at  $1120$  and  $1040\text{ cm}^{-1}$  result from CH and CO stretching, respectively[128]. O-H stretching accounts for the peak at  $3420\text{ cm}^{-1}$  in the FTIR spectrum of CVN8, while C-H stretching accounts for the peak at  $2922\text{ cm}^{-1}$ . This indicates that the available hydroxyl groups on the chitosan molecule can potentially form crosslinks with vanillin[17]. At  $1630\text{ cm}^{-1}$  in the FTIR spectrum of CVN8, the amine band appeared due to vibration. Vanillin interacted with hydroxyl and amino groups in the chitosan matrix, proving the presence of these groups[129]. The C-O stretching vibration is responsible for the peak at  $1247\text{ cm}^{-1}$ . The creation of hydrogen bonds between PVA and NC is responsible for the lowering in the peak. [130]. In FTIR spectrum of CVN12, the peak at  $1261\text{ cm}^{-1}$  is due to C-C stretching of PVA. C-O stretching is responsible for the peak at  $1629\text{ cm}^{-1}$ [131]. The C=O stretching peak in the FTIR spectrum of CVN16 is at  $1632\text{ cm}^{-1}$ . The peak at  $3424\text{ cm}^{-1}$  is O-H bonds[132].

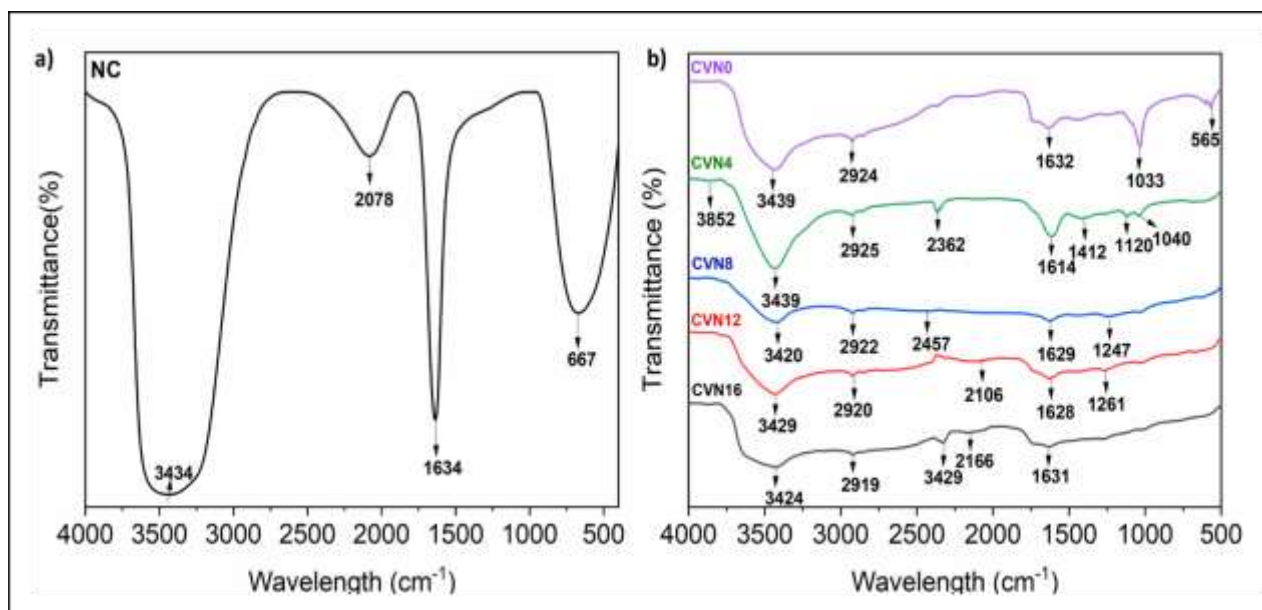


Figure 29: FTIR Spectrum of a) NC and b) hydrogel membranes with varying NC compositions

#### 4.2.2. CuO-Ag NPs and their incorporated membranes

The PVA-Chitosan composite membranes crosslinked with vanillin and incorporated with NPs showed characteristic peaks in Fig. 30(b) indicating the presence of its constituents and successful blending of polymers. Peaks at 3450 cm<sup>-1</sup> (O-H stretching), 2945 cm<sup>-1</sup> (C-H stretching), and 2170 cm<sup>-1</sup> (C=O stretching) indicated the presence of PVA, while peaks at around 1650 cm<sup>-1</sup> (amide-1 bending) and 1250 cm<sup>-1</sup> (C-H bending) indicated the presence of chitosan[133]. The overlapped peaks of nanocellulose were also observed at 3300 cm<sup>-1</sup> (O-H stretching), 2900 cm<sup>-1</sup> (C-H stretching), and 1050 cm<sup>-1</sup> (C-O stretching)[114].

The nanoparticles also showed their characteristic peaks in Fig. 30(a), such as for CuO, the peaks observed at 630 cm<sup>-1</sup> (Cu-O bending) and 1057 cm<sup>-1</sup> (Cu-O stretching)[134]. For Ag NPs, the overlapped peaks observed at 1636 cm<sup>-1</sup> (N-H bending) and 1400 cm<sup>-1</sup> (C=C stretching)[135]. As the concentration of the NPs increased, the peaks became sharper, indicating a higher concentration of NPs in the composite membrane. The regular bonds of constituents in composites show that the addition of filler, crosslinker and NPs shown no significant influence on chemical structures i.e., no chemical bonding formed during the blending, Mhatre, Bhagwat[136] observed similar conclusions. The results show the successful fabrication of composite membranes, with the different peaks indicating the presence of the constituent materials and NPs.



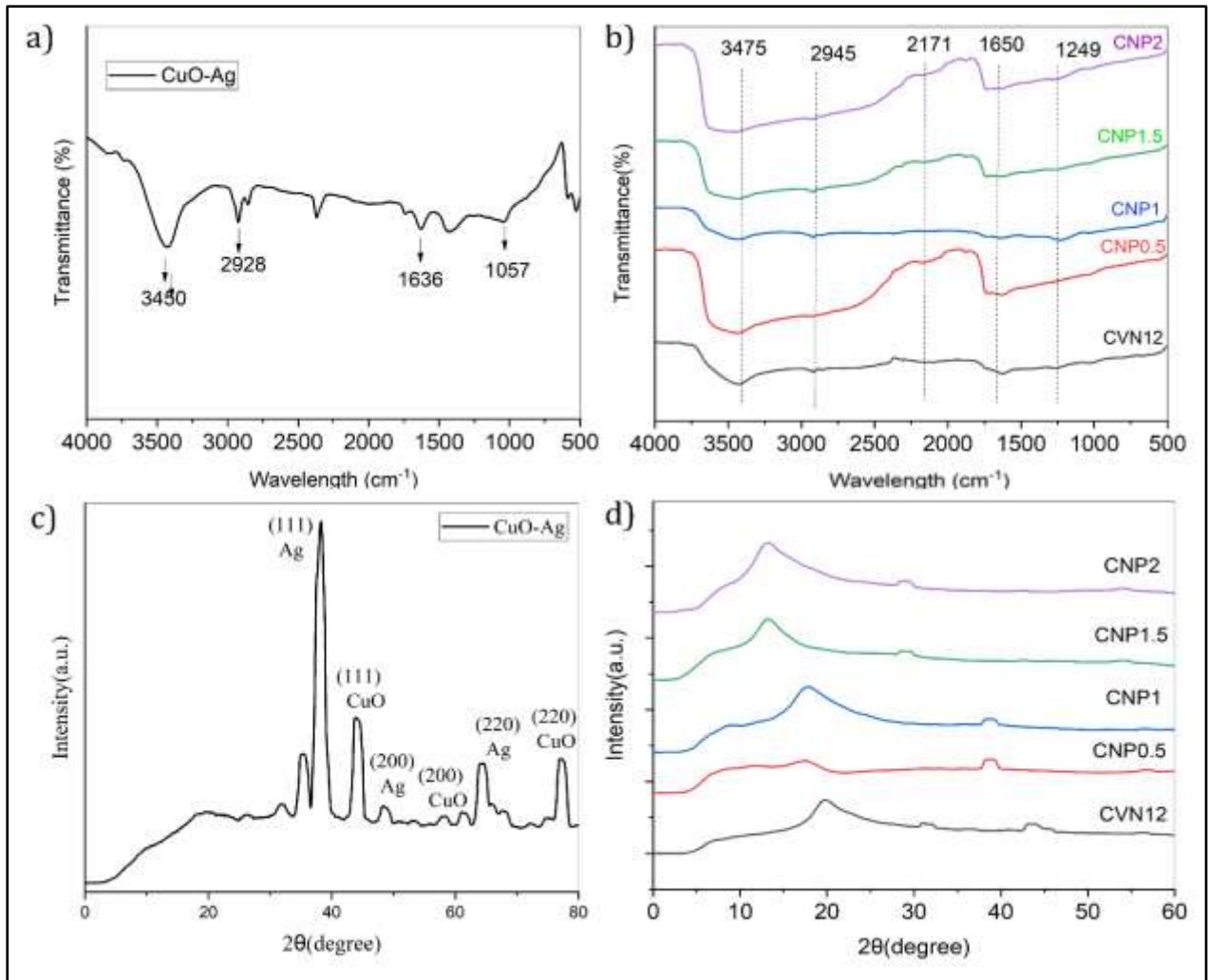


Figure 30: FTIR spectra of (a) CuO-Ag nanoparticles and (b) composite membranes, as well as XRD patterns of (c) CuO-Ag nanoparticles and (d) composite membranes.

### 4.3. Scanning Electron Microscopy (SEM)

#### 4.3.1. Nanocellulose incorporated membranes

SEM analysis was used to investigate the surface morphology and cross-section of formulated membranes. SEM results were shown in Fig. 31. In Fig.31(a) results showed that hydrogels become dense after the addition of nanocellulose, and no pores were found. In Fig. 31(b and c) it can be seen from results that the surfaces become rough with addition of nanocellulose. Nanocellulose (NC) was visible as a collection of tiny white dots that were dispersed throughout the sample[137]. On the surface of the formed membrane, a void of pores was observed. The addition of NC had a synergistic impact, resulting in a more uniform output. Therefore, it can be concluded that the surface of CVN membranes is affected by

incorporating NC into the main polymer matrix. It is revealed that surface of film with 0.3gm of vanillin shows compact structure[129].

The cross-sectional surface of CVN hydrogel membranes with varying NC compositions were also examined. Even distribution of NC can be seen in Fig. 31. The distribution of NC in CVN hydrogel membranes has a significant impact on the mechanical properties of nanocomposite membranes[130].

EDX results depict unique amounts of energy released by atoms of each element during transfer. Elemental analysis shown in Fig.31. Analysis of CVN membranes through EDX spectrophotometer confirmed the presence of C, N and O. The analysis confirmed that CVN0 membrane contains 57.9% C, 4% N and 42.1% O. Similarly, CVN12 membrane contains 54.8% C, 5.5% N and 39.7% O and CVN16 contains 51.9% C, 5.1% N and 43% O.

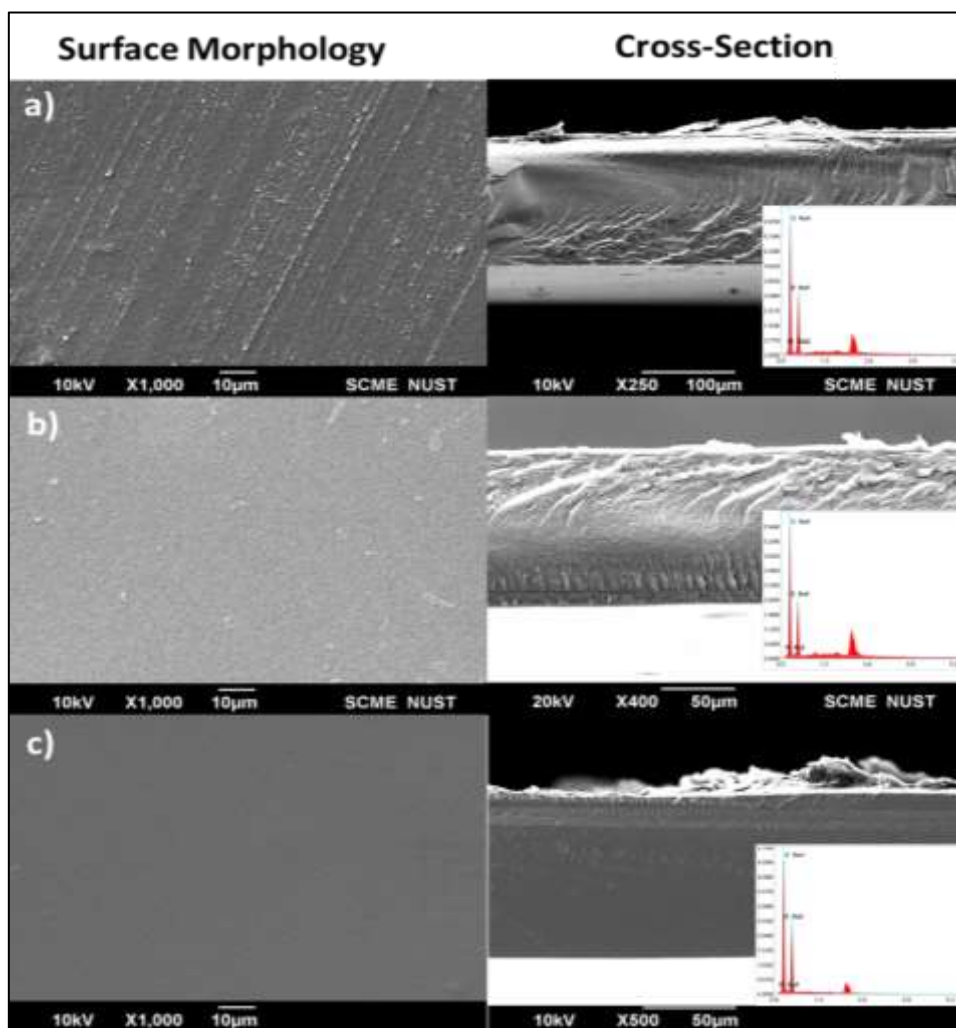


Figure 31:SEM images of surface and cross section of a) CVN0, b) CVN12, c) CVN16

### 4.3.2. CuO-Ag NPs and their incorporated membranes

The morphology and surface structure of the fabricated PVA-Chitosan composite membranes crosslinked with vanillin and incorporated with CuO-Ag NPs were investigated using scanning electron microscopy (SEM) and energy-dispersive X-ray spectroscopy (EDX). The SEM image and EDX of synthesized nanoparticles of copper oxide and silver are depicted in Fig32. (a-b).

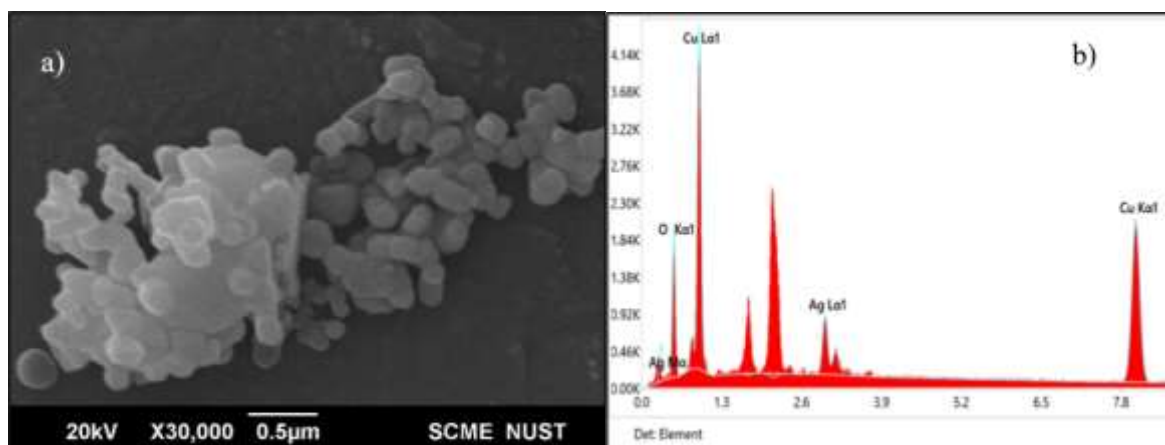


Figure 32: Copper oxide and silver nanoparticle blend a) SEM image b) EDX

The SEM images of the fabricated membranes are shown in Fig. 33 (a-e), and it can be observed that the membrane surface appeared compact and without any pores at magnifications up to 1000x which shows the excellent compatibility of PVA and Chitosan polymer. The membrane without NPs had a poreless, rough surface structure. However, as the concentration of NPs increased, the surface became rougher, this may be due to the well dispersion of NPs in the matrix which is also observed by Yang, Ren [138], but upon further increasing the NP concentration, the surface became smooth and more compact. This indicates the homogeneity and uniformity of the fabricated membranes also indicated by Gobi and Babu [126].

Furthermore, the EDX analysis was performed to determine the elemental composition of the fabricated membranes. The results, as shown in Fig. 33(f-j) indicated unique amounts of energy released from atoms of every element during the transfer. The analysis of the CVN membranes through the EDX spectrophotometer confirmed the presence of carbon, nitrogen, oxygen, copper, and silver. It was also found that the weight percentage of Cu and Ag indicated a positive correlation between concentration and the observed increase of NPs.

EDX analysis confirmed the presence of the desired elements in the composite membranes. These results suggest that the fabricated membranes have potential applications in various fields, including wound dressing, water purification and separation processes.

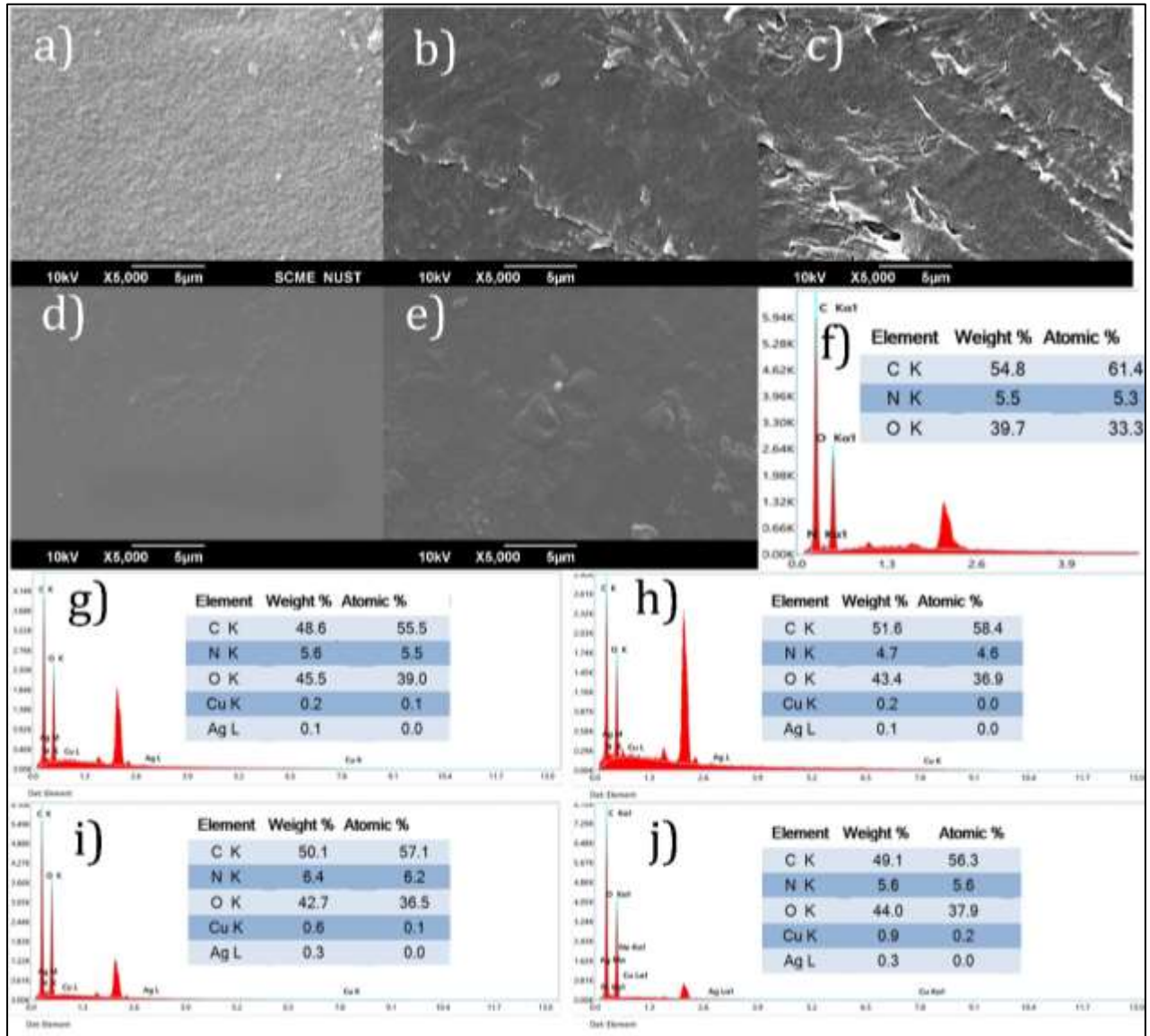


Figure 33: SEM images and EDX analysis of CVN12, CNP0.5, CNP1, CNP1.5, and CNP2 membranes. (a-e) SEM images showcasing the surface morphologies and nanoparticle distributions of the membranes respectively. (f-j) EDX analysis displaying the elemental composition and distribution across the membrane surface respectively.

## 4.4. Mechanical Properties

### 4.4.1. Nanocellulose incorporated membranes

The key benefit of incorporating nanocellulose in hydrogel membrane was to improve its mechanical strength[139]. Tensile tests showed that polymers and nanocellulose interact with each other at the interface. The results were presented in Fig. 34.

The inclusion of NC was found to improve the failure strength of hydrogel membranes. When nanocellulose is incorporated into the hydrogel membrane, it forms a strong network of intermolecular hydrogen bonds and entanglements that provide additional mechanical strength to the membrane[128]. Tensile strength improves as the amount of nanocellulose increases in hydrogel membrane. Maximum tensile stress was shown with 12% concentration of NC i.e.  $50\text{N/mm}^2$ . Due to agglomeration and PVA crystallinity, mechanical properties decline with increasing nanocellulose concentrations. Higher concentrations of nanocellulose resulted in lower breaking stress values. In case of 16% NC concentration, tensile stress is  $24\text{N/mm}^2$ . It could be because of the elevated amount of NC in the PVA matrix, which could make it stick together more quickly. Overall, PVA film crystallinity also improved with increased nanocellulose concentration. Too much nanocellulose would make it hard for the PVA matrix to stick together, which reduce mechanical strength of membrane[114].

The Young's modulus values for the CVN0, CVN4, CVN8, CVN12 and CVN16 membranes were found to be 0.2143, 0.5225, 0.5038, 0.5406 and 0.14860 respectively.

The hydrogel membrane's elongation at break increases with the addition of NC. This improvement may be attributed to an increase in the spacing between the polymeric chains that occurs when NC was incorporated. The elongation at break results for hydrogel membranes were presented in Fig. 34. The maximum elongation break was found in the case of 12%NC i.e., 94%. As a result of interaction between PVA chains and NC, the stiffness and mechanical properties were improved.

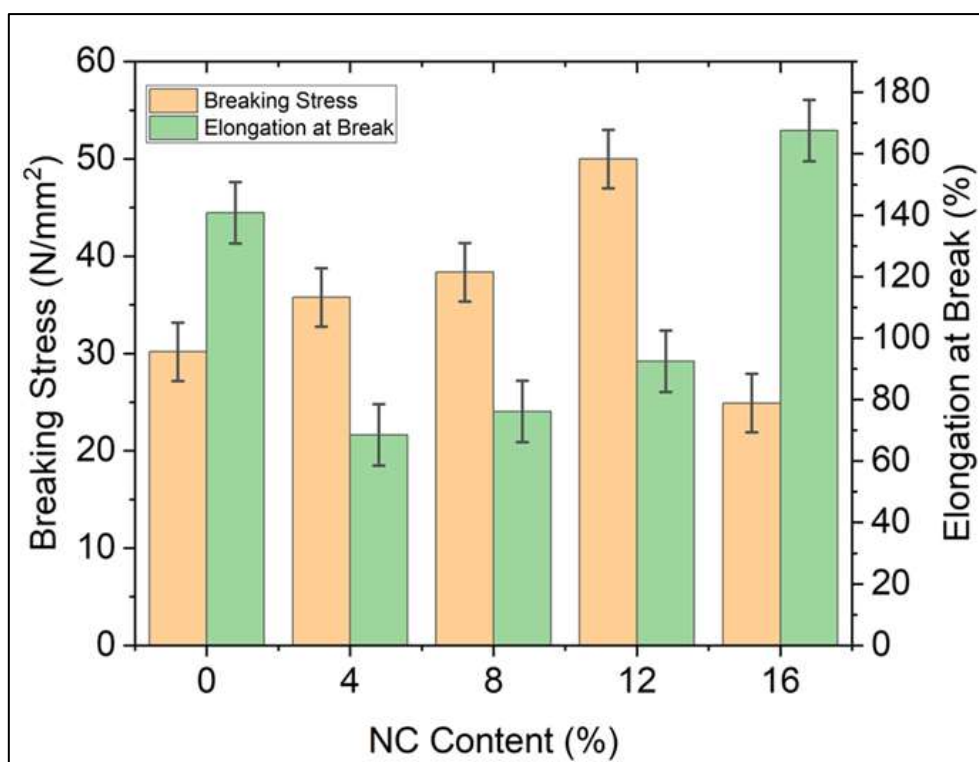


Figure 34: Mechanical properties of hydrogel membranes with varying NC compositions

#### 4.4.2. CuO-Ag incorporated membranes

The stress-strain graph for each membrane is shown in Fig.35. The stress values for the CVN0, CVN12, CNP0.5, CNP1, CNP1.5, and CNP2 membranes were found to be  $30.18 \pm 1.02$ ,  $49.985 \pm 2.31$ ,  $37.605 \pm 1.56$ ,  $34.325 \pm 2.225$ ,  $24.065 \pm 2.02$ , and  $21.120 \pm 3.012$  MPa, respectively. The corresponding strain values were 140.86, 92.455, 86.315, 79.44, 37.9, and 27.08%.

The slope of the linear section of the stress-strain curve was used to compute the Young's modulus values. The Young's modulus values for the CVN0, CVN12, CNP0.5, CNP1, CNP1.5, and CNP2 membranes were found to be 0.2143, 0.5406, 0.4357, 0.4321, 0.6350, and 0.5163 respectively.

According to the data, the inclusion of CuO-AgNPs resulted in an increase in the stress and Young's modulus values of the membranes. This is due to the nanoparticles improving intermolecular interactions between the polymer chains, resulting in a stronger and more compact structure. However, the strain values decreased with the addition of nanoparticles, indicating that the membranes became more brittle, similar trends were observed by Malik,



Duan [140] and Yang, Ren [138] that upon increasing the concentration of NPs, the extended flow of polymer chains lowers the plasticity of hydrogel membranes making them little brittle. Studies show that the breaking stress to disrupt the human skin is 35MPa [141], which is comparable to the mechanical strength of presented membranes, hence these membranes are competitive candidates to be utilize as reliable dressing materials.

The highest stress and Young's modulus values were observed for the CNP1.5 membrane, which had a CuO-AgNPs concentration of 1.5 mg/g. This suggests that an optimal concentration of nanoparticles can improve the mechanical properties of the membranes.

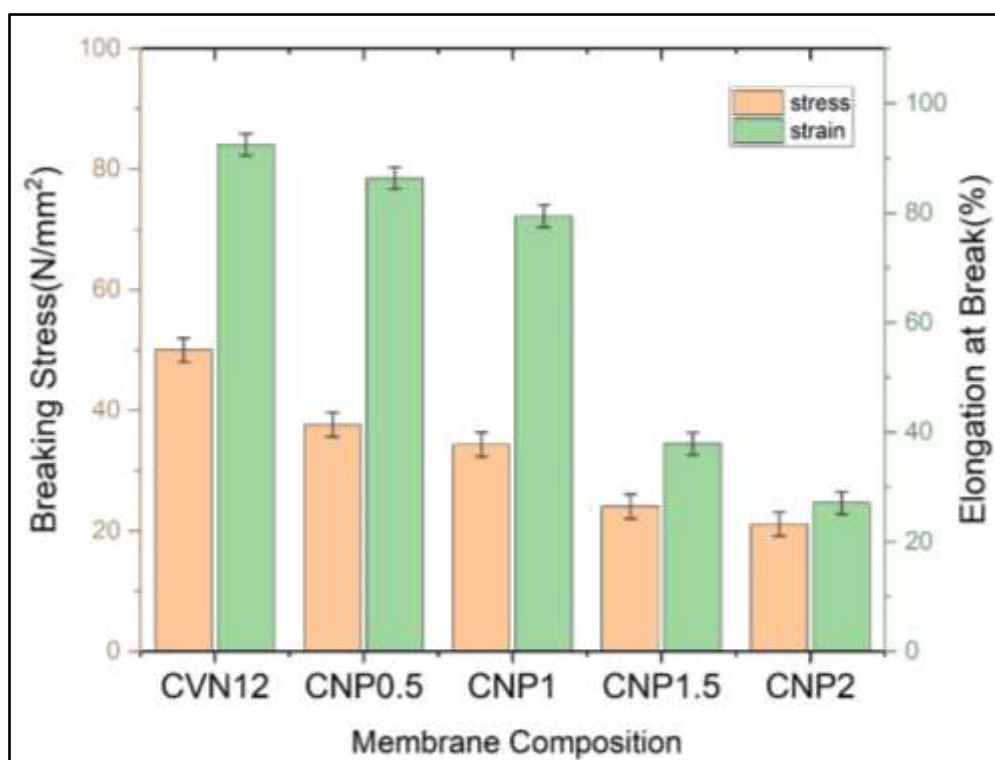


Figure 35: Mechanical properties of hydrogel membranes with varying CuO-Ag NP compositions

## 4.5. Thermogravimetric Analysis (TGA)

### 4.5.1. Nanocellulose incorporated membranes

The thermal behavior analysis of Chitosan/Vanillin/PVA hydrogel membrane with different NC concentration was studied using TGA and results were shown in Fig. 36. The weight loss percentage and derivative of weight loss percentage was recorded against temperature. Thermal degradation was recorded in three stages.

In the case of CVN0, it was observed that during the stage 1, the weight loss was in the region of 30 to 115°C which was caused by the loss of weakly bounded moisture on membrane surface due to evaporation[115]. The weight loss in this region was around 5%. The weight loss in the region of 117 to 214°C showed thermal degradation of vanillin[139]. Here the weight loss was 8%. In the second stage, thermal degradation was observed from 214 to 366°C. This was due to thermal degradation of PVA and chitosan. The weight loss in this case was 49%. In final stage of degradation, which occurred after 366°C was due to carbonization of components present in nanocomposite membrane[130]. The weight loss in this case was 19%. So total mass loss was 81%.

In the case of CVN4, slight change was observed in thermal degradation of hydrogel membrane. The weight loss due to evaporation was 7%. Weight loss due to degradation of vanillin was 6%. During the stage 2, weight loss due to thermal degradation of PVA and chitosan was 47%. During the third stage, weight loss due to carbonization of components was 19%. So, the total mass loss was 79%.

In the case of CVN8, during the stage 1, weight loss due to evaporation was 6%. Thermal degradation of vanillin was 5%. During the second stage of degradation, weight loss due to PVA and chitosan degradation was 47%. In the third stage, thermal degradation due to carbonization of components was 15%. So, the total mass loss was 73%.

In the case of CVN12, during the first stage, thermal degradation due to evaporation was 5%. Thermal degradation due to vanillin was 6%. During the second stage, weight loss due to thermal degradation of PVA and chitosan was 43%. In the third stage, weight loss due to carbonization of components was 14%. So, the total mass loss was 68%.

In the case of CVN16, during stage 1, weight loss due to evaporation was 3%. Thermal degradation due to vanillin was 7%. During stage 2, weight loss due to degradation of PVA and chitosan was 48%. During the third stage, weight loss due to carbonization of components was 20%. So, the total mass loss was 78%.

So, from the results it can be deduced that with the addition of NC to hydrogel membrane, thermal stability of hydrogel membrane improved. In the case of CVN12 i.e. 12%NC composition, showed most thermally stable. With more increase of NC, thermal stability of hydrogel membrane started decreasing.



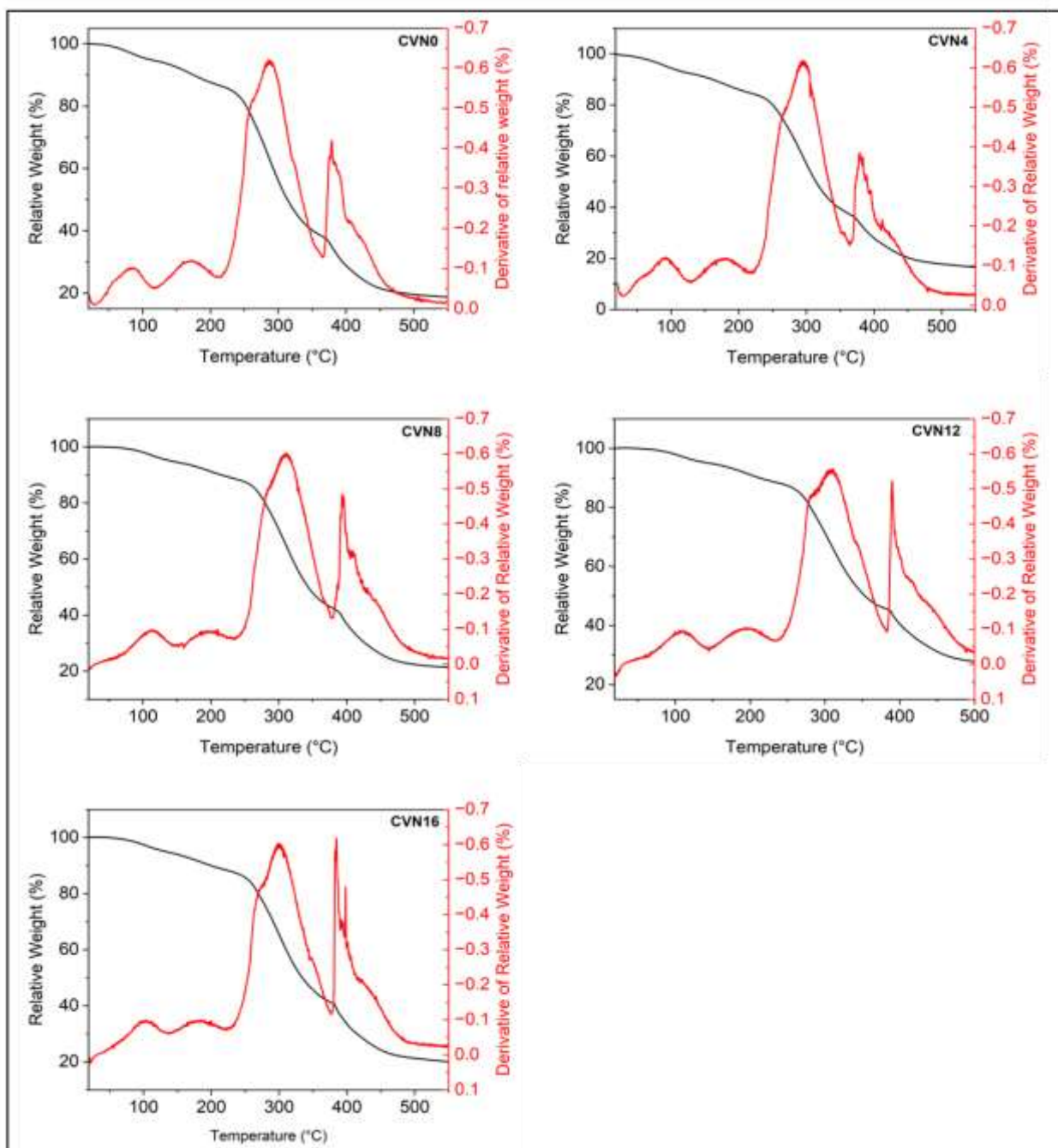


Figure 36: Thermal degradation (TGA) study of hydrogel membranes with varying NC compositions

#### 4.5.2. CuO-Ag incorporated membranes

The thermal behavior analysis of Chitosan/Vanillin/PVA/NC hydrogel membrane with different CuO-Ag NPs concentration was studied using TGA and results were shown in Fig. 37. The weight loss percentage and derivative of weight loss percentage was recorded against temperature. Thermal degradation was recorded in three stages.

In the case of CNP0.5, slight change was observed in thermal degradation of hydrogel membrane. The weight loss due to evaporation was 4%. Weight loss due to degradation of vanillin was 8%. During the stage 2, weight loss due to thermal degradation of PVA and chitosan was 44%. During the third stage, weight loss due to carbonization of components was 14%. So, the total mass loss was 70%.

In the case of CNP1, during the stage 1, weight loss due to evaporation was 5%. Thermal degradation of vanillin was 9%. During the second stage of degradation, weight loss due to PVA and chitosan degradation was 58%. In the third stage, thermal degradation due to carbonization of components was 19%. So, the total mass loss was 91%.

In the case of CNP1.5, during the first stage, thermal degradation due to evaporation was 4%. Thermal degradation due to vanillin was 10%. During the second stage, weight loss due to thermal degradation of PVA and chitosan was 58%. In the third stage, weight loss due to carbonization of components was 14%. So, the total mass loss was 86%.

In the case of CNP2, during stage 1, weight loss due to evaporation was 3%. Thermal degradation due to vanillin was 12%. During stage 2, weight loss due to degradation of PVA and chitosan was 45%. During the third stage, weight loss due to carbonization of components was 13%. So, the total mass loss was 73%.

So, from the results it can be deduced that with the addition of CuO-Ag NPs to hydrogel membrane, thermal stability of hydrogel membrane improved. In the case of CNP2 i.e. 2mg NPs composition is considered most thermally stable. With increase of NPs concentration, the stability of hydrogel membranes is seen increasing.

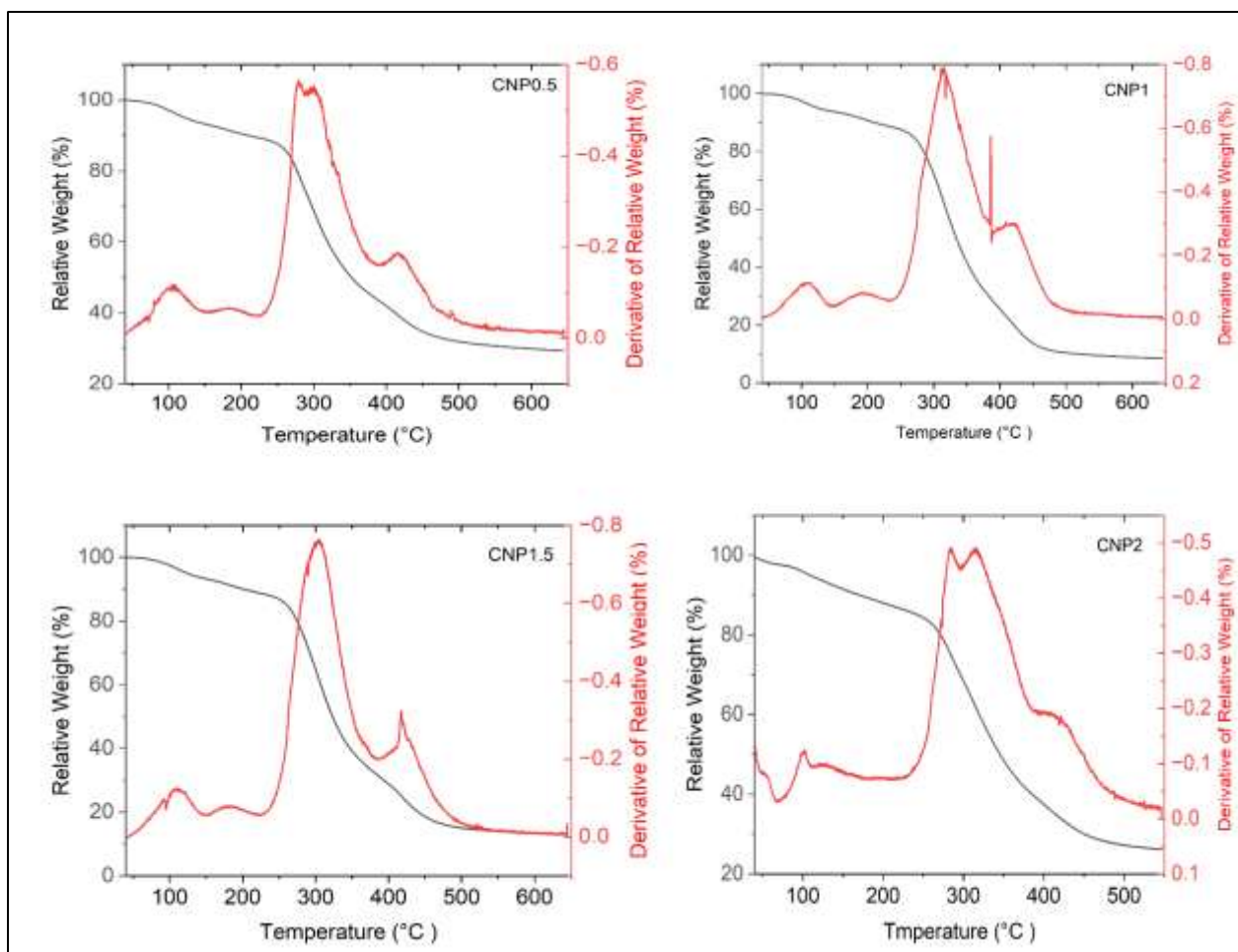


Figure 37: Thermal degradation (TGA) study of hydrogel membranes with varying CuO-Ag NPs concentration

## 4.6. Surface Roughness

### 4.6.1. Nanocellulose incorporated membranes

Surface roughness of CVN hydrogel membranes at different NC concentrations was shown in Fig. 38. Surface roughness increased drastically with increasing NC concentrations, as expected. The maximum value of surface roughness was obtained in case of 16%NC i.e. 1300nm. Since, there is a large miscibility degree difference between PVA and NC, the addition of NC can lead to the formation of a high amorphous-like structure[121]. A moderately rough surface can enhance the surface area available for cell attachment, leading to improved cell adhesion and proliferation. This may play a role in the creation of new tissue and hasten wound healing. An extremely rough surface, on the other hand, may cause damage to newly formed tissue and impede the healing process.

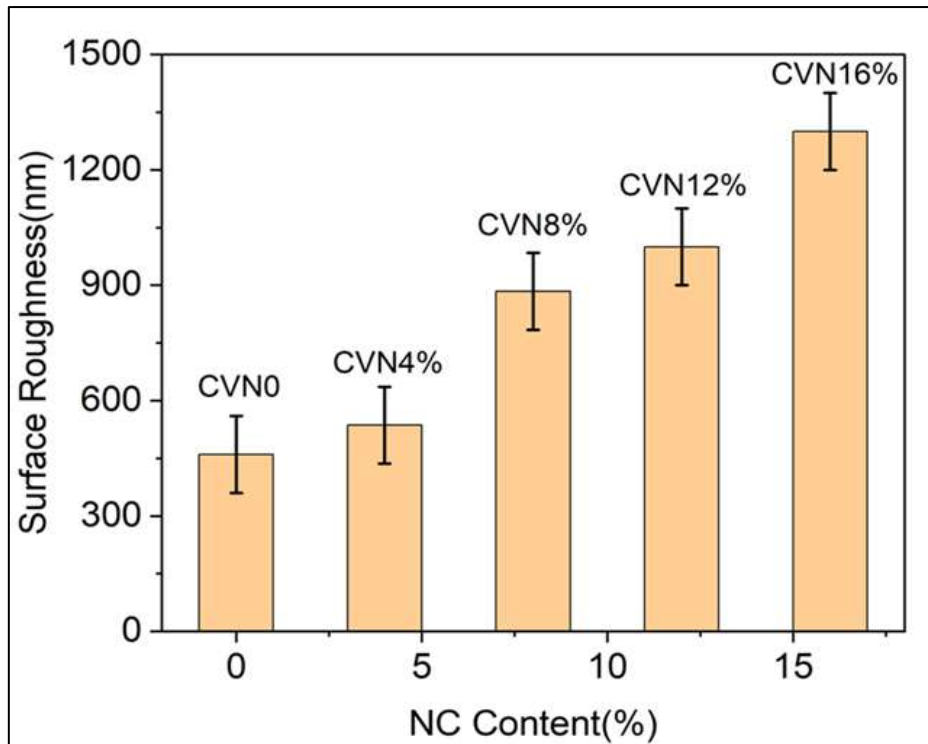


Figure 38: Surface roughness of hydrogel membranes with varying NC compositions

#### 4.6.2. CuO-Ag incorporated membranes

The surface roughness of materials plays a crucial role in determining their physical and mechanical properties, as well as their performance in various applications. In this study, the surface roughness of different samples, including CVN12, CNP0.5, CNP1, CNP1.5, and CNP2, was evaluated and presented in Fig. 39. The surface roughness values were found to be 1000 nm, 611 nm, 697 nm, 1440 nm, and 1805 nm, respectively. The incorporation of nanoparticles (NPs) in the composite membranes had a noticeable effect on the surface roughness. The roughness values increased as the concentration of NPs increased. For instance, CVN12, which did not contain any NPs, had a surface roughness of 1000 nm. In comparison, CNP0.5, CNP1, CNP1.5, and CNP2, which contained increasing concentrations of NPs, exhibited surface roughness values of 611 nm, 697 nm, 1440 nm, and 1805 nm, respectively. This suggests that the presence of NPs contributed to the formation of surface irregularities and enhanced the overall roughness of the membranes[142]. The increased roughness can be attributed to factors such as the interaction between the NPs and the polymer matrix, the formation of agglomerates or clusters of NPs on the surface, and changes in the surface morphology due to the presence of NPs. Yang, Ren[138] fabricated Chitosan-

PVA membranes and incorporated with NPs, they also reported similar results i.e., surface roughness increased upon the addition of NPs.

Understanding the surface roughness characteristics is essential for optimizing material properties and designing effective surface modifications for specific applications, such as promoting cell adhesion, improving wettability, and enhancing mechanical stability.

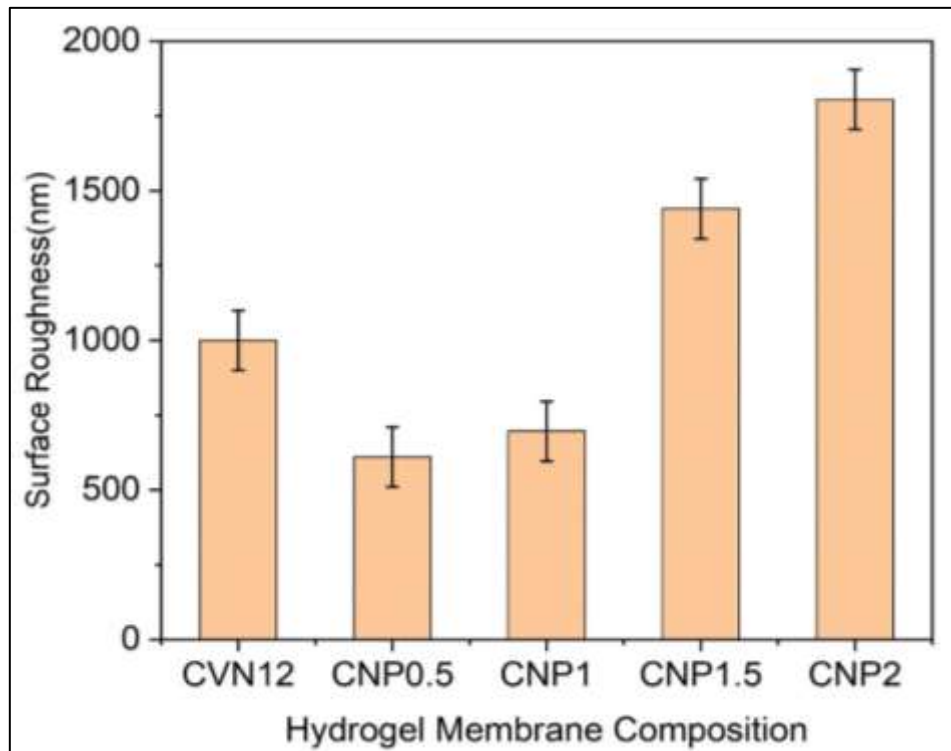


Figure 39: Surface roughness of hydrogel membranes with varying CuO-Ag NP concentration

## 4.7. Contact Angle Measurement

### 4.7.1. Nanocellulose incorporated membranes

One of the most useful structural analysis tools for characterizing hydrogel membranes is the measurement of water contact angle. Fig.40 photographically illustrates a surface covered in water droplets of CVN 0, CVN 4, CVN 8, CVN 12 and CVN 16 respectively. As a rule of thumb, hydrophilic materials have contact angles less than 90 degrees, while hydrophobic materials have contact angles greater than 90 degrees[143]. As it is observed in fig.40, pure PCV membrane exhibits  $68.5^\circ$  angle which shows hydrophilic nature. Now by addition of NC contact angle increases to  $99.7^\circ$  which exhibits its hydrophobic nature. Similarly, hydrogel

membrane with NC 8% concentration has angle of  $92.6^\circ$  showing hydrophobic nature. Hydrogel membrane with NC concentration 12% and 16% shows  $74.3^\circ$  and  $57^\circ$  angle respectively which depicts their hydrophilic nature.

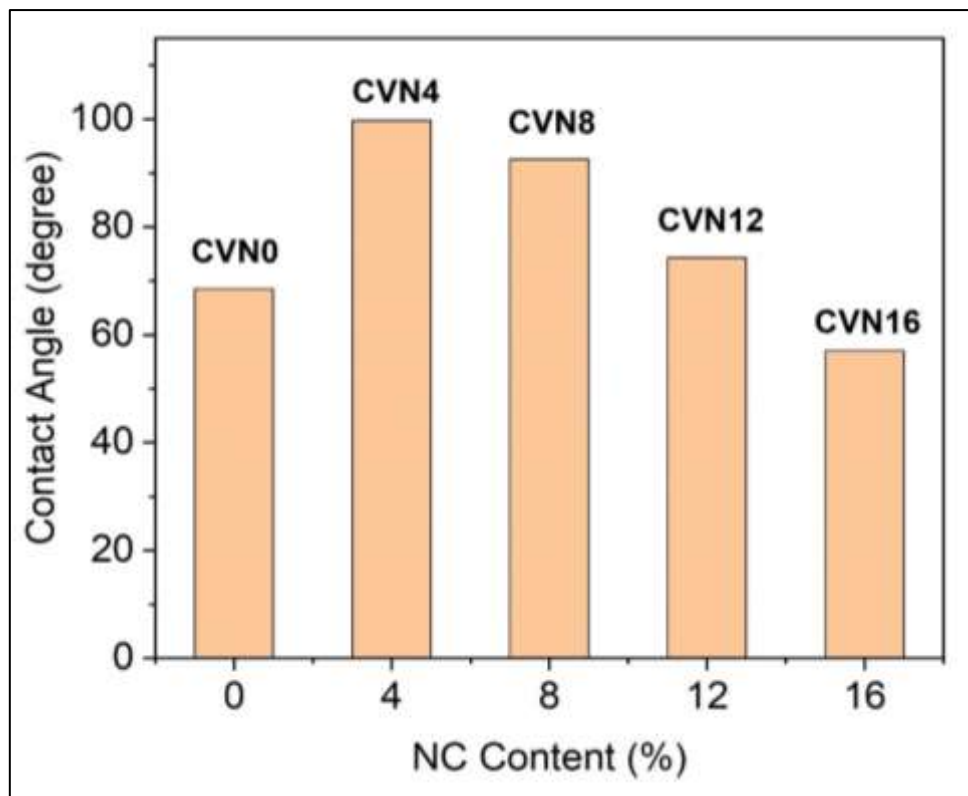


Figure 40: Contact angle measurement of hydrogel membranes with varying NC compositions

#### 4.7.2. CuO-Ag incorporated membranes

Contact angle measurements were carried to assess the hydrophilicity/hydrophobicity of the fabricated membranes and illustrated in Fig.41. The contact angle measurement results showed that the CVN12 membrane is highly hydrophobic with a contact angle of  $89^\circ$  at 0 seconds, which decreased to  $81.9^\circ$  after 120 seconds. The membranes with CuO-Ag NPs showed a decrease in contact angle compared to the CVN12 membrane. The CNP1 membrane had the lowest contact angle at both time intervals with  $44.8^\circ$  at 0 seconds and  $34.3^\circ$  after 120 seconds, indicating that it is the most hydrophilic membrane. The CNP0.5 and CNP1.5 membranes also showed a decrease in contact angle, while the CNP2 membrane showed an increase in contact angle compared to the CNP1.5 membrane. These results suggest that the addition of CuO-Ag NPs can enhance the hydrophilicity of the membranes, and the effect depends on the concentration of the nanoparticles.

The increased wettability of the membranes can be due to the decrease in contact angle with increasing time. The presence of nanoparticles in the membranes influenced their surface characteristics dramatically, as seen by the significant decrease in contact angle for the CNP0.5, CNP1, and CNP1.5 membranes which is evident by other studies as well[144, 145]. Ardebilchi Marand, Almasi[144] incorporated NiO nanoparticles in their chitosan composite membranes, the inclusion of nanoparticles (NPs) in the hydrogel membrane formulation led to a noticeable reduction in the contact angle, aligning with the outcomes observed in this investigation.

These membranes exhibited hydrophilic behavior, indicating that the addition of nanoparticles had increased their surface energy. On the other hand, the CNP2 membrane showed hydrophobic behavior, indicating that the surface energy of the membrane was decreased due to the presence of a high concentration of nanoparticles. The contact angle measurements revealed that adding nanoparticles to Chitosan/PVA membranes had a significant effect on their surface properties, which can be used in the development of water filtration membranes, drug delivery systems, and tissue engineering scaffolds.

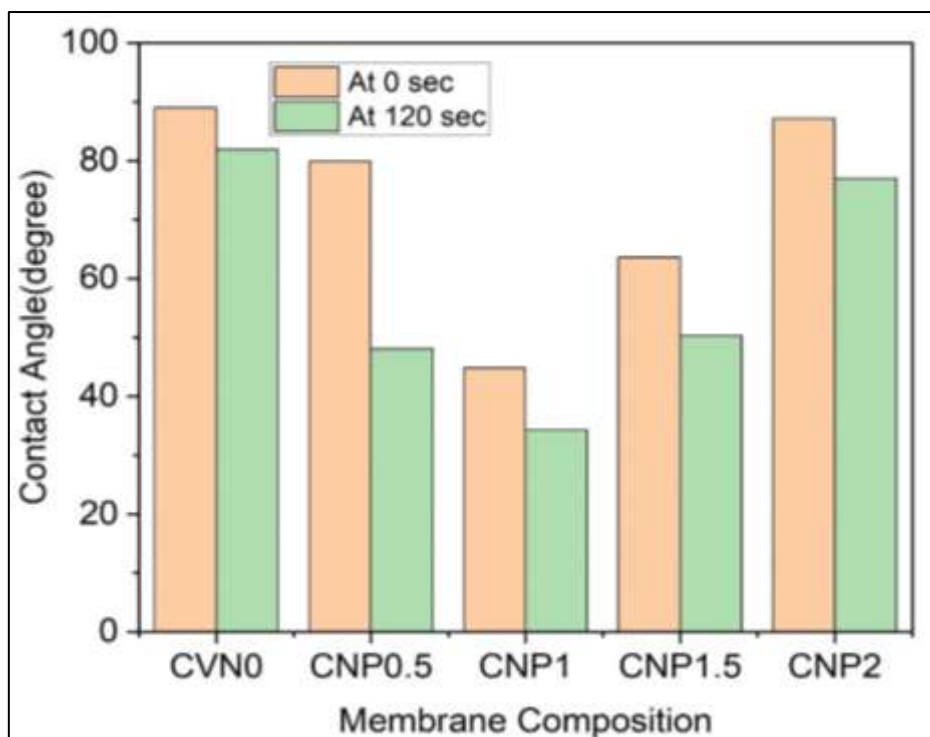


Figure 41: Contact angle measurement of hydrogel membranes with varying CuO-Ag NP concentration

## 4.8. Moisture Retention Capability

### 4.8.1. Nanocellulose incorporated membranes

Moisture retention capability is a process to determine loss of water vapor from membranes. MRC of hydrogel membrane with varying NC composition is shown in Fig. 42. The moisture retention capability of all membranes lies within the range of 94 to 95%. Hence, addition of NC in hydrogel membrane did not affect the moisture retention capability of membranes.

The excellent moisture retention capability was ascribed to the hydrophilic nature of both PVA and nanocellulose, which enables them to readily interact with water molecules and form hydrogen bonds[60]. PVA's hydroxyl group (OH) possesses the capability to absorb and retain a significant amount of moisture[21]. CVN nanocomposite membranes have been recommended for use in wound dressings, where high moisture retention is desirable to utilize hydrogel membranes effectively[146].

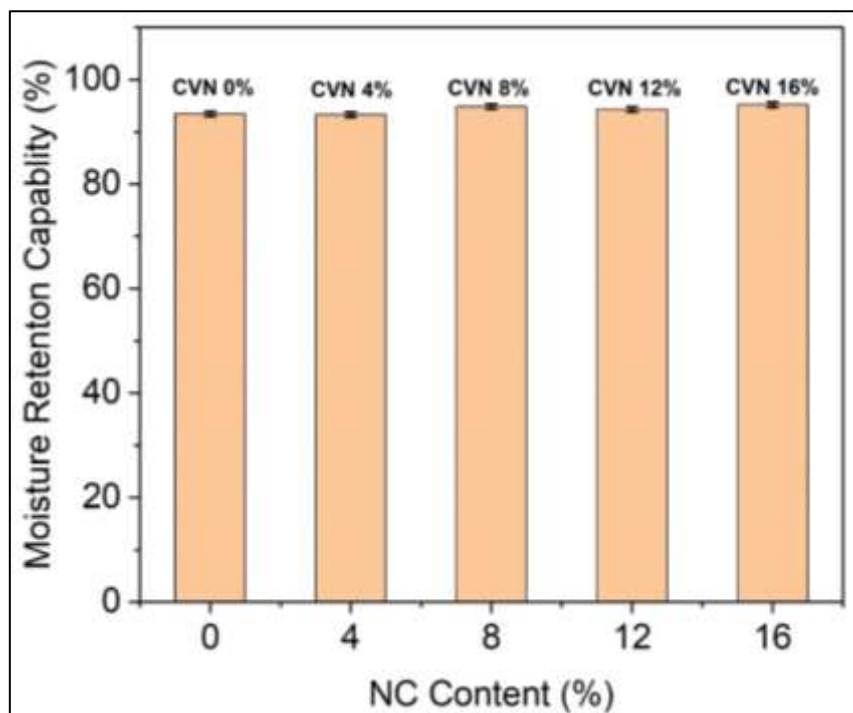


Figure 42: Moisture retention capability of hydrogel membranes with varying NC compositions



#### 4.8.2. CuO-Ag incorporated membranes

The Moisture Retention Capacity (MRC) analysis is a reliable method to assess the water holding capacity and biodegradability potential of hydrogel wound dressings. The findings of MRC analysis are depicted in Fig.43. The increase in nanoparticle (NP) concentration within the membrane led to an increase in void volume occupied by water molecules, thereby causing an increase in MRC values from 94.35% for CVN12 to 98.84% for CNP2. This could be attributable to increased hydroxyl group availability as a result of reduced polymeric chain interactions, resulting in increased water absorbance by NPs. [147]. The obtained MRC values are superior to those reported in previous studies on chitosan-based hydrogels incorporated with NPs (e.g., Affes, Maalej[148] and Hamdi, Nasri[148]).

These findings suggest that the incorporation of nanoparticles in the fabricated membranes holds great potential for wound dressing applications. These membranes promote effective wound healing without eschar formation or inflammation, making them promising candidates for clinical use.

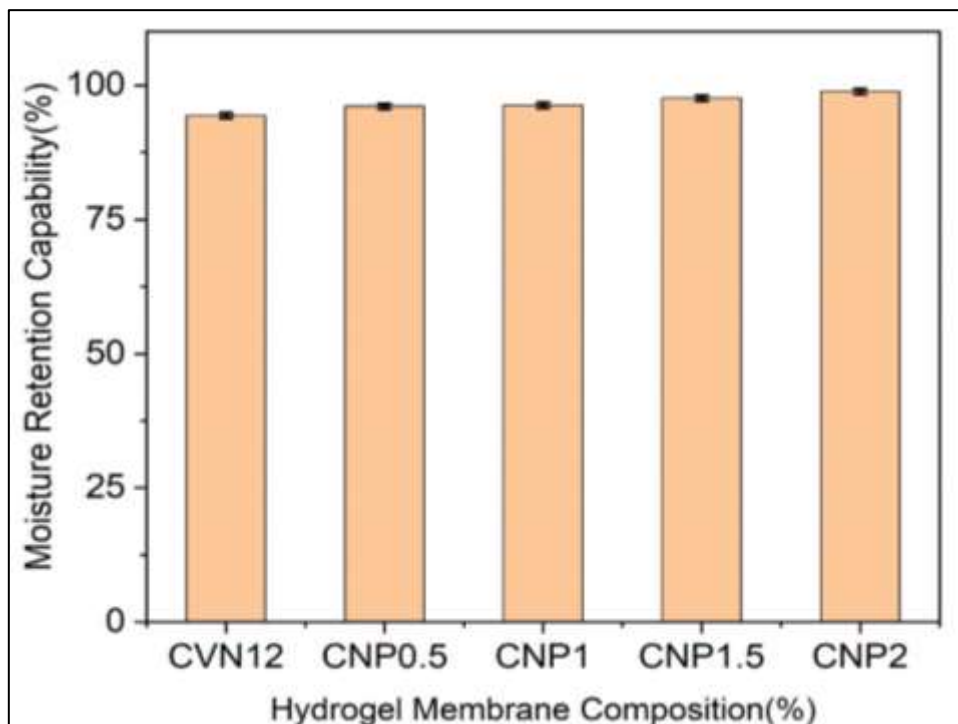


Figure 43: Moisture retention capability of hydrogel membranes with varying CuO-Ag NP concentration

## 4.9. Water Vapor Transmission Rate (WVTR)

### 4.9.1. Nanocellulose incorporated membranes

The WVTR of hydrogel membranes with varying NC compositions were shown in Fig.44. A closed bottle served as a positive control, while an open bottle served as a negative control. WVTR was determined to be 1163 g/m<sup>2</sup>h in the case of an open bottle. When a bottle was covered with hydrogel membranes, however, the value reduced dramatically, as seen in Fig.44 (a). The addition of nanocellulose resulted in a decreasing trend of WVTR, with higher values being obtained for lower amounts of nanocellulose. The highest WVTR value was obtained with 4% nanocellulose i.e.163gm/mm<sup>2</sup>hr. It gradually decreased as the amount of nanocellulose increased i.e., 8%, 12% and 16% respectively. The lowest value of WVTR was obtained in the case of 16%NC i.e.101gm/mm<sup>2</sup>hr. This is due to the fact that adding nanocellulose greatly reduced the PVA peak intensity in hydrogels. As a result, it was hypothesized that nanocellulose operated as a barrier in the PVA chain packing. WVTR readings for CVN hydrogel membranes were substantially lower than for an open bottle. Therefore, these hydrogel membranes can lessen the amount of moisture that escapes through the wound. Approximately 8.34 g/m<sup>2</sup> per hour is the amount of water transmitted by healthy skin. Scar formation will occur if the WVTR is too high. But at a slower rate, wound exudate accumulation is more likely to occur. Accumulated wounds promote bacterial proliferation. Under these conditions, picking the right water vapor transmission rate is crucial. The acceptable range for water vapor transmission in the literature is 91-189 g/m<sup>2</sup> hr[132]. All CVN formulations depicted WVTR in this interval. Thus, hydrogel membranes could be used as wound dressings because they let a good amount of water vapor through.

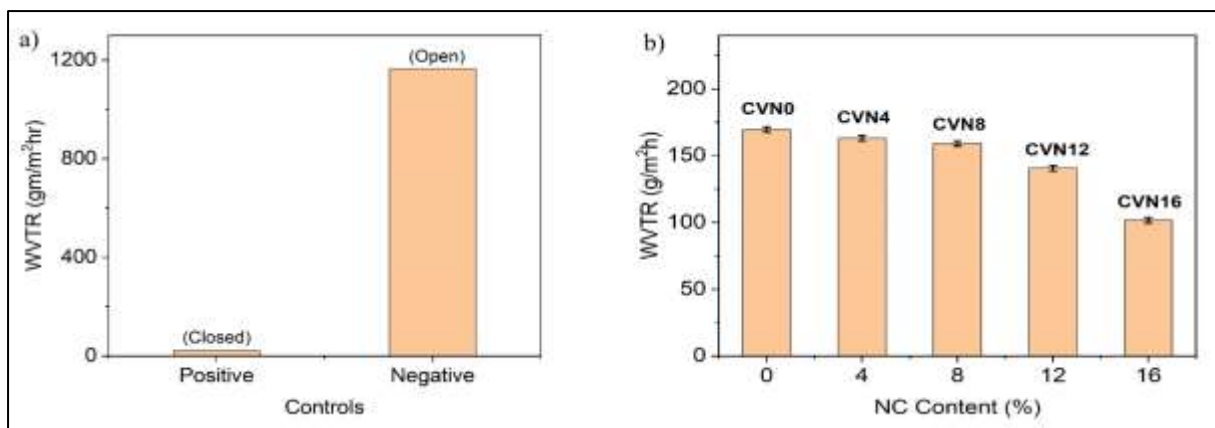


Figure 44: a) Positive and negative controls b) WVTR of hydrogel membranes with varying NC compositions

#### 4.9.2. CuO-Ag incorporated membranes

In Fig. 45(b), a declining trend for WVTR was seen after the addition of CuO-Ag NPs. The higher values were attained with fewer CuO-Ag NPs. WVTR reached its highest value of 132.3 g/m<sup>2</sup>h for 0.5 mg of CuO-Ag NPs, and it gradually declined to 129.6, 116.5, and 100.3 g/m<sup>2</sup>h for 1 mg, 1.5 mg, and 2 mg, respectively. This is explained by the fact that the intensity of the PVA peak fell dramatically as the number of CuO-Ag NPs grew, implying that the NPs acted as a barrier in the PVA chain packing. The WVTR values for PVA/Ch/V/NC/CuO-AgNPs nanocomposite membranes were substantially lower when compared to those obtained for an open bottle. Therefore, these hydrogel membranes have the capacity to lessen the passage of water vapour from the wound bed. About 8.34 g/m<sup>2</sup> per hour of water is transferred from normal skin. When this threshold is breached, the quantity increases dramatically to 209 g/m<sup>2</sup> hr. for granulating wounds. For acute wounds, the WVTR is 12.6 g/m<sup>2</sup> hr. If WVTR is too high, scarring will develop, and lower rates increase the chance of wound exudate accumulation. Bacterial growth is ultimately accelerated by the accumulation of wounds. Given this circumstance, the best rate for water vapour transport should be chosen. Therefore, 92–190 g/m<sup>2</sup> hr is the optimal range for water vapour transport. All of the formulations' WVTR values fall within this desirable range. In light of their capacity to transmit water vapour, the produced hydrogel membranes have the potential to be employed as wound dressings.

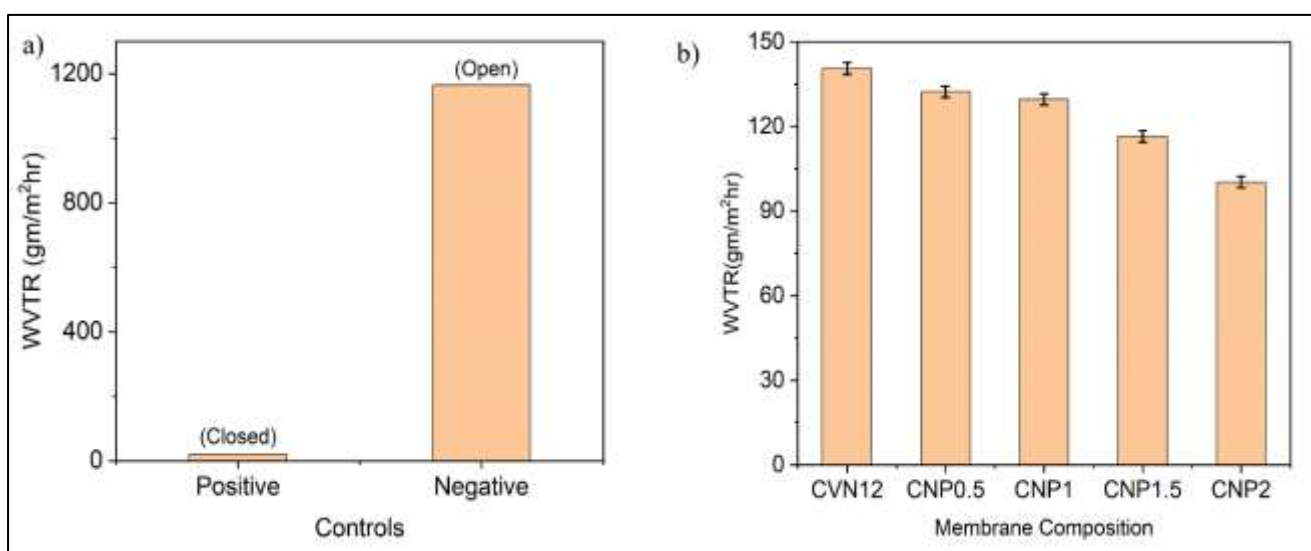


Figure 45: a) Positive and negative controls b) WVTR of hydrogel membranes with varying CuO-Ag NP concentration

## 4.10. Gel Fraction

### 4.10.1. Nanocellulose incorporated membranes

The gel fraction test measures the extent of cross-linking within a hydrogel membrane. Fig. 46 shows the gel fraction of hydrogel membranes with varying NC compositions. The establishment of chemical bonds between polymer chains results in the formation of a network structure, which gives the hydrogel its physical properties. [47]. As NC concentration rises, the gel fraction value falls. This corresponded to an increase in cross-linking and water uptake properties of nanocellulose. This increase can be ascribed to high surface area and aspect ratio of nanocellulose. This provides more reactive sites for cross-linking, as well as its hydrophilic nature, which can lead to increased water uptake by the hydrogel. Hence, showing better thermal and mechanical properties[149].

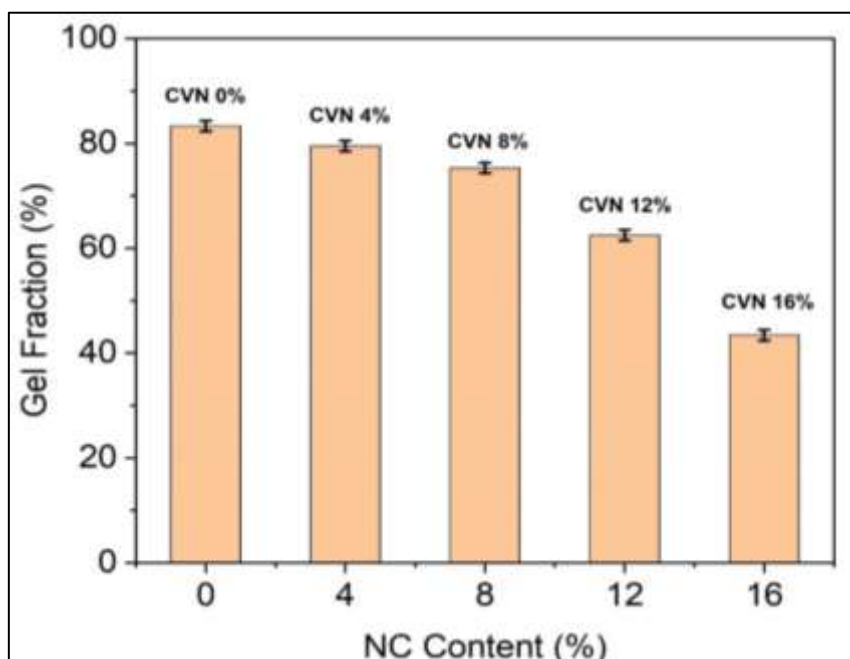


Figure 46: Gel Fraction of hydrogel membranes with varying NC concentration

### 4.10.2. CuO-Ag incorporated membranes

The values of the gel fraction marginally decreased with the addition of CuO-Ag NPs, as shown in Fig.47. Less crosslinking and subsequently a substantial growth of the hydrogel network resulted from this. CuO-Ag NPs' interaction with OH and NH<sub>2</sub> functional groups through hydrogen bonding is responsible for this reduction.[150]. The results were in the

approximately of 70%. The hydrophilic properties of CuO-Ag, which draw more water, may be to blame for the decline in gel fraction. The hydrogel structure weakens as the water absorption increases because more water molecules are present and permeate it.[139]. This decrease in the gel fraction value made it easier for copper oxide and silver ions to be released from the polymeric matrix and contribute to the healing process of wounds.

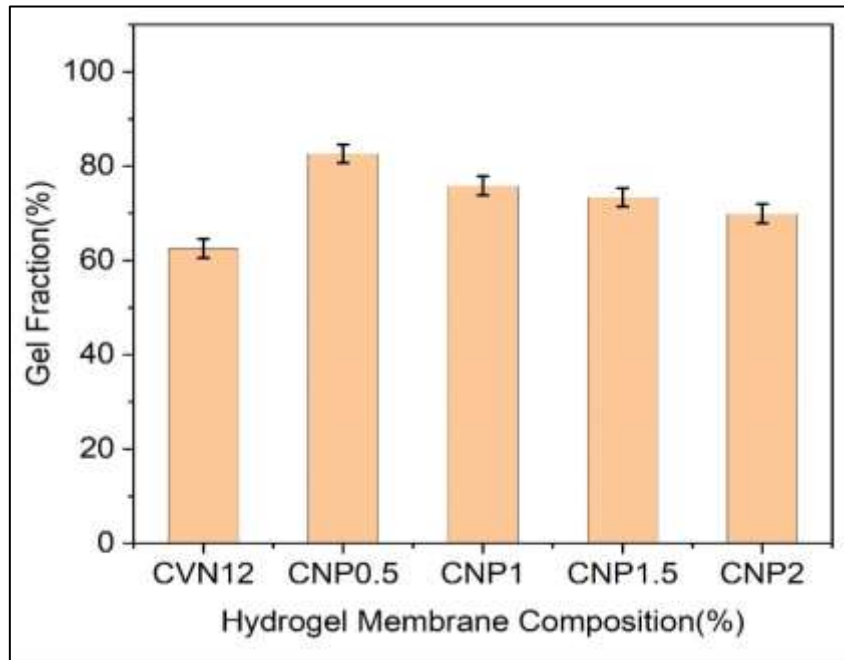


Figure 47: Gel Fraction of hydrogel membranes with varying CuO-Ag concentration

## 4.11. Porosity

### 4.11.1. Nanocellulose incorporated membranes

For wound dressing application, absorption capacity of the membrane is critical. A hydrogel membrane with high porosity will absorb more impurities from the wound surface and prevent the wound from infection. Furthermore, the transfer of oxygen and nutrients is also facilitated. The porous network is also important for cell proliferation. Results of porosity were depicted in Fig.48. The figure clearly demonstrates that a higher concentration of NC in a hydrogel membrane results in a less porous structure. The value of porosity in case of 4%NC observed was 57% and it decreased to 53% in case 116%NC. NC has a large surface area and a lot of hydroxyl groups on its surface, which can form hydrogen bonds with water molecules. This makes it easier for the membrane to absorb water. This can cause the membrane to swell and decrease its porosity[151].

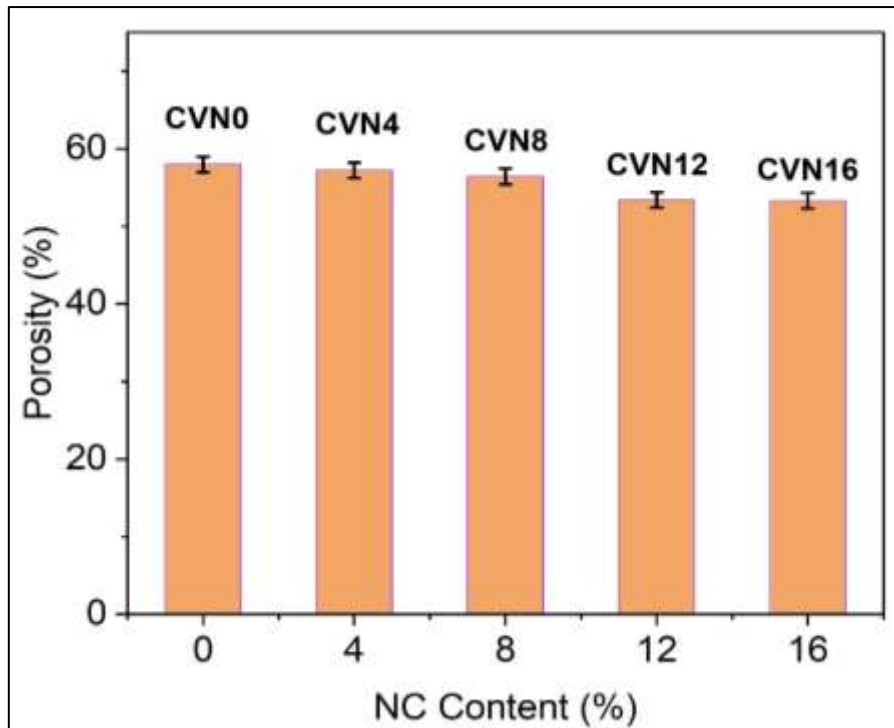


Figure 48: Porosity of hydrogel membranes with varying NC concentration

#### 4.11.2. CuO-Ag incorporated membranes

Considering the specimen PVA/Ch/V/NC, when CuO-Ag NPs were incorporated the porosity reduced, when the number of nanoparticles was increased gradually as shown in Fig.49. Porosity and density are inversely associated; as hydrogel density increased, porosity dropped. This might be because the penetration of solvent molecules into the network was impacted by the presence of CuO-Ag NPs. Mehrabani also reports that the addition of nanoparticles reduces porosity.[152].

After the addition of CuO-Ag NPs, the porosity of all the nanocomposites ranged from 48.39 to 55.07%. The high values attained indicated that there would be a large surface area available for the absorption of wound exudates. The high porosity is beneficial for the flow of nutrients and oxygen as well. Consequently, they make excellent wound dressings.

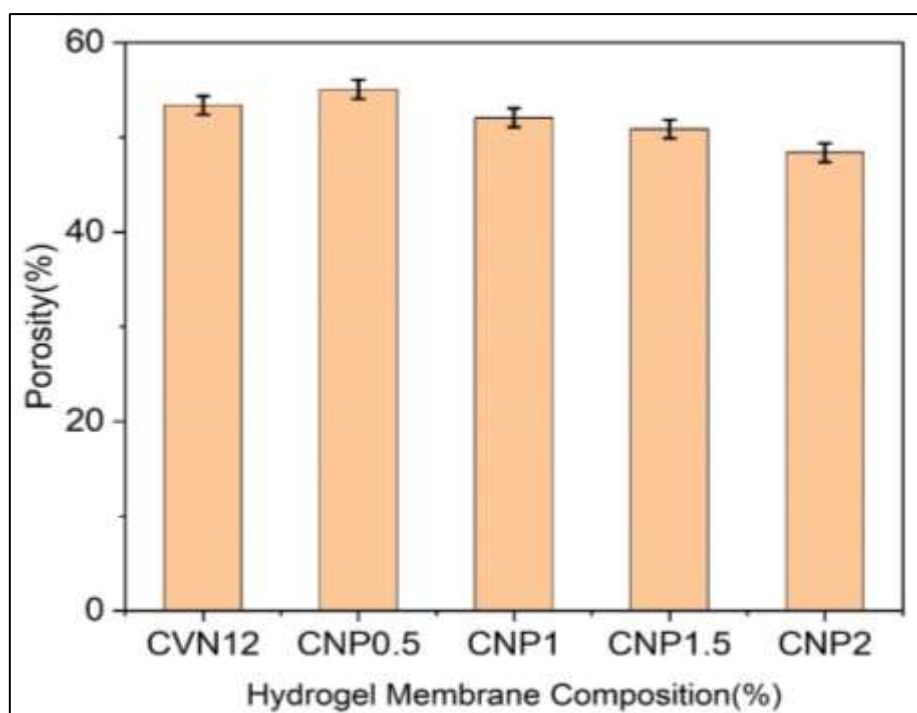


Figure 49: Porosity of hydrogel membranes with varying CuO-Ag concentration

## 4.12. Swelling Ability

### 4.12.1. Nanocellulose incorporated membranes

Hydrophilicity of functional groups can influence swelling. Polymeric chains hydrate and relax as more water was incorporated into the matrix[146]. pH, temperature, swelling environment, polymer nature, and degree of crosslinking are all factors that influence swelling[153]. PVA, chitosan, and nanocellulose hydrophilic functional groups were involved in film swelling[154]. Swelling percentage increases as crosslinking density decreases[155], possibly due to decreased polymeric chain entanglement. As can be seen in Fig.50, the swelling hits its peak value while it was submerged in water. Addition of NC increases swelling, and maximum swelling was observed in case of CVN16.

When compared to the results obtained with distilled water as in Fig.50 (a), the swelling percentage was significantly higher when using phosphate buffer solution. The ionic charge electrostatic repulsion promoted swelling, which wedges polymeric chain accumulation and promotes network expansion[143]. The osmotic pressure that existed between the solution and the polymer network dropped as the ionic strength of the solution rose. As a result, water molecule diffusion is delayed within the polymer network[156]. That's the underlying cause

behind reduction in swelling that was observed in the phosphate buffer solution. The swelling volume transition is caused by salts. The addition of mobile ions changes the ionic strength of water, resulting in a swelling volume transition. Thus, electrostatic repulsions separate the excess counter ions in the solution. As a result, the ability to swell increases. Fig.50 (b) depicts the swelling percentages for phosphate buffer solution and maximum swelling was observed in case of CVN16.

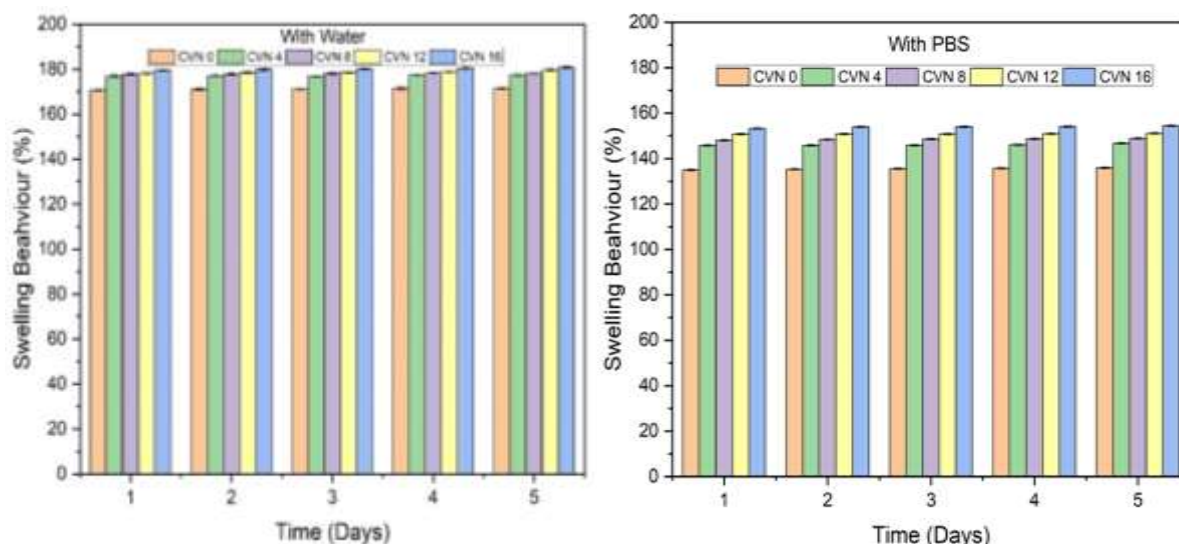


Figure 50: Swelling behaviour of hydrogel membranes with varying NC concentration a) with deionized water b) phosphate buffer solution

#### 4.12.2. CuO-Ag incorporated membranes

The Fig.51 (a) represents the swelling of different composite membranes at various time intervals. The findings show that the concentration of nanoparticles (NPs) in the membrane matrix influences the swelling behaviour of hydrogel membranes. The incorporation of NPs in the hydrogel membranes increased the voids in the matrix, which were occupied by water molecules and caused an increase in swelling ratio[157]. As shown in the Fig.51 (a), for water, the swelling ratio increased with increasing NP concentration, with CNP 2 showing the highest swelling ratio of 191.67% followed by CNP1.5 as 188.05 % compared to other samples. In the case of phosphate buffer solution, the swelling ratios were comparatively lower because the PBS had a lower pH and higher ionic strength compared to water. The charged functional groups in the hydrogel may interact more strongly with the ions in the PBS, leading to a reduced swelling ratio compared to water[158]. The maximum value for swelling with PBS was observed for CNP2 which is 170.16% as shown in Fig.51 (b).



Additionally, the phosphate ions in PBS may have a competitive effect with water molecules in the swelling of hydrogels. These factors could contribute to the lower swelling ratio observed in PBS compared to water. The results are consistent with Kumar, Behl[159] and Ahmed, Niazi[160].

However overall, the membranes shown excellent swelling ratios and these results suggest that the incorporation of NPs into hydrogel membranes can improve their swelling behavior, which is important for their intended use in wound dressing materials.

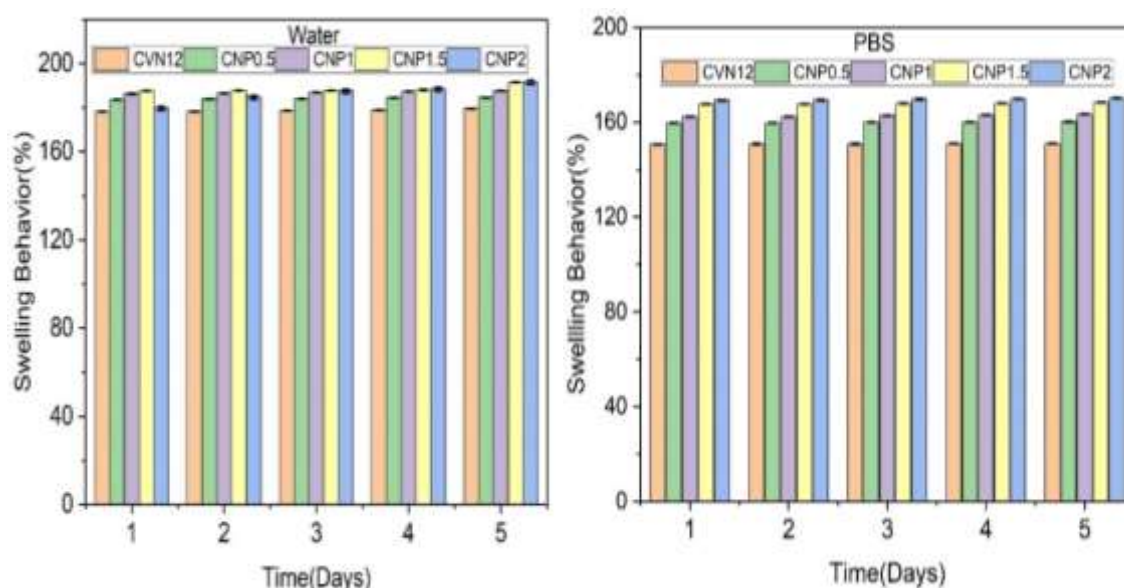


Figure 51: Swelling behaviour of hydrogel membranes with varying CuO-Ag NP concentration a) with deionized water b) phosphate buffer solution

## 4.13. Biodegradability

### 4.13.1. Nanocellulose incorporated membranes

In this study, a biodegradability test was performed on hydrogel membrane to assess its environmental impact. The hydrogel membrane was buried in the soil and monitored over a certain period. Weight of membranes were measured every week. Results showed that the hydrogel membrane gradually degraded in the soil environment, with visible signs of degradation observed after a few weeks. The results were shown in Fig.52. These findings indicate that hydrogel membrane has promising potential as an environmentally friendly material.

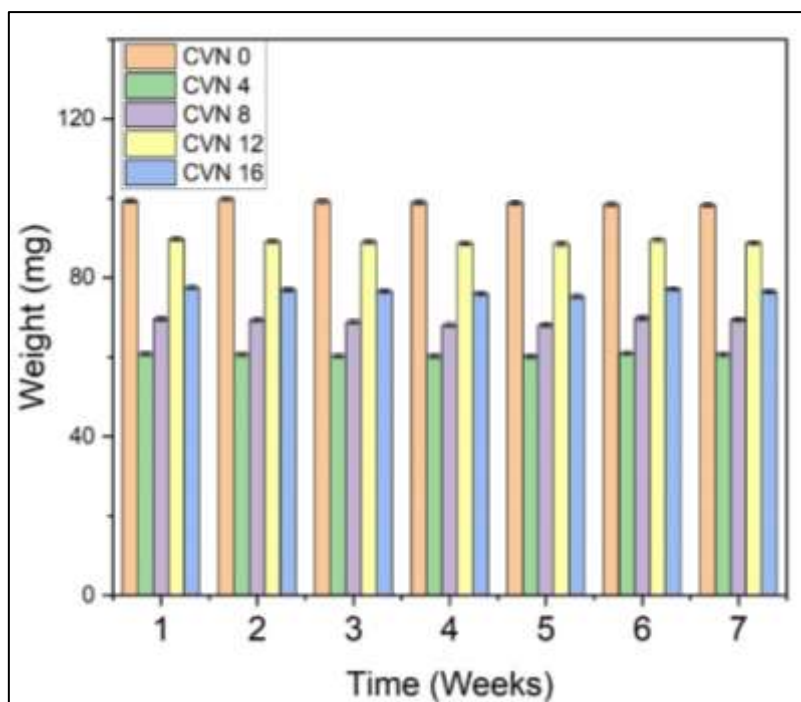


Figure 52: Biodegradability of hydrogel membranes with varying NC concentration

#### 4.13.2. CuO-Ag incorporated membranes

The biodegradability of a hydrogel membrane was evaluated in this study to determine its potential environmental impact. The hydrogel membrane was subjected to a burial test in soil, and its weight was recorded weekly for a specified period. The outcomes demonstrated that the hydrogel membrane underwent gradual degradation in the soil environment, with evident degradation indications observed after a few weeks. The experimental results are depicted in Fig.53, showing the weight loss percentage of the samples over a period of 7 weeks. Among the samples, CVN0 exhibited the lowest weight loss percentage throughout the entire duration. On the other hand, CNP2 initially had the highest weight loss percentage in the first week, but the percentage gradually decreased in the subsequent weeks. Overall, the results suggest that all samples underwent some degree of degradation in the soil environment, with CNP 1.5 showing the highest weight loss percentage in week 7. The results show that the addition of NPs promoted the decomposition of the original polymeric matrix. Moreover, results are aligned with the studies from Gobi and Babu[126] and Morgado, Lisboa[161] chitosan-PVA membranes.

These findings suggest that the hydrogel membrane exhibits promising potential as a sustainable and environmentally friendly material due to its biodegradable properties, which

could reduce its environmental impact when discarded. The results of this study contribute to advancing the development of sustainable materials that could potentially replace conventional materials and mitigate environmental damage caused by waste accumulation

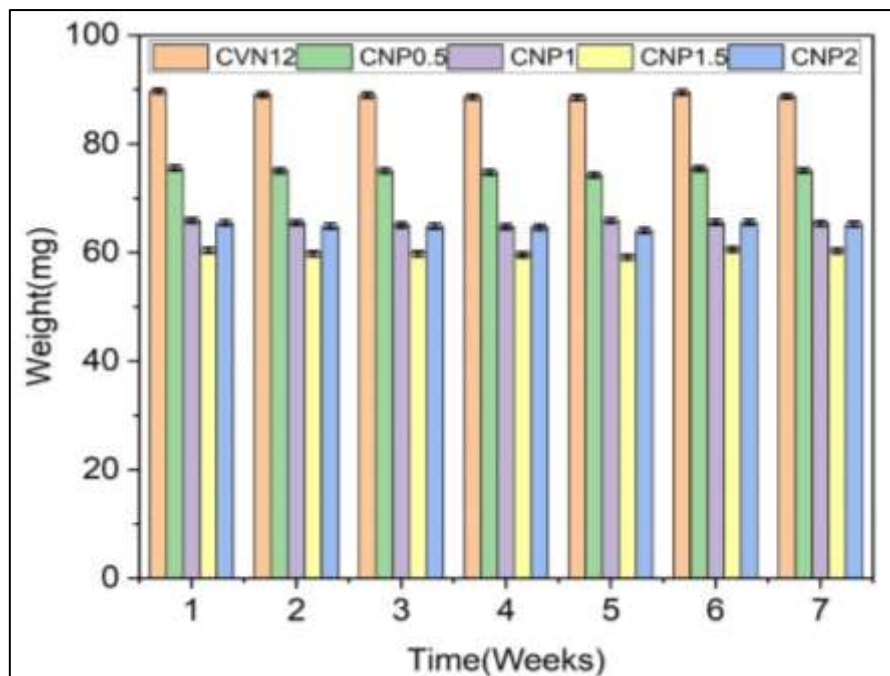


Figure 53: Biodegradability of hydrogel membranes with varying CuO-Ag concentration

#### 4.14. Cell-based Cytotoxicity Assay

The cytotoxicity and cell viability of four different samples (CNP 0.5, CNP 1, CNP 1.5, and CNP 2) were measured at three different concentrations (20, 40, and 80  $\mu\text{g}/\text{mL}$ ) and portrayed in Fig. 54. The cytotoxicity percentage represents the percentage of cells that died due to exposure to the sample, while the cell viability percentage represents the percentage of cells that remained alive after exposure.

At the lowest concentration level, all samples showed low cytotoxicity percentages ranging from 5.36% to 13.77%, with CNP 1.5 showing the least toxicity. At the medium concentration level, the cytotoxicity percentages slightly increased, with CNP 0.5 exhibiting the highest value at 18.10%. The cell viability percentages remained relatively high for all samples, with CNP 1.5 showing the highest viability. At the highest concentration level, the cytotoxicity percentages substantially increased for all samples, with CNP 1.5 showing the lowest toxicity and CNP 0.5 showing the highest. The cell viability percentages decreased for

all samples, ranging from 81.89% to 94.63%. Overall, CNP 1.5 showed the least toxicity at all concentration levels, while CNP 0.5 exhibited the highest cytotoxicity at the highest concentration level. The general trend of increasing cytotoxicity and decreasing cell viability upon increasing the concentration of NPs is consistent with the previous studies[162].

The CNP 1.5 sample showed the highest cell viability at this concentration level while CNP 0.5 showed the least cell viability. The CNP 1.5 sample consistently showed the highest cell viability at all concentration levels, indicating that it was the most effective in promoting cell growth and proliferation. The reason for the low cytotoxicity observed in the synthesized membranes can be attributed to the non-chemical crosslinking process, as indicated by the FTIR results. The crosslinking of PVA and chitosan was achieved through the physical bonding facilitated by vanillin. This finding is consistent with the research conducted by Supriya Bhatt, Thakur[133].

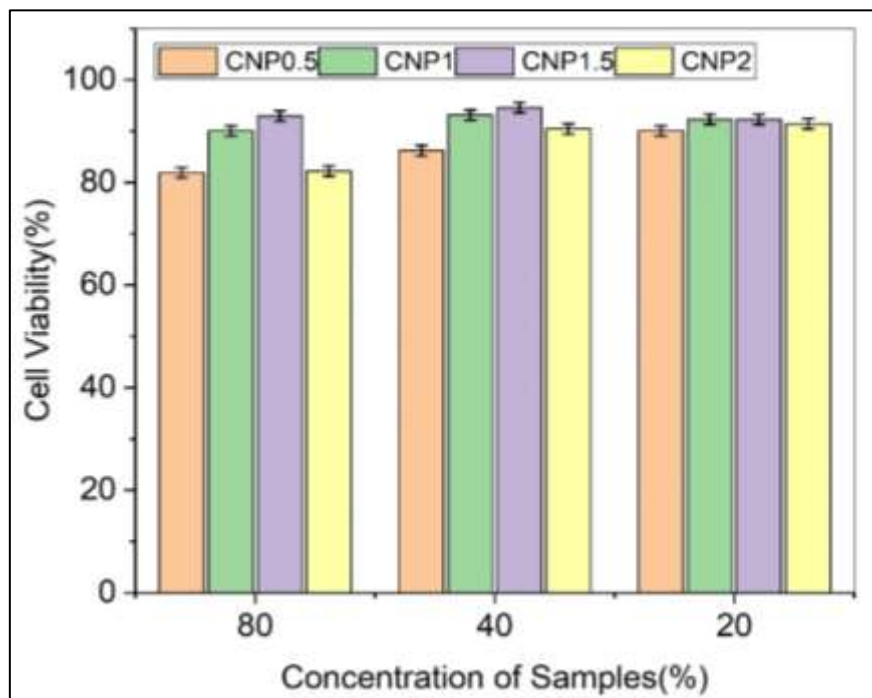


Figure 54: depiction of cytotoxicity evaluation of fabricated membranes through cell viability assay

#### 4.15. Antibacterial Activity Measurement

Fig.55 (e) presents the measurement of inhibition zone diameters resulting from the antibacterial assessment of the developed hydrogels against Gram-negative Escherichia Coli and Gram-positive Staphylococcus Aureus using the disc diffusion method, while Fig.55 (a-

d) displays the Kirby-Bauer agar plates. Notably, clear inhibition zones were observed against both strains of pathogens. Gentamicin served as the positive control in this experiment, whereas CVN12 membrane served as the negative control. The zone of inhibition formed was  $17 \pm 0.5$  mm and  $8 \pm 0.3$  mm against E. Coli and S. aureus for CNP2. As the number of NPs increased in hydrogels, the better inhibition zones were recorded, similar results were reported by Malik, Duan[17] using chitosan-vanillin membrane with AgNPs and Ahmed, Niazi[121] employing PVA-starch membrane. The reported results encourage the use of synthesized membranes as wound healing material.

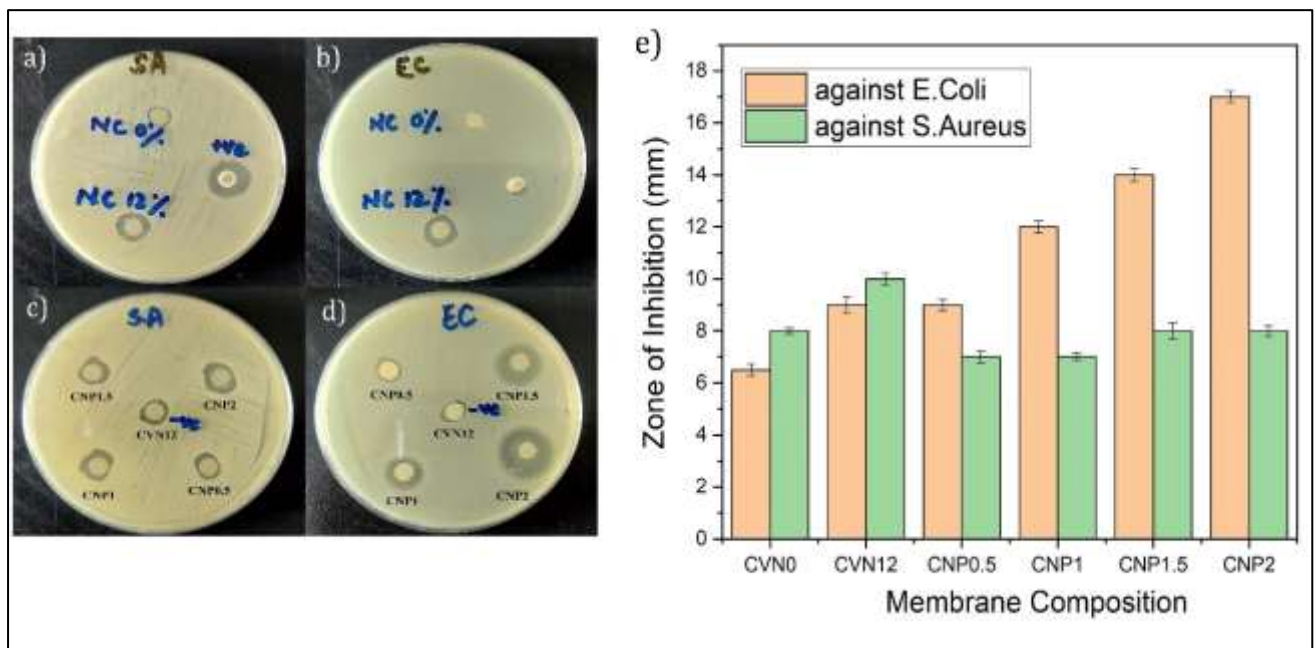


Figure 55: Photograph showing the zone of inhibition formed around PVA-Chitosan hydrogel membranes against E. coli and S. aureus (a,b,c,d) and e) graphical representation of antibacterial activity

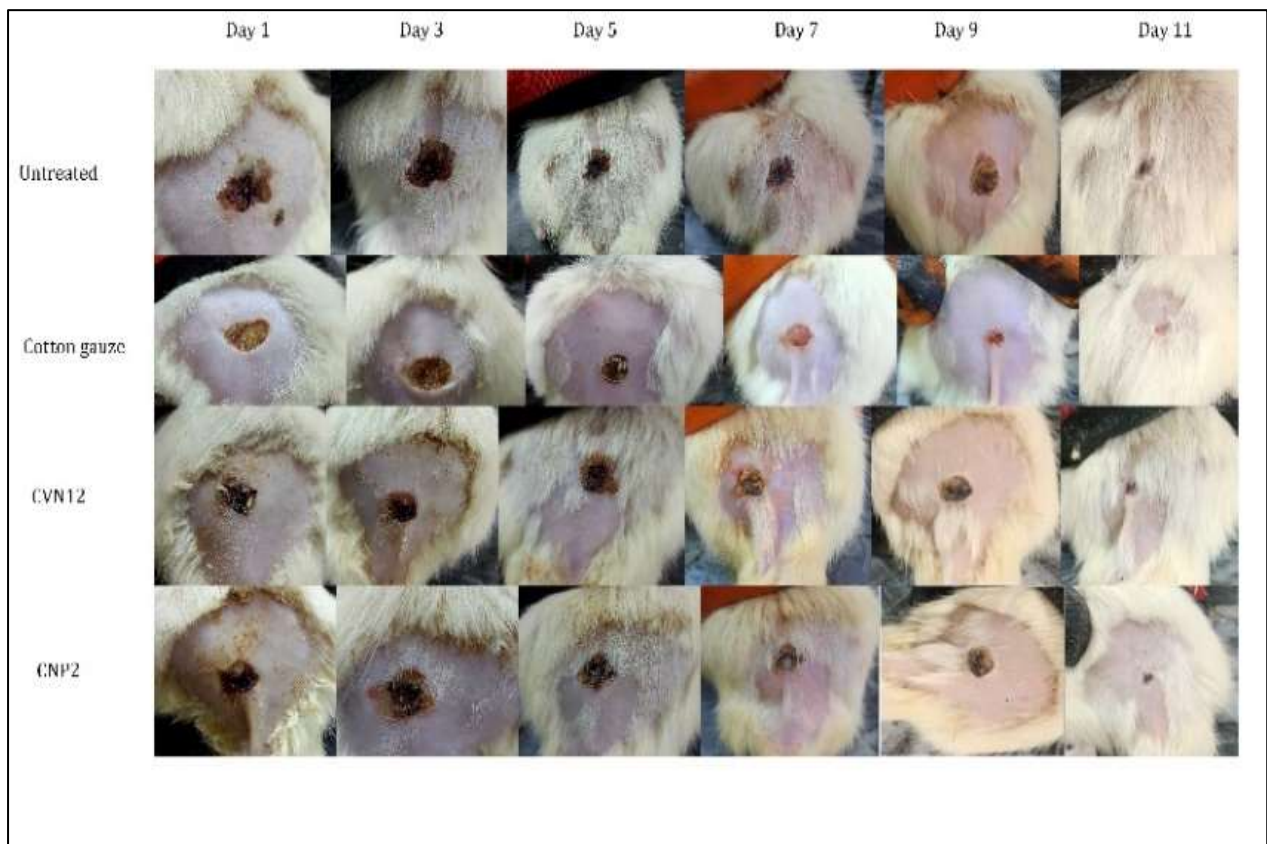
#### 4.16. In-vivo Wound Healing Experiment

The wound healing potential of the fabricated membranes was assessed in male Wister rats by creating full thickness wounds on the dorsal side of each rat. The progression of wound healing was monitored at multiple time points (1st, 3rd, 5th, 7th, 9th and 11th day). Fig. 56 (a-b) visually and graphically represents the wound healing efficacy of the different NP treatments at varying concentrations over the course of the study.

The first three days showed insignificant healing in G1 and G2 however G3 and G4 showed comparatively better healing i.e., 23.07 and 12.62% respectively. On day five and day seventh all concentrations of CVN12 and CNP2 showed an increase in healing efficiency where G3 and G4 reached 32.7% and 22.3%, respectively for day five and showing similar results for day seventh. On day nine, the healing efficiency of all concentrations of CVN12 and CNP2 showed a further increase, with the highest efficiency recorded in G3 and G4 at 42.3 % and 41.7%, respectively.

Finally, at day 11, the highest wound healing efficiency was seen in G4 with 70.9%, followed by G3 with 51.9%, G2 with 55.7%, and G1 with 52.3%.

Given the superior outcomes observed in comparison to cotton gauze, it can be inferred that CNP2 manufactured membranes have significant advantages in facilitating full thickness burn wound healing. According to the findings, G4 had the highest wound healing efficiency in the rat model, and good re-epithelization was also noted, showing its potential for wound healing applications.





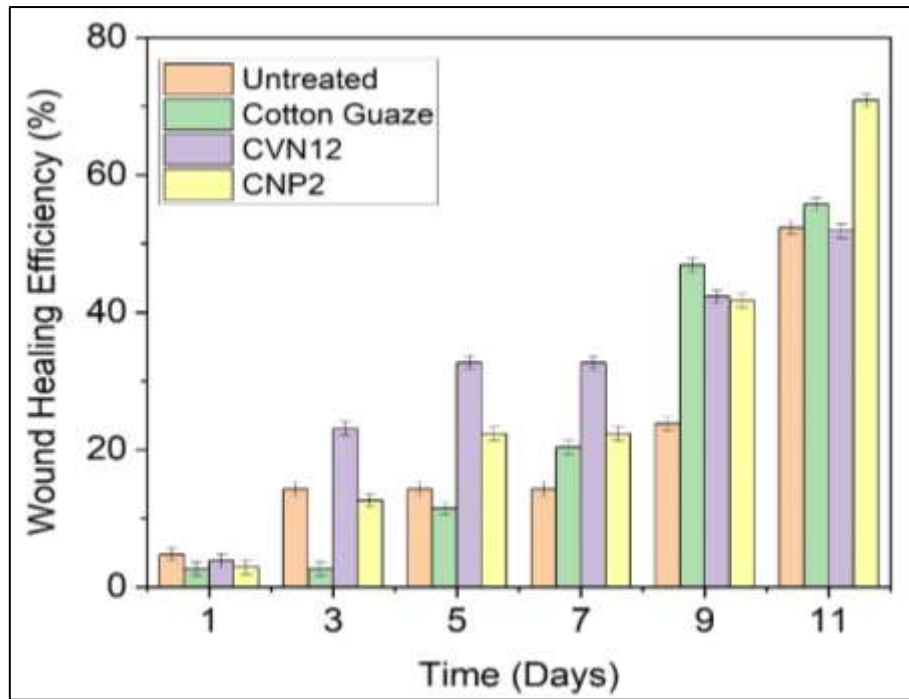


Figure 56: Photographic representation of burn wounds induced in the animal model a)  
 Photographic results b) Graphical representation of wound healing efficiency

## Conclusion

A thorough examination of the creation and evaluation of Chitosan-PVA hydrogel membranes reinforced with nanocellulose, crosslinked with vanillin and incorporated with nanoparticles for prospective applications in wound healing was carried out in this study. The membranes exhibited desirable properties such as competitive mechanical strength, hydrophilic nature, high moisture retention, superior swelling behavior, biodegradability, and excellent cell viability. Both gram-positive and gram-negative bacteria were significantly inhibited by the manufactured membranes' antibacterial properties. Furthermore, in an animal model, these membranes demonstrated remarkable potential in enhancing the process of wound healing.

Various nanocellulose compositions were incorporated into a polymeric matrix to create membranes with superior thermal and mechanical properties. The hydrogel membranes showed remarkable swelling properties. When nanocellulose was added, the WVTR went down and the hydrophilicity went up. Microscopy and X-ray diffraction studies show that the PVA/chitosan matrix contains NC in a uniform distribution. FTIR research showed that the -NH groups of NC and the -OH groups of PVA and chitosan bond together through hydrogen bonds. The improved thermal and mechanical properties can be attributed to the hydrogen bonding. Hydrophilicity of PVA and nanocellulose were credited for the high moisture retention of up to 96%.

The results of this study highlight the potential of Chitosan-PVA hydrogel membranes as multifunctional wound dressings with wound healing efficiency of 70.9% with a wide range of advantageous properties. The incorporation of nanoparticles enhanced the antimicrobial activity with a maximum of 17mm inhibition zone and overall performance of the membranes. This research significantly contributes to the understanding of various aspects, such as mechanical stability, degradability, toxicity, and efficacy, when developing wound healing materials. The combination of Chitosan-PVA hydrogel reinforced with nanocellulose and vanillin along with nanoparticles as antimicrobial agent offers a promising approach to address these aspects and provide an optimized wound healing solution.

The development and characterization of Chitosan-PVA hydrogel membranes for wound healing are presented in this paper in detail. The demonstrated properties and performance of



these membranes highlight their potential for use as effective wound dressings in clinical settings. The findings strongly support the notion that these hydrogel membranes hold significant promise as viable candidates for healing applications, particularly in the treatment of second and third degree burn injuries.

## **Future Recommendations**

Wound dressing is a potential market to be explored, in future

- 1) Green synthesis can be investigated for synthesis of nanoparticles. Various algae sources can be considered for this
- 2) The nanoparticles can also be synthesized by in-situ technique for better dispersion
- 3) Organic and natural wound healing agents e.g., kelp, cloves and other herbs can be examined
- 4) Biological characterization including cell proliferation, tissue growth and protein absorption can be done
- 5) For drug delivery, various model drugs can be loaded into the matrix and their release profile be investigated
- 6) For diabetic patients, medications like insulin can be coupled with medicines that promote wound healing
- 7) Due to the paucity of studies on the cytotoxic effects of nanomaterials in films, the key future possibility for hydrogel membranes is the safety enhancement of antimicrobial nanofillers.
- 8) The regulated release of antibacterial chemicals must be accomplished in order to create effective and long-lasting antibacterial membranes.

## References

1. Pang, Q., et al., *Smart flexible electronics- integrated wound dressing for real- time monitoring and on- demand treatment of infected wounds*. *Advanced Science*, 2020. **7**(6): p. 1902673.
2. Zhu, J., et al., *Hyaluronic acid and polyethylene glycol hybrid hydrogel encapsulating nanogel with hemostasis and sustainable antibacterial property for wound healing*. *ACS applied materials & interfaces*, 2018. **10**(16): p. 13304-13316.
3. Zhang, L.-j., et al., *Dermal adipocytes protect against invasive Staphylococcus aureus skin infection*. *Science*, 2015. **347**(6217): p. 67-71.
4. Zhang, M., et al., *Multifunctional chitosan/alginate hydrogel incorporated with bioactive glass nanocomposites enabling photothermal and nitric oxide release activities for bacteria-infected wound healing*. *International Journal of Biological Macromolecules*, 2023. **232**: p. 123445.
5. Han, G. and R. Ceilley, *Chronic wound healing: a review of current management and treatments*. *Advances in therapy*, 2017. **34**: p. 599-610.
6. Zhang, M., et al., *Super-ductile, injectable, fast self-healing collagen-based hydrogels with multi-responsive and accelerated wound-repair properties*. *Chemical Engineering Journal*, 2021. **405**: p. 126756.
7. AshaRani, P., et al., *Cytotoxicity and genotoxicity of silver nanoparticles in human cells*. *ACS nano*, 2009. **3**(2): p. 279-290.
8. Cheng, H., et al., *Sprayable hydrogel dressing accelerates wound healing with combined reactive oxygen species-scavenging and antibacterial abilities*. *Acta biomaterialia*, 2021. **124**: p. 219-232.
9. Zheng, Z., et al., *Catechol modified quaternized chitosan enhanced wet adhesive and antibacterial properties of injectable thermo-sensitive hydrogel for wound healing*. *Carbohydrate Polymers*, 2020. **249**: p. 116826.
10. Wang, J., et al., *UV cross-linked injectable non-swelling dihydrocaffeic acid grafted chitosan hydrogel for promoting wound healing*. *Carbohydrate Polymers*, 2023. **314**: p. 120926.
11. Itzhakov, R., et al., *Oligochitosan and oxidized nucleoside-based bioderived hydrogels for wound healing*. *Carbohydrate Polymers*, 2023. **314**: p. 120947.
12. Tian, B. and J. Liu, *Smart stimuli-responsive chitosan hydrogel for drug*

- delivery: A review*. International Journal of Biological Macromolecules, 2023: p. 123902.
13. Barleany, D.R., et al., *Synthesis and characterization of chitosan/polyvinyl alcohol crosslinked poly (N-isopropylacrylamide) smart hydrogels via  $\gamma$ -radiation*. Materials Today: Proceedings, 2023.
  14. Karthick, S.A., K. Manjari, and M.G. Devi, *Biocompatible and bioactive PVA/Sericin/Chitosan nanofibrous wound dressing matrix*. Applied Surface Science Advances, 2023. **13**: p. 100362.
  15. Khorasani, M.T., et al., *Enhanced antimicrobial and full-thickness wound healing efficiency of hydrogels loaded with heparinized ZnO nanoparticles: in vitro and in vivo evaluation*. International Journal of Biological Macromolecules, 2021. **166**: p. 200-212.
  16. Sadeghi-Aghbash, M., et al., *Fabrication and development of PVA/Alginate nanofibrous mats containing Arnebia Euchroma extract as a burn wound dressing*. Reactive and Functional Polymers, 2022. **181**: p. 105440.
  17. Malik, U.S., et al., *Vanillin cross-linked hydrogel membranes interfacial reinforced by carbon nitride nanosheets for enhanced antibacterial activity and mechanical properties*. Chinese Chemical Letters, 2023. **34**(4): p. 108071.
  18. Do, N.H., et al., *Recent developments in chitosan hydrogels carrying natural bioactive compounds*. Carbohydrate Polymers, 2022. **294**: p. 119726.
  19. Jagadamma, S., et al., *Substrate quality alters the microbial mineralization of added substrate and soil organic carbon*. Biogeosciences, 2014. **11**(17): p. 4665-4678.
  20. Sood, R. and D.S. Chopra, *Optimization of reaction conditions to fabricate Ocimum sanctum synthesized silver nanoparticles and its application to nano-gel systems for burn wounds*. Materials Science and Engineering: C, 2018. **92**: p. 575-589.
  21. Kamoun, E.A., E.-R.S. Kenawy, and X. Chen, *A review on polymeric hydrogel membranes for wound dressing applications: PVA-based hydrogel dressings*. Journal of advanced research, 2017. **8**(3): p. 217-233.
  22. Potts, R., *Skin barrier: principles of percutaneous absorption*. Archives of dermatology, 1997. **133**(7): p. 924-924.
  23. Boateng, J.S., et al., *Wound healing dressings and drug delivery systems: a*

- review*. Journal of pharmaceutical sciences, 2008. **97**(8): p. 2892-2923.
24. Gurtner, G.C., et al., *Wound repair and regeneration*. Nature, 2008. **453**(7193): p. 314-321.
  25. Winter, G.D., *Formation of the scab and the rate of epithelization of superficial wounds in the skin of the young domestic pig*. Nature, 1962. **193**(4812): p. 293-294.
  26. Ndlovu, S.P., et al., *Gelatin-based hybrid scaffolds: Promising wound dressings*. Polymers, 2021. **13**(17): p. 2959.
  27. Edwards, J.V., et al., *Modified cotton gauze dressings that selectively absorb neutrophil elastase activity in solution*. Wound Repair and Regeneration, 2001. **9**(1): p. 50-58.
  28. Wichterle, O. and D. Lim, *Hydrophilic gels for biological use*. Nature, 1960. **185**(4706): p. 117-118.
  29. Mathur, A.M., S.K. Moorjani, and A.B. Scranton, *Methods for synthesis of hydrogel networks: A review*. Journal of Macromolecular Science, Part C: Polymer Reviews, 1996. **36**(2): p. 405-430.
  30. Alexander, C., *Temperature-and pH-responsive smart polymers for gene delivery*. Expert Opinion on Drug Delivery, 2006. **3**(5): p. 573-581.
  31. Bignotti, F., et al., *Synthesis, characterisation and solution behaviour of thermo-and pH-responsive polymers bearing L-leucine residues in the side chains*. Polymer, 2000. **41**(23): p. 8247-8256.
  32. Liu, F. and M.W. Urban, *Recent advances and challenges in designing stimuli-responsive polymers*. Progress in polymer science, 2010. **35**(1-2): p. 3-23.
  33. Hoffman, A.S., *Hydrogels for biomedical applications*. Advanced drug delivery reviews, 2012. **64**: p. 18-23.
  34. Akhtar, M.F., M. Hanif, and N.M. Ranjha, *Methods of synthesis of hydrogels... A review*. Saudi Pharmaceutical Journal, 2016. **24**(5): p. 554-559.
  35. Bashir, S., et al., *Fundamental concepts of hydrogels: Synthesis, properties, and their applications*. Polymers, 2020. **12**(11): p. 2702.
  36. Buenger, D., F. Topuz, and J. Groll, *Hydrogels in sensing applications*. Progress in Polymer Science, 2012. **37**(12): p. 1678-1719.
  37. Guo, W., et al., *pH- Stimulated DNA Hydrogels Exhibiting Shape- Memory Properties*. Advanced Materials, 2015. **27**(1): p. 73-78.

38. Das, N., *Preparation methods and properties of hydrogel: A review*. Int. J. Pharm. Pharm. Sci, 2013. **5**(3): p. 112-117.
39. Yang, Z., et al., *Acute toxicity of high dosage carboxymethyl chitosan and its effect on the blood parameters in rats*. Journal of Materials Science: Materials in Medicine, 2012. **23**: p. 457-462.
40. Chan, P., et al., *Synthesis and characterization of chitosan-g-poly (ethylene glycol)-folate as a non-viral carrier for tumor-targeted gene delivery*. Biomaterials, 2007. **28**(3): p. 540-549.
41. Anitha, A., et al., *Synthesis, characterization, cytotoxicity and antibacterial studies of chitosan, O-carboxymethyl and N, O-carboxymethyl chitosan nanoparticles*. Carbohydrate polymers, 2009. **78**(4): p. 672-677.
42. Ullah, F., et al., *Classification, processing and application of hydrogels: A review*. Materials Science and Engineering: C, 2015. **57**: p. 414-433.
43. Pyarasani, R.D., T. Jayaramudu, and A. John, *Polyaniline-based conducting hydrogels*. Journal of Materials Science, 2019. **54**(2): p. 974-996.
44. Mohamed, N.A. and M.M. Fahmy, *Synthesis and antimicrobial activity of some novel cross-linked chitosan hydrogels*. International journal of molecular sciences, 2012. **13**(9): p. 11194-11209.
45. Zhang, D., et al., *Carboxyl-modified poly (vinyl alcohol)-crosslinked chitosan hydrogel films for potential wound dressing*. Carbohydrate polymers, 2015. **125**: p. 189-199.
46. Hwang, M.-R., et al., *Gentamicin-loaded wound dressing with polyvinyl alcohol/dextran hydrogel: gel characterization and in vivo healing evaluation*. Aaps Pharmscitech, 2010. **11**: p. 1092-1103.
47. Kamoun, E.A., et al., *Poly (vinyl alcohol)-alginate physically crosslinked hydrogel membranes for wound dressing applications: characterization and bio-evaluation*. Arabian Journal of Chemistry, 2015. **8**(1): p. 38-47.
48. Yang, J.M., W.Y. Su, and M.C. Yang, *Evaluation of chitosan/PVA blended hydrogel membranes*. Journal of Membrane Science, 2004. **236**(1-2): p. 39-51.
49. Huang, M.-H. and M.-C. Yang, *Evaluation of glucan/poly (vinyl alcohol) blend wound dressing using rat models*. International journal of pharmaceuticals, 2008. **346**(1-2): p. 38-46.
50. Hago, E.-E. and X. Li, *Interpenetrating polymer network hydrogels based on*

- gelatin and PVA by biocompatible approaches: Synthesis and characterization*. Advances in Materials Science and Engineering, 2013. **2013**.
51. Fahmy, A., et al., *Poly (vinyl alcohol)-hyaluronic acid membranes for wound dressing applications: synthesis and in vitro bio-evaluations*. Journal of the Brazilian Chemical Society, 2015. **26**: p. 1466-1474.
  52. Padol, A.R., et al., *Safety evaluation of silk protein film (a novel wound healing agent) in terms of acute dermal toxicity, acute dermal irritation and skin sensitization*. Toxicology international, 2011. **18**(1): p. 17.
  53. Das, S., et al., *Recent advances in hydrogels for biomedical applications*. Asian J Pharm Clin Res, 2018. **11**: p. 62-8.
  54. Bhardwaj, U., et al., *PLGA/PVA hydrogel composites for long-term inflammation control following sc implantation*. International journal of pharmaceutics, 2010. **384**(1-2): p. 78-86.
  55. Abdullah, Z.W., et al., *PVA, PVA blends, and their nanocomposites for biodegradable packaging application*. Polymer-Plastics Technology and Engineering, 2017. **56**(12): p. 1307-1344.
  56. Jayasekara, R., et al., *Biodegradability of a selected range of polymers and polymer blends and standard methods for assessment of biodegradation*. Journal of Polymers and the Environment, 2005. **13**: p. 231-251.
  57. Fukushima, K. and G. Camino, *Polymer nanocomposites biodegradation*. Functional and physical properties of polymer nanocomposites, 2016: p. 57-91.
  58. Subhashree, S. and P.S. Kumar, *New analytical strategies amplified with carbon-based nanomaterial for sensing food pollutants*. Chemosphere, 2022. **295**: p. 133847.
  59. Tănase, E.E., et al., *Preparation and characterization of biopolymer blends based on polyvinyl alcohol and starch*. Romanian Biotechnological Letters, 2015. **20**(2): p. 10307.
  60. Pal, K., A. Banthia, and D. Majumdar, *Preparation of transparent starch based hydrogel membrane with potential application as wound dressing*. Trends Biomater Artif Organs, 2006. **20**(1): p. 59-67.
  61. van den Broek, L.A., et al., *Chitosan films and blends for packaging material*. Carbohydrate polymers, 2015. **116**: p. 237-242.

62. Butnaru, E., et al., *Poly (vinyl alcohol)/chitosan/montmorillonite nanocomposites for food packaging applications: Influence of montmorillonite content*. High Performance Polymers, 2016. **28**(10): p. 1124-1138.
63. Pal, K., A.K. Banthia, and D.K. Majumdar, *Preparation and characterization of polyvinyl alcohol-gelatin hydrogel membranes for biomedical applications*. Aaps Pharmscitech, 2007. **8**: p. E142-E146.
64. Zhang, R., W. Xu, and F. Jiang, *Fabrication and characterization of dense chitosan/polyvinyl-alcohol/poly-lactic-acid blend membranes*. Fibers and Polymers, 2012. **13**: p. 571-575.
65. Li, H.-Z., S.-C. Chen, and Y.-Z. Wang, *Thermoplastic PVA/PLA blends with improved processability and hydrophobicity*. Industrial & Engineering Chemistry Research, 2014. **53**(44): p. 17355-17361.
66. Zou, G.-X., P.-Q. Jin, and L.-Z. Xin, *Extruded starch/PVA composites: Water resistance, thermal properties, and morphology*. Journal of Elastomers & Plastics, 2008. **40**(4): p. 303-316.
67. Aloui, H., et al., *Synergistic effect of halloysite and cellulose nanocrystals on the functional properties of PVA based nanocomposites*. ACS Sustainable Chemistry & Engineering, 2016. **4**(3): p. 794-800.
68. Qua, E., et al., *Preparation and characterization of poly (vinyl alcohol) nanocomposites made from cellulose nanofibers*. Journal of Applied Polymer Science, 2009. **113**(4): p. 2238-2247.
69. Li, Q., et al., *Synthesis and characterization of chitosan-based hydrogels*. International journal of biological macromolecules, 2009. **44**(2): p. 121-127.
70. Tamura, H., et al., *Biomedical applications of chitin hydrogel membranes and scaffolds*. Carbohydrate Polymers, 2011. **84**(2): p. 820-824.
71. Xu, T., et al., *Synthesis, characteristic and antibacterial activity of N, N, N-trimethyl chitosan and its carboxymethyl derivatives*. Carbohydrate Polymers, 2010. **81**(4): p. 931-936.
72. Delben, F., S. Stefancich, and R. Muzzarelli, *Chelating ability and enzymatic hydrolysis of water-soluble chitosans*. Carbohydrate polymers, 1992. **19**(1): p. 17-23.
73. Ai, H., et al., *Antioxidant, antifungal and antiviral activities of chitosan from the larvae of housefly, Musca domestica L*. Food chemistry, 2012. **132**(1): p.



- 493-498.
74. Ong, S.-Y., et al., *Development of a chitosan-based wound dressing with improved hemostatic and antimicrobial properties*. *Biomaterials*, 2008. **29**(32): p. 4323-4332.
  75. Peniche, C., W. Argüelles-Monal, and F. Goycoolea, *Chitin and chitosan: major sources, properties and applications*, in *Monomers, polymers and composites from renewable resources*. 2008, Elsevier. p. 517-542.
  76. Islam, A., M. Riaz, and T. Yasin, *Structural and viscoelastic properties of chitosan-based hydrogel and its drug delivery application*. *International journal of biological macromolecules*, 2013. **59**: p. 119-124.
  77. Buschmann, M.D., et al., *Chitosans for delivery of nucleic acids*. *Advanced drug delivery reviews*, 2013. **65**(9): p. 1234-1270.
  78. Chen, S.-H., et al., *Assessment of reinforced poly (ethylene glycol) chitosan hydrogels as dressings in a mouse skin wound defect model*. *Materials Science and Engineering: C*, 2013. **33**(5): p. 2584-2594.
  79. Giri, T.K., et al., *Modified chitosan hydrogels as drug delivery and tissue engineering systems: present status and applications*. *Acta Pharmaceutica Sinica B*, 2012. **2**(5): p. 439-449.
  80. He, P., S.S. Davis, and L. Illum, *In vitro evaluation of the mucoadhesive properties of chitosan microspheres*. *International journal of pharmaceutics*, 1998. **166**(1): p. 75-88.
  81. Lehr, C.-M., et al., *In vitro evaluation of mucoadhesive properties of chitosan and some other natural polymers*. *International journal of Pharmaceutics*, 1992. **78**(1-3): p. 43-48.
  82. Peppas, N.A. and J.J. Sahlin, *Hydrogels as mucoadhesive and bioadhesive materials: a review*. *Biomaterials*, 1996. **17**(16): p. 1553-1561.
  83. De Campos, A.M., A. Sánchez, and M.a.J. Alonso, *Chitosan nanoparticles: a new vehicle for the improvement of the delivery of drugs to the ocular surface. Application to cyclosporin A*. *International journal of pharmaceutics*, 2001. **224**(1-2): p. 159-168.
  84. Ueno, H., T. Mori, and T. Fujinaga, *Topical formulations and wound healing applications of chitosan*. *Advanced drug delivery reviews*, 2001. **52**(2): p. 105-115.
  85. Minami, S., et al., *Chitin and chitosan activate complement via the alternative*

- pathway. *Carbohydrate Polymers*, 1998. **36**(2-3): p. 151-155.
86. Ishihara, M., et al. *Photocrosslinkable chitosan: an effective adhesive with surgical applications*. in *International Congress Series*. 2001. Elsevier.
  87. Pangburn, S., P. Trescony, and J. Heller, *Lysozyme degradation of partially deacetylated chitin, its films and hydrogels*. *Biomaterials*, 1982. **3**(2): p. 105-108.
  88. Freier, T., et al., *Controlling cell adhesion and degradation of chitosan films by N-acetylation*. *Biomaterials*, 2005. **26**(29): p. 5872-5878.
  89. Habibi, Y., L.A. Lucia, and O.J. Rojas, *Cellulose nanocrystals: chemistry, self-assembly, and applications*. *Chemical reviews*, 2010. **110**(6): p. 3479-3500.
  90. Dash, R., Y. Li, and A.J. Ragauskas, *Cellulose nanowhisker foams by freeze casting*. *Carbohydrate polymers*, 2012. **88**(2): p. 789-792.
  91. Moon, R.J., et al., *Cellulose nanomaterials review: structure, properties and nanocomposites*. *Chemical Society Reviews*, 2011. **40**(7): p. 3941-3994.
  92. Nayigiziki, F.X., *Physical characterization and antimicrobial properties of PVA-cellulose nanofiber based films*. 2016, University of Missouri-Columbia.
  93. Heiligtag, F.J. and M. Niederberger, *The fascinating world of nanoparticle research*. *Materials today*, 2013. **16**(7-8): p. 262-271.
  94. Devouard, B., et al., *Magnetite from magnetotactic bacteria; size distributions and twinning*. *American Mineralogist*, 1998. **83**(11-12\_Part\_2): p. 1387-1398.
  95. Li, N., P. Zhao, and D. Astruc, *Anisotropic gold nanoparticles: synthesis, properties, applications, and toxicity*. *Angewandte Chemie International Edition*, 2014. **53**(7): p. 1756-1789.
  96. Taylor, M.G., et al., *Catalyst design based on morphology-and environment-dependent adsorption on metal nanoparticles*. *ACS Catalysis*, 2015. **5**(11): p. 6296-6301.
  97. Chavali, M.S. and M.P. Nikolova, *Metal oxide nanoparticles and their applications in nanotechnology*. *SN applied sciences*, 2019. **1**(6): p. 607.
  98. POOLE, C., P.. Jr., OWENS, FJ, "Introduction to Nano Technology", *A John Wiley & Sons. INC, New Jersey*, 2003: p. 72.
  99. Niculescu, A.-G., C. Chircov, and A.M. Grumezescu, *Magnetite nanoparticles: Synthesis methods—A comparative review*. *Methods*, 2022. **199**: p. 16-27.

100. Parashar, M., V.K. Shukla, and R. Singh, *Metal oxides nanoparticles via sol-gel method: a review on synthesis, characterization and applications*. Journal of Materials Science: Materials in Electronics, 2020. **31**: p. 3729-3749.
101. Galema, S.A., *Microwave chemistry*. Chemical Society Reviews, 1997. **26**(3): p. 233-238.
102. Chikan, V. and E.J. McLaurin, *Rapid nanoparticle synthesis by magnetic and microwave heating*. Nanomaterials, 2016. **6**(5): p. 85.
103. Swihart, M.T., *Vapor-phase synthesis of nanoparticles*. Current opinion in colloid & interface science, 2003. **8**(1): p. 127-133.
104. Li, J., Q. Wu, and J. Wu, *Synthesis of Nanoparticles via Solvothermal and Hydrothermal Methods 12*. 2016.
105. Patra, J.K. and K.-H. Baek, *Green nanobiotechnology: factors affecting synthesis and characterization techniques*. Journal of Nanomaterials, 2015. **2014**: p. 219-219.
106. Raghunath, A. and E. Perumal, *Metal oxide nanoparticles as antimicrobial agents: a promise for the future*. International journal of antimicrobial agents, 2017. **49**(2): p. 137-152.
107. Gubin, S.P., *Magnetic nanoparticles*. 2009: John Wiley & Sons.
108. Jones, N., et al., *Antibacterial activity of ZnO nanoparticle suspensions on a broad spectrum of microorganisms*. FEMS microbiology letters, 2008. **279**(1): p. 71-76.
109. Bruna, T., et al., *Silver nanoparticles and their antibacterial applications*. International Journal of Molecular Sciences, 2021. **22**(13): p. 7202.
110. Franci, G., et al., *Silver nanoparticles as potential antibacterial agents*. Molecules, 2015. **20**(5): p. 8856-8874.
111. Teirumnieks, E., et al., *Antibacterial and anti-viral effects of silver nanoparticles in medicine against COVID-19—a review*. Laser Physics, 2020. **31**(1): p. 013001.
112. Weldegebrieal, G.K., *Synthesis method, antibacterial and photocatalytic activity of ZnO nanoparticles for azo dyes in wastewater treatment: A review*. Inorganic Chemistry Communications, 2020. **120**: p. 108140.
113. Liu, J., et al., *Soluble soybean polysaccharide films containing in-situ generated silver nanoparticles for antibacterial food packaging applications*. Food Packaging and Shelf Life, 2022. **31**: p. 100800.

114. Sarwar, M.S., et al., *Preparation and characterization of PVA/nanocellulose/Ag nanocomposite films for antimicrobial food packaging*. Carbohydrate Polymers, 2018. **184**: p. 453-464.
115. Naqvi, S.M.K., et al., *Fabrication and characterization of polyvinyl alcohol/chitosan/moringa-extract hydrogel patch for wound-healing applications*. Materials Express, 2021. **11**(1): p. 107-115.
116. Asamoah, R., et al., *A comparative study of antibacterial activity of CuO/Ag and ZnO/Ag nanocomposites*. Advances in Materials Science and Engineering, 2020. **2020**: p. 1-18.
117. Kohli, R., *Methods for monitoring and measuring cleanliness of surfaces*, in *Developments in surface contamination and cleaning*. 2012, Elsevier. p. 107-178.
118. Ramachandran, V.S. and J.J. Beaudoin, *Handbook of analytical techniques in concrete science and technology: principles, techniques and applications*. 2000: Elsevier.
119. SanAgustin, J.T., et al., *Scanning electron microscopy to examine cells and organs*, in *Methods in cell biology*. 2009, Elsevier. p. 81-87.
120. Yang, J., et al., *Fabrication and surface modification of macroporous poly (L- lactic acid) and poly (L- lactic- co- glycolic acid)(70/30) cell scaffolds for human skin fibroblast cell culture*. Journal of Biomedical Materials Research: An Official Journal of The Society for Biomaterials, The Japanese Society for Biomaterials, and The Australian Society for Biomaterials and the Korean Society for Biomaterials, 2002. **62**(3): p. 438-446.
121. Ahmed, A., et al., *In-vitro and in-vivo study of superabsorbent PVA/Starch/g-C<sub>3</sub>N<sub>4</sub>/Ag@ TiO<sub>2</sub> NPs hydrogel membranes for wound dressing*. European Polymer Journal, 2020. **130**: p. 109650.
122. Dehnad, D., et al., *Optimization of physical and mechanical properties for chitosan–nanocellulose biocomposites*. Carbohydrate Polymers, 2014. **105**: p. 222-228.
123. Thangavel, P., et al., *Biomimetic hydrogel loaded with silk and l- proline for tissue engineering and wound healing applications*. Journal of Biomedical Materials Research Part B: Applied Biomaterials, 2017. **105**(6): p. 1401-1408.
124. Kord, B., et al., *Preparation and characterization of nanofibrillated Cellulose/Poly (Vinyl Alcohol) composite films*. Maderas. Ciencia y

- tecnología, 2016. **18**(4): p. 743-752.
125. Baker, S., et al., *Phyto-nano-hybrids of Ag-CuO particles for antibacterial activity against drug-resistant pathogens*. Journal of Genetic Engineering and Biotechnology, 2020. **18**(1): p. 1-8.
  126. Gobi, R. and R.S. Babu, *In-vitro study on chitosan/PVA incorporated with nickel oxide nanoparticles for wound healing application*. Materials Today Communications, 2023. **34**: p. 105154.
  127. Lan, W., et al., *Developing poly (vinyl alcohol)/chitosan films incorporate with d-limonene: Study of structural, antibacterial, and fruit preservation properties*. International journal of biological macromolecules, 2020. **145**: p. 722-732.
  128. Narasagoudr, S.S., et al., *Ethyl vanillin incorporated chitosan/poly (vinyl alcohol) active films for food packaging applications*. Carbohydrate polymers, 2020. **236**: p. 116049.
  129. Zhang, Z.-H., et al., *Enhancing mechanical properties of chitosan films via modification with vanillin*. International journal of biological macromolecules, 2015. **81**: p. 638-643.
  130. Jahan, Z., M.B.K. Niazi, and Ø.W. Gregersen, *Mechanical, thermal and swelling properties of cellulose nanocrystals/PVA nanocomposites membranes*. Journal of industrial and engineering chemistry, 2018. **57**: p. 113-124.
  131. Asamoah, R., et al., *Synthesis and characterization of zinc and copper oxide nanoparticles and their antibacteria activity*. Results in Materials, 2020. **7**: p. 100099.
  132. Khorasani, M.T., et al., *Incorporation of ZnO nanoparticles into heparinised polyvinyl alcohol/chitosan hydrogels for wound dressing application*. International journal of biological macromolecules, 2018. **114**: p. 1203-1215.
  133. Bhatt, S.S., G. Thakur, and M. Nune, *Preparation and characterization of PVA/Chitosan cross-linked 3D scaffolds for liver tissue engineering*. Materials Today: Proceedings, 2023.
  134. Prass, G.S. and A.S.C. d'Oliveira, *Processing and characterization of AISI 316L coatings modified with Cu and CuO nanoparticles*. Surface and Coatings Technology, 2023. **461**: p. 129465.
  135. Pauzi, N., et al., *Silver nitrate concentration on silver nanoparticles formation*

- attached on cellulose nanocrystal matrix*. Materials Today: Proceedings, 2023.
136. Mhatre, A., et al., *Chitosan/gelatin/PVA membranes for mammalian cell culture*. Carbohydrate Polymer Technologies and Applications, 2021. **2**: p. 100163.
  137. Nishiyama, Y., P. Langan, and H. Chanzy, *Crystal structure and hydrogen-bonding system in cellulose I $\beta$  from synchrotron X-ray and neutron fiber diffraction*. Journal of the American Chemical Society, 2002. **124**(31): p. 9074-9082.
  138. Yang, L., et al., *Preparation and characterization of PVA/arginine chitosan/ZnO NPs composite films*. International Journal of Biological Macromolecules, 2023. **226**: p. 184-193.
  139. Parsa, P., A. Paydayesh, and S.M. Davachi, *Investigating the effect of tetracycline addition on nanocomposite hydrogels based on polyvinyl alcohol and chitosan nanoparticles for specific medical applications*. International journal of biological macromolecules, 2019. **121**: p. 1061-1069.
  140. Malik, U.S., et al., *Vanillin cross-linked hydrogel membranes interfacial reinforced by carbon nitride nanosheets for enhanced antibacterial activity and mechanical properties*. Chinese Chemical Letters, 2022: p. 108071.
  141. Pal, K., A. Banthia, and D.J.T.B.A.O. Majumdar, *Preparation of transparent starch based hydrogel membrane with potential application as wound dressing*. 2006. **20**(1): p. 59-67.
  142. Xu, J., et al., *Characterization of zinc oxide nanoparticles-epoxy resin composite and its antibacterial effects on spoilage bacteria derived from silvery pomfret (*Pampus argenteus*)*. Food Packaging and Shelf Life, 2019. **22**: p. 100418.
  143. Qi, X., et al., *Investigation of Salecan/poly (vinyl alcohol) hydrogels prepared by freeze/thaw method*. Carbohydrate polymers, 2015. **118**: p. 60-69.
  144. Marand, S.A., H. Almasi, and N.A. Marand, *Chitosan-based nanocomposite films incorporated with NiO nanoparticles: Physicochemical, photocatalytic and antimicrobial properties*. International Journal of Biological Macromolecules, 2021. **190**: p. 667-678.
  145. Munshi, A., et al., *Effect of nanoparticle size on sessile droplet contact angle*. Journal of Applied Physics, 2008. **103**(8).

146. Lumbreras-Aguayo, A., et al., *Poly (methacrylic acid)-modified medical cotton gauzes with antimicrobial and drug delivery properties for their use as wound dressings*. Carbohydrate polymers, 2019. **205**: p. 203-210.
147. Kanmani, P. and J.-W. Rhim, *Physicochemical properties of gelatin/silver nanoparticle antimicrobial composite films*. Food chemistry, 2014. **148**: p. 162-169.
148. Affes, S., et al., *Controlled size green synthesis of bioactive silver nanoparticles assisted by chitosan and its derivatives and their application in biofilm preparation*. Carbohydrate polymers, 2020. **236**: p. 116063.
149. Tanpichai, S. and K. Oksman, *Cross-linked nanocomposite hydrogels based on cellulose nanocrystals and PVA: Mechanical properties and creep recovery*. Composites Part A: Applied Science and Manufacturing, 2016. **88**: p. 226-233.
150. Abd El-Mohdy, H., *Radiation synthesis of nanosilver/poly vinyl alcohol/cellulose acetate/gelatin hydrogels for wound dressing*. Journal of Polymer Research, 2013. **20**(6): p. 177.
151. Kasai, D., et al., *An investigation into the influence of filler Piper nigrum leaves extract on physicochemical and antimicrobial properties of chitosan/poly (vinyl alcohol) blend films*. Journal of Polymers and the Environment, 2019. **27**: p. 472-488.
152. Mehrabani, M.G., et al., *Preparation of biocompatible and biodegradable silk fibroin/chitin/silver nanoparticles 3D scaffolds as a bandage for antimicrobial wound dressing*. International journal of biological macromolecules, 2018. **114**: p. 961-971.
153. Baghaie, S., et al., *Wound healing properties of PVA/starch/chitosan hydrogel membranes with nano Zinc oxide as antibacterial wound dressing material*. Journal of Biomaterials Science, Polymer Edition, 2017. **28**(18): p. 2220-2241.
154. Vrana, N., et al., *Cell encapsulation within PVA- based hydrogels via freeze-thawing: A one- step scaffold formation and cell storage technique*. Journal of tissue engineering and regenerative medicine, 2009. **3**(7): p. 567-572.
155. Yiamsawas, D., et al., *Synthesis and swelling properties of poly [acrylamide-co-(crotonic acid)] superabsorbents*. Reactive and Functional Polymers, 2007. **67**(10): p. 865-882.

156. Abdeen, Z., *Swelling and reswelling characteristics of cross-linked poly (vinyl alcohol)/chitosan hydrogel film*. Journal of Dispersion Science and Technology, 2011. **32**(9): p. 1337-1344.
157. Noori, S., M. Kokabi, and Z. Hassan, *Poly (vinyl alcohol)/chitosan/honey/clay responsive nanocomposite hydrogel wound dressing*. Journal of Applied Polymer Science, 2018. **135**(21): p. 46311.
158. Sadeghi, M. and M. Yarahmadi, *Synthesis and characterization of superabsorbent hydrogel based on chitosan-g-poly (acrylic acid-coacrylonitrile)*. African Journal of Biotechnology, 2011. **10**(57): p. 12265-12275.
159. Kumar, A., T. Behl, and S. Chadha, *Synthesis of physically crosslinked PVA/Chitosan loaded silver nanoparticles hydrogels with tunable mechanical properties and antibacterial effects*. International journal of biological macromolecules, 2020. **149**: p. 1262-1274.
160. Ahmed, A., et al., *Enhancing the thermal, mechanical and swelling properties of PVA/starch nanocomposite membranes incorporating gC 3 N 4*. Journal of Polymers and the Environment, 2020. **28**: p. 100-115.
161. Morgado, P.I., et al., *Poly (vinyl alcohol)/chitosan asymmetrical membranes: Highly controlled morphology toward the ideal wound dressing*. Journal of membrane science, 2014. **469**: p. 262-271.
162. Hiep, N.T., et al., *Microwave-assisted synthesis of chitosan/polyvinyl alcohol silver nanoparticles gel for wound dressing applications*. International Journal of Polymer Science, 2016. **2016**.